EFFECT OF STRESS ON INITIATION AND PROPAGATION OF LOCALIZED CORROSION IN ALUMINIUM ALLOYS

By

SUKANTA GHOSH

A thesis submitted to
University of Birmingham
for the degree of
DOCTOR OF PHILOSOPHY

Metallurgy and Materials
School of Engineering
University of Birmingham
November 2007

1st of 5 files

Introductory material and chapters 1 and 2

The remaining chapters and the appendices are in four additional files

By convention sweet, by convention bitter, by convention hot, by convention cold, by convention colour: but in reality nothing exists except atoms and empty space; everything else is opinion.

…….Democritus of Abdera

ACKNOWLEDGEMENTS

I would like to express my sincere gratitude to my supervisors, Dr. Brian J. Connolly and Dr. Alison J. Davenport for their invaluable guidance and supervision throughout this study.

Special thanks go to Dr. Vincent Vignal and Dr. Roland Oltra of Université de Bourgogne, France for their kind assistance during the experiments performed in their laboratory. I have learnt a lot about the microelectrochemical and mechanistic aspects of corrosion research from Dr. Vignal through his enthusiastic and expert guidance. I would also like to thank Dr. Marco Stampanoni and Dr. Amela Groso of the Swiss Light Source, for their help during the X-ray synchrotron tomography experiments.

I would like to thank the Overseas Research Students Awards Scheme, UK and the Department of Metallurgy and Materials, University of Birmingham, UK for the financial support for my PhD study.

I also owe a lot to my friends in the ‘Grace House’ for providing such a nice and affectionate atmosphere for living and without them last three years definitely would have felt much longer. I would like to express my appreciation for help throughout my course of study from the members of the corrosion group, especially Tony Horner, Chris Cooper, Farkhanda, and Rob Winsley.

I can not end without thanking my family whose constant encouragement and love I have relied throughout my study in the UK.

ABSTRACT

High strength aluminium alloy AA2024 is susceptible to localized corrosion in the form of pitting and intergranular corrosion (IGC). The corrosion behaviour of this alloy is strongly influenced by the presence of different intermetallic particles. In this study, the effect of applied stress and the role of intermetallic particle removal by surface treatment on the initiation and propagation of localized corrosion are investigated.

It was found that applying a stress to as polished AA2024 leads to a drop in breakdown potential. However, no detectable effect of stress on breakdown was observed for an Al-0.099 Cu model alloy without intermetallic particles. Direct observation of the effect of stress on as polished AA2024 in a FEG-SEM shows the development of micro/nano crevices adjacent to intermetallic particles. It is likely that these crevices are initiation sites for localized corrosion, lowering the breakdown potential in stressed AA2024. A micro-capillary electrochemical cell technique was used to investigate the electrochemical behaviour of individual intermetallic particles and their behaviour has been compared with the particle free matrix in unstressed conditions. Initiation sites for localized attack and its morphology have been studied in detail using SEM, AFM, and optical profilometry. The electrochemical behaviour of specific intermetallic particles and the particle free matrix of AA2024 have been studied as a function of stress state using the micro-capillary electrochemical cell in combination with an in situ stressing stage. These experiments emphasized the role of intermetallic particles as the possible key contributing factor in determining the corrosion properties of the alloy under stressed conditions.

The propagation of localized corrosion sites in AA2024 in chloride environments was also found to be affected by stress. In situ X-ray synchrotron microtomography experiments were used to observe the evolution of corrosion attack as a function of continuous exposure time. It was found that application of stresses of 70% yield strength or above has a significant effect on the localized corrosion propagation. The outcome of this work provides quantitative growth rates of intergranular corrosion in three dimensional space as a function of stress state in real time.

Combination of all the above studies (stressed vs. unstressed along with as received vs. surface treated) will help us in better understanding the importance of applied stress, surface treatment and constituent intermetallic particles on localized corrosion initiation and propagation.

TABLE OF CONTENTS

1 INTRODUCTION

Aluminium and its alloys are used extensively in the modern industrial world for various applications. Aluminium is second only to iron as the most important metal of commerce [1]. Various properties of aluminium alloys like good thermal conductivity, exceptional electrical conductivity, high strength to weight ratio, high fracture toughness and excellent corrosion resistance have made them very popular for numerous industrial applications. Broad use of aluminium alloys can vary from aluminium foils for food packaging to the structural components of aircraft, marine and aerospace vehicles [2, 3]. Since 1930, modern aircraft have been built almost universally from aluminium alloys (predominantly using Al-Cu-Mg (2XXX) series and Al-Zn-Mg-Cu (7XXX) series alloys). The main focus of this current study will be on aluminium alloy 2024 which is extensively used in the aircraft industry for applications such as fuselage skins, fuselage frames, and wings due to its high strength to weight ratio and high fracture toughness [4-7]. Corrosion resistance of most aluminium alloys results from the naturally occurring, tenacious surface oxide film. Rupture of the passive film may create different types of corrosion attack and make the aluminium alloy especially susceptible to localized corrosion and, in some cases, subsequent environmentally assisted cracking. Corrosion of aluminium alloys thus has been a topic of interest to many researchers for the last few decades.

Like other high strength aluminium alloys, AA2024 is prone to localized corrosion such as pitting and intergranular corrosion (IGC) which can be potential sites for initiation of cracks, resulting in catastrophic failure. Localized corrosion is normally considered as a very complex process involving a combination of many controlling

factors (e.g., local chemistry, local physical metallurgy, local stress state, etc.). Hence, information on the mechanism of localized corrosion and the distinct physicochemical properties associated with the localized corrosion site has always been an issue of prime importance, since this knowledge can lead to the development of component life prediction models and novel effective corrosion protection systems.

Localized corrosion of aluminium alloy 2024-T351 is strongly influenced by the presence of "second-phase" intermetallic particles or constituent particles that form during ingot solidification due to the presence of impurity elements such as iron and manganese in amounts which exceed the solid solubility limit [8-11]. After cold working, clusters or bands of these particles are normally found to be aligned parallel to the rolling direction. Two predominant categories of intermetallic particles have been distinguished on the surface of AA2024 [6, 7, 9]. The first type appeared as round and smooth with size ranging from 1-5 μm and are identified as Al_2CuMg ('S' phase particle). The second type of particle (consists of Al-Cu-Fe-Mn) is in the range of 10-30 μm with rectangular or elongated shape and identified with the composition of $Al_6(CuFeMn)$ or other stoichiometric relationship [commonly referred as Fe-Mn rich particle or in short 'Fe-Mn' particle]. It is generally believed that Fe-Mn rich intermetallic particles act as cathodic sites during the corrosion process whereas 'S' phase particles show initial anodic behaviour. However, 'S' phase particle can then dealloy to form Cu rich particle remnants/surface that is cathodically active. Thus, 'S' phase intermetallic particles have, in particular, been identified as the key contributor to the poor corrosion resistance of AA2024 [12-15].

Initiation of localized corrosion is a key stage in determining the corrosion performance of a particular alloy. In this study, the role of individual intermetallic particles in initiating pitting corrosion has been investigated using a micro-capillary

electrochemical cell technique (or “Micro-Cell” technique [16, 17]) with an exposure area of 40 μm diameter. Microelectrochemical experiments with such a small exposure area will allow better understanding of the corrosion behaviour of individual microstructural features (e.g., intermetallic particles, particle free matrix etc) by comparing their relative corrosion behaviour with each other.

It has also been previously shown that the presence of coarse intermetallic particles like Fe-Mn rich and ‘S’ phase particles in high strength wrought alloys do not necessarily add any beneficial effect to the alloy properties, but they remain in the microstructure as natural impurities as their removal would not be cost effective [5, 18]. The presence of these types of intermetallic particles in the alloy surface significantly decrease the resistance to localized corrosion [18]. As a result, to improve the corrosion resistance and the adhesion of coatings or paints on the surface, a surface treatment is often required [19]. A typical surface treatment involves different steps such as cleaning, coating and finally painting. Chromate conversion coating is the most widely used surface treatment technique but because of the carcinogenic nature of the hexavalent chromium, users are forced to find an alternative. It has been shown that the ‘S’ phase particles can be selectively removed from the AA2024 surface by etching the samples with NaOH followed by HNO_3 desmutting treatment in the presence of chloride ions [19]. The effectiveness of these intermetallic particles removal in improving the corrosion properties of AA2024 has been investigated in detail during this current study.

The primary goal of this study is to investigate the effect of applied stress on localized corrosion initiation and propagation in aluminium alloys. Application of stress can change the local microstructural features and subsequently the electrochemical activity for localized corrosion site initiation. Whereas several studies of the applied stress / corrosion relationship of stainless steel have been explored, limited research has

been performed on aluminium alloys. Previous investigators have shown that applied stress affects the localized corrosion behaviour of structural metal by influencing dissolution rate [20-22], passivity [23-25], and localized corrosion initiation and propagation [26-34]. In aluminium alloys, deformation is thought to produce surface defects such as slip lines, microcracks, decohesion between phases as well as making the surface rougher [35]. It has also been hypothesized [35] that all these surface defects could serve as potential sites for pit initiation by making passive film less stable than a flat surface.[1]

However, the role of intermetallic particles on initiation of localized corrosion in a stressed aluminium alloy has not, as yet, been well understood or, in fact, rigorously investigated. The corrosion properties of the intermetallic particles under stress (due to change in the morphology and stress distribution around the irregular shaped particles) might also influence the overall corrosion properties of the alloy. Large scale corrosion measurement on an alloy surface does not always allow the possibility to identify the individual contribution from each of those above mentioned deformation features under stressing conditions. Hence ambiguities still remain about the key contributing microstructural feature in determining the corrosion performance of a stressed specimen.

With this in mind, an effort (using two different experimental approaches) has been made in this study to separate out the contribution from intermetallic particles and matrix deformations towards determining the overall corrosion performance of a stressed specimen. Firstly, the corrosion properties of stressed AA2024 specimens are compared with the corrosion properties of intermetallic particle free Al-Cu binary alloy specimens under stressing conditions. Comparison of the corrosion character of these two alloys

[1] No investigations were performed on the passive films in this dissertation.

indicates the possible crucial and perhaps governing role of the intermetallic particles. In addition, micro-capillary electrochemical cell experiments (with an exposure of 40 μm diameter) have been performed on specific features of AA2024 (e.g., intermetallic particles, particle free matrix etc) as a function of stress state (both in the elastic and plastic domain). These experiments allow better understanding of the corrosion behaviour of individual microstructural features under stress. Earlier it has been hypothesized that the presence of delamination at the particle/matrix interface creates micro/nano crevices which in turn enhance the electrochemical reactivity of a stressed specimen [36]. In this current study, in situ stressing analysis of the AA2024 surface as a function of stress state within a FEG-SEM has been used to investigate the presence of delamination at the particle/matrix interface. Emphasis has been placed on understanding the behaviour of individual intermetallic particle morphology as a function of stress and its possible effects on localized corrosion behaviour of the alloy.

Several techniques such as confocal laser scanning microscopy [37, 38], microcapillary electrochemical cell technique [39-42], scanning Kelvin probe force microscopy [43, 44], and AFM [45-48] have previously been used to investigate the localized corrosion initiation associated with the intermetallic particles in the aluminium alloys. Compared to the techniques available for studying localized corrosion initiation process, not many techniques have been developed to understand the localized corrosion growth kinetics in the propagation stage. Growth kinetics of localized corrosion (predominantly pitting and intergranular) in aluminium alloys have been studied predominantly using two techniques, namely the foil penetration technique [29, 49-52] and X-ray radiography [53-55]. However, during the last few years researchers have been trying to develop more accurate and convenient techniques for further studies of the

growth rate. Better understanding and quantification of the growth rate in bulk aluminium alloys will contribute to the ongoing effort of life prediction modelling.

High resolution, in situ X-ray synchrotron microtomography has been used to record the three dimensional evolution of localized corrosion sites in an aqueous chloride solution, as a function of applied stress and exposure time. The two most predominant forms of localized corrosion, pitting and intergranular corrosion are three dimensional in nature. IGC growth rate measurement is a fundamental problem and most of the techniques previously used are based on conventional two dimensional methods. Conventional two dimensional techniques have limitations and accurate quantitative measurements of IGC rate are difficult to obtain using these techniques. The true size, complex shape, distribution and connectivity of phases and defects such as intergranular corrosion can not be obtained from a 2D section.

X-ray synchrotron microtomography is a relatively new, non-destructive technique which has been used recently in many areas of materials science and engineering to obtain 3D information of materials. X-ray synchrotron microtomography can overcome the limitations of 2D technique and allows for the characterization of evolving features within the bulk of the material with spatial resolutions close to 1 μm (or less). The outcome of this work will provide, for the first time, quantitative growth rates of intergranular corrosion as a function of stress state in real time.

In this PhD dissertation the combination of all the above studies (stressed vs. unstressed along with as received vs. surface treated) will help us in better understanding the importance of constituent intermetallic particles, surface treatment, and applied stress on the initiation and propagation stages of localized corrosion of aluminium alloys.

This dissertation is effectively separated into four distinctly themed sections. Experimental results, discussion and conclusions for each of these four sections are presented in Chapter 4, 5, 6, and 7.

Chapter 4 of this dissertation mainly discusses the effect of surface treatment on removing deleterious intermetallic particles from the alloy surface and the resulting beneficial effects on improving the corrosion properties of AA2024-T351.

Chapter 5 presents a detailed investigation on the electrochemical behaviour of individual intermetallic particles through micro-capillary electrochemical cell experiments. The relative corrosion behaviour of different intermetallic particles in AA2024-T351 along with the behaviour of particle free matrix has been characterized in this chapter. These electrochemical studies are thought to provide insight in the contribution of different intermetallic particles towards the initiation of pitting corrosion in AA2024-T351.

Chapter 6 discusses the result of the current investigation on the effect of applied elastic and plastic tensile stress in initiating localized corrosion in aluminium alloys. The main focus of this chapter is to compare the corrosion properties of unstressed samples with stressed samples and to identify the microstructural features responsible for changing the corrosion behaviour under stressing conditions. One of the key focuses of this chapter is to investigate the role of the intermetallic particles present in the AA2024-T351 microstructure in enhancing localized corrosion activities under stress.

Chapter 7 discusses the effect of stress on the growth and development of localized corrosion (i.e., intergranular corrosion) in a high strength aluminium alloy. In this chapter, the use of high resolution in situ X-ray synchrotron microtomography to record the three dimensional evolution of localized corrosion sites in an aqueous chloride solution, as a function of applied stress and exposure time has been discussed in detail.

This work provides quantitative growth rates of intergranular corrosion under stressing condition and in three dimensions.

An overall summary of this current project along with key findings is presented in Chapter 8. Possibilities of further experiments in certain areas have been discussed in the form of future work in Chapter 9.

2 LITERATURE REVIEW

2.1 Physical Metallurgy of Age Hardening Aluminium Alloys

Wrought aluminium products are produced from cast ingots and through different mechanical and thermal treatments their structures are changed. About 85% of the aluminium and its alloys are used for wrought product like rolled plate, sheet, foil, extrusions, tube, rod, bar and wire [5]. Although aluminium and its alloys are one of the most versatile of the common foundry metals, the discussion in this section will be confined to the wrought form only. Depending on the composition and structure, each series of aluminium alloys behave differently and variation of their properties depend on their processing history. Wrought alloys are of two types: non-heat treatable (i.e., the 1XXX, 3XXX, 4XXX, and 5XXX series) and heat treatable (the 2XXX, 6XXX, and 7XXX series). Aluminium alloys are either thermally treated or mechanically treated to develop the desired balance of mechanical properties required for consistence component service performance. The heat treatable alloys achieve their strength by precipitation hardening after the thermal treatment.

The most common thermal treatment consists of solution treatment, quenching and aging [5, 56, 57]. The purpose of the solution treatment is to bring the entire alloying elements to complete solid solution and ideally it should be performed in a single phase field near the solidus temperature. Homogenization is an important criterion for this step. After the solution treatment, the next processing step is to cool the alloy or quench it to room temperature. The objective is to get the maximum supersaturation of the alloying elements for the next aging step. The alloy in this stage remains as supersaturated solid

solution (SSSS). Sometimes, the alloy is cold-worked after quenching in order to improve its response to ageing. In case of heat-treatable aluminium alloys, developments of properties occur in the age-hardening stage where controlled decomposition of the SSSS is achieved by age hardening at room temperature (natural aging) or at elevated temperature (artificial aging) [58, 59]. During the aging treatment the soluble alloying elements are precipitated (mostly together with aluminium as aluminium compounds) in an optimize size and distribution. The time and temperature of the aging treatment depends on the alloy system and it could vary from room temperature to elevated temperature.

The strength of an age-hardened alloy is mainly dependent on the precipitate-dislocation interaction. Figure 2.1 schematically shows the relationship between the microstructure and the aging behaviour. Hardness increases as a function of time during aging (Zone 1) with the appearance of precipitates in the matrix. If the precipitates are fine and uniformly dispersed throughout the matrix, they hinder the movement of dislocations and thereby increase the yield stress of the material (Zone 2). However, over-ageing could easily coarsen the precipitates and they become more widely spaced. This causes the dislocations to loop around the precipitates (Zone 3) and as a result the yield strength decreases [5, 60].

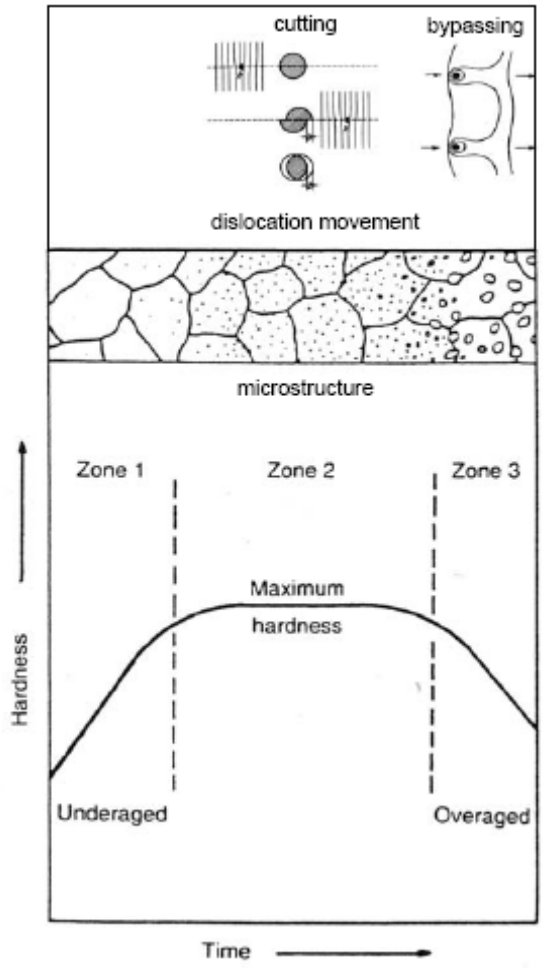

Figure 2.1 Relationship between aging and microstructure of an age hardenable aluminium alloy. Hardness starts increasing as a function of time during aging (Zone 1) with the appearance of precipitates in the matrix. In Zone 2 uniformly dispersed fine precipitates results into the maximum strength of the material. Overageing in Zone 3 coarsens the precipitates and yield strength decreases [5].

2.1.1 The 2xxx Series

The precipitation-hardening phenomenon at room temperature (i.e., natural aging) following quenching was discovered by Wilm in Germany in 1906 [61]. In 1931 the continuing demand of the aircraft industry for lighter-weight structures led to the development of alloy 2024-T3 which is classified as a high strength aluminium alloy and responds to strengthening by heat treatment. The main focus of the current study will be

on the 2024-T351 alloy which is widely used in the aircraft industry for applications such as fuselage skins, fuselage frames, and wings [4-7]. 'T' symbolizes that the alloy is heat-treatable, and the T3 treatment consists of solution heat treating, water quenching, cold-working and natural aging [56, 62]. Moreover, the presence of the digits '51' at the end of a temper designation denote a tensile stretching operation that can be carried out immediately after quenching to decrease residual stresses and, in some cases, to increase the mechanical properties of the alloy, for example 'T351' [56].

The main alloying element in the 2XXX series alloys is copper. Strength of the alloy is increased by the addition of copper while magnesium[2] is added to accelerate the precipitation hardening as well as to achieve benefits from natural aging effects [56, 63].

As AA2024 is a heat treatable alloy, a broad range of mechanical properties can be obtained using different working and aging combinations. Apart from T351, the other commonly used tempers for AA2024 are O, T3, T4, T6 and T8 [5, 64, 65]. Typical mechanical properties of AA2024 with different tempers are given in Table 2.1. Cold work prior to age hardening (e.g., T3 and T8 tempers) increase the density of dislocations which act as a precursor sites for nucleation of fine precipitates and thereby having beneficial effects on the mechanical properties of the alloy.

Impurities play an important role in the properties of these alloys. Aluminium alloy 2024 is widely used in the aircraft industry because of its specific strength and good balance between fracture toughness and fatigue crack growth [4-7, 66]. However, the presence of impurities will promote the formation of coarse intermetallic constituent particles as will be discussed in the following section in detail. Presence of large

[2] Addition of magnesium increases the retained vacancy concentration after solutionization and quench. Magnesium interacts with vacancies to enhance precipitate nucleation. Moreover, Mg additions also lower the stacking fault energy of the aluminium alloy which may enhance nucleation of plate-like precipitates.

constituent phases have detrimental effect on the fracture toughness of the aluminium alloys as it is generally accepted that the fracture of brittle constituent particles lead to preferential paths for crack advance and reduce fracture toughness [4, 56, 67]. Apart from that, fatigue cracks are also shown to initiate from those coarse constituent particles [19, 68, 69]. Hence, several high-toughness versions of the 2XXX alloys are developed with tighter control of the impurities and thereby improving the fracture and fatigue properties [2, 56].

Table 2.1 Typical mechanical properties of AA2024 with different tempers.

Temper	Tensile Strength (MPa)	Yield Strength (MPa)		Reference
O	185	75	Annealed	[1, 63, 64]
T3	485	345	Solution heat treated, cold worked and naturally aged	[1, 5, 56, 64, 70]
T351	470	325 - 345	Solution heat treated, stress relieved by stretching at 0.5-3% permanent set, cold worked and naturally aged	[1, 5, 64, 70]
T4	470	325	Solution heat treated and naturally aged	[1, 5, 63, 64]
T6	475	395	Solution heat treated and artificially aged at 190˚C for 12 hours	[63, 64, 71]
T8	480	450	Solution heat treated, cold worked and artificially aged at 190˚C for 12 hours	[1, 5, 63, 71]

2.1.1.1 Second Phase Constituents in AA2024

AA2024 is characterized by the presence of “second-phase” microstructural particles which are produced when alloying element content exceeds the solid solubility limit. The second phase particles of concern are mainly of three types: constituent intermetallic particles, dispersoids and fine precipitates.

2.1.1.1.1 Constituent Intermetallic Particles

Formation of this type of second phase particles occurs interdendritically by eutectic decomposition during ingot solidification, primarily from iron and silicon impurities [4]. These particles are generally coarser (0.5 to 30 μm) and can be either soluble or insoluble when subjected to solution heat treatments or homogenisation treatments. Presence of wide variety of intermetallic phases in aluminium alloys due to the high electronegativity and trivalence of aluminium has been the subject of considerable study for the last few decades [56, 57, 72, 73].

One group of intermetallic particles usually contain impurity elements like iron or silicon and are virtually insoluble [57]. The most common phases of this type present in a wrought 2024 are $(Fe,Mn)_3SiAl_{12}$, $Al_6(CuFeMn)$, $FeMnAl_6$, $Al_7Cu_2(Fe,Mn)$, $Al_2Cu(Mn,Fe)_3$ Cu_2FeAl_7, $Al_{20}Cu_2(Fe,Mn)_3$, $Cu_2Mg_8Si_5Al_4$ [9, 37, 45, 56, 57, 72-77]. Other complex intermetallic phases reported to be present in the aluminium alloys that contain Si, Fe, Mn and/or Cu are Al_8Fe_2Si, Al_5FeSi, $Al_{21}Fe_3Si_5$, $Al_5(FeMn)_3Si_2$, $Al_{19}Fe_4MnSi_2$, $\alpha Al(Fe,Mn)Si$, $\alpha Al_{12}Mn_3Si$, $(Fe,Mn)_xSi(Al,Cu)_y$ [45, 73, 75, 78]. As the solubility of iron in pure aluminium is reduced by alloying elements, intermetallic particles containing iron are insoluble [4]. Although silicon has appreciable solubility in

aluminium, its solubility is decreased by alloying elements like magnesium [4]. The size distributions of insoluble intermetallic particles are controlled by the rate of ingot solidification, the chemical composition, and the extent and nature of bulk deformation. Particle size decreases as solidification rate increases, as iron and/or silicon content decreases, and as the amount of deformation increases [4].

The major alloying elements form the second group of intermetallic particles which are soluble and typical examples are Mg_2Si, Al_2Cu and Al_2CuMg, [5-7, 9, 79, 80]. Al_2Cu particles (θ-phase) are less often observed in AA2024 compared to Al_2CuMg. Al_2Cu particles are small, rounded (about 1-2 μm) and generally found as isolated individual particles [75].

In most of the cases intermetallic particles do not serve any useful purpose in high strength wrought aluminium alloys like 2024 but they are present in commercial alloys because their removal is not cost effective [5]. During the thermo-mechanical treatment subsequent to the ingot formation, the intermetallic particles are broken down into fragments aligned in bands along the rolling direction [7, 8]. The intermetallic particles can also form clusters after they are broken down during the rolling process [81].

However, among all the reported constituent intermetallic particles, two categories (based on size, composition and shapes) have predominantly been distinguished on the surface of aluminium 2024 alloy as shown in Figure 2.2. The first type appeared as round and smooth with size range of 1-5 μm and they are identified as Al_2CuMg (‘S’ phase) [6, 7, 9, 14, 82]. Sometime these ‘S’ phase particles are reported to be as large as 10 μm in diameter [10]. The crystal structure of ‘S’ phase is orthorhombic with lattice spacing of a = 0.400, b = 0.923 and c = 0.714 nm [5, 63, 75, 83]. The second type of particle (consists of Al-Cu-Fe-Mn) is in the size range of 10 to 30 μm, characterized by a rectangular or elongated shape and identified with a composition of Al_6(CuFeMn) or other

stoichiometric relationship [commonly referred as 'Fe-Mn' particle/Fe-rich intermetallic particle] [9, 11, 70]. Compositions of these particles vary considerably from particle to particle. Some particles contained mainly Fe and Cu with small amount of Mn, while others contained Si as well [75]. These constituent particles are found to possess complex crystal structure, although in few occasions they are identified as a complex rhombohedral phase [75]. In some cases, Fe-containing particles are found to have Cu-rich surface layers compared to the bulk [6, 19].

Chen *et al.* [8] found that the average density of the constituent intermetallic particles in AA2024-T3 with a projected surface area > 1 μm^2 is about ~ 323,000 particles per cm^2. Buchheit *et al.* [9] reported that different intermetallic particles covered about 4.2% of the total alloy surface of AA2024-T3.

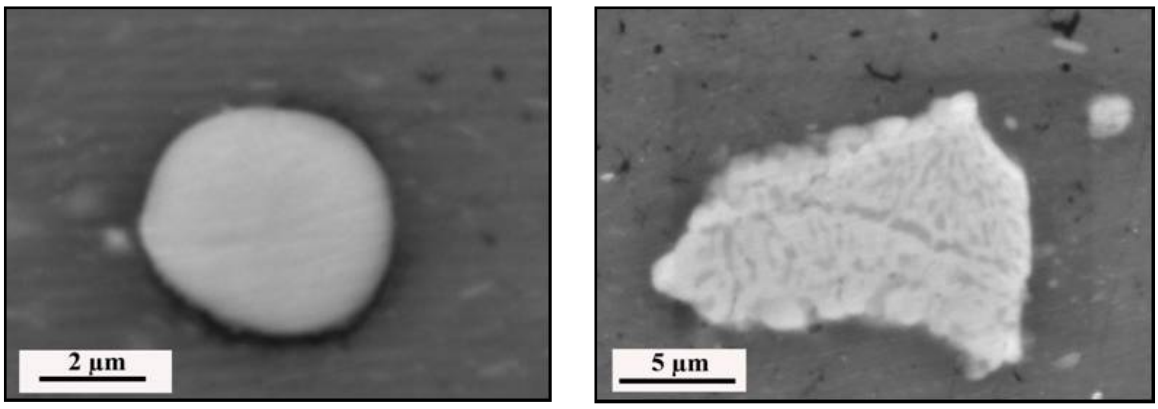

Figure 2.2 SEM micrographs of two predominant categories of intermetallic particles in AA2024, (a) smooth and rounded Al_2CuMg ('S' phase particle) and (b) irregular and elongated Al-Cu-Fe-Mn containing particle [Fe-Mn particle] [19, 84].

2.1.1.1.2 Dispersoids

These smaller submicron particles (typically 0.05 to 0.5 μm) are formed during ingot homogenization [5]. Guillaumin *et al.* [7] found rod shaped dispersoids in AA2024 as $Al_{20}Mn_3Cu_2$ with an average length of 200 nm. Figure 2.3 shows the transmission electron micrograph of such rod shaped $Al_{20}Mn_3Cu_2$ dispersoid. The presence of this type of dispersoid in AA2024 is also confirmed by other researchers [45, 56, 57, 66, 76, 85]. Though normally dispersoids are uniformly distributed throughout the matrix, the presence of dispersoid free zones around the coarse intermetallic particles has been observed [7, 45]. Other types of dispersoids in AA2024 were identified as $Cr_2Mg_3Al_{18}$ and $ZrAl_3$ [66, 86]. $Al_{20}Mn_3Cu_2$ dispersoids (~0.28 μm) are larger in sizes compared to $Cr_2Mg_3Al_{18}$ (~0.08 μm) and $ZrAl_3$ (~0.035 μm). Most of these compounds contain one of the transition metals which have modest solubility and diffuse slowly in solid aluminium. Distribution of these dispersoids and spacing between them has an important effect on the mechanical properties of AA2024 [66].

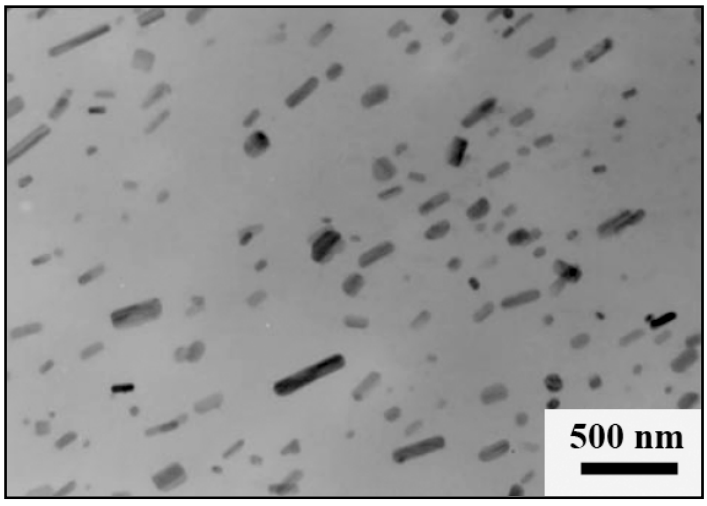

Figure 2.3 Transmission electron micrograph of dispersoids in aluminium alloy 2024. The major dispersoids is identified as $Al_{20}Mn_3Cu_2$ [66].

2.1.1.1.3 Fine Age Hardening Precipitates

Fine precipitates (up to 0.1 μm) which form during age-hardening heat treatments have the largest effect on strengthening of heat treatable aluminium alloys. The most commonly found precipitates in AA2024 are Al_2CuMg (S-phase) [5, 57, 59, 63, 72, 87-90] and Al_2Cu (θ-phase) [57, 76, 86, 88]. However, fine, nanometer-sized and lathe-shaped 'S' phase precipitates are far more important in controlling the mechanical properties of AA2024 than Al_2Cu precipitates [10].

Precipitation sequence in Al-Cu-Mg alloy starting from super saturated solid solution (SSSS) can be represented as:

$$SSSS \rightarrow GPzones \rightarrow S'(Al_2CuMg) \rightarrow S(Al_2CuMg)$$ [59, 83, 91-93]

GP (Guinier-Preston) zones are localized concentrations of clustering of Cu and Mg atoms in the form of disks on the (110) aluminium planes and are fully coherent with the matrix. GP zones are sometimes known as GPB zones (Guinier-Preston-Bagaryatsky). S' is an intermediate precipitate, semicoherent with matrix, and normally precipitates heterogeneously on dislocations, but can also precipitate homogeneously within the matrix [59, 89]. Since S' precipitates on the dislocations, an increase in dislocation density by cold working prior to quenching increases the amount of S' precipitate and subsequently produces a fine distribution of equilibrium S precipitates which are incoherent with the matrix [59, 88]. The metastable phase S' is regarded as a precursor to the equilibrium phase S and both of them are reported to have similar composition and structure [83, 91, 92, 94]. For all practical purposes S and S' may be considered to be the same phase [83].

As discussed earlier, like other age hardenable alloys, AA2024 derives its strength from the interaction of dislocation with the fine precipitate formed during aging treatment. The needle or plate shaped S-phase precipitates with a long side of about 100 nm [7, 95] are uniformly distributed in the matrix (see Figure 2.4).

Apart from precipitating in the dislocations, Al_2CuMg phases also precipitate at the grain boundaries with either no sign of a precipitate free zone [7] or a slight precipitate free zone [95]. Figure 2.5a and Figure 2.5b show the precipitation of Al_2CuMg phases at grain boundaries and a precipitate free zone adjacent to the grain boundary, respectively.

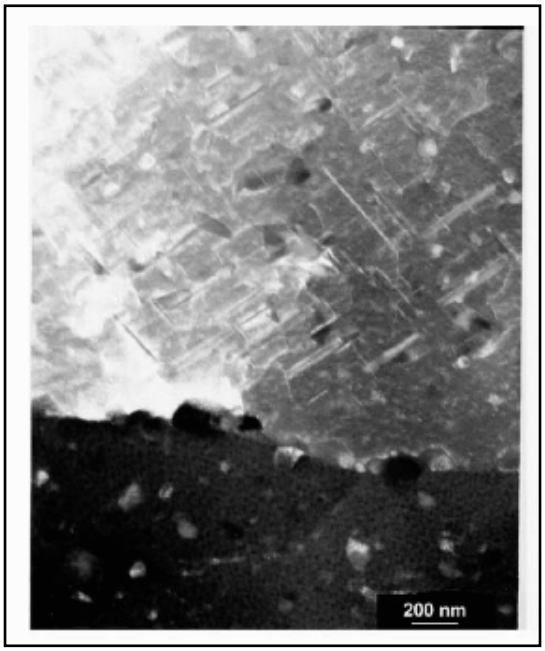

Figure 2.4 TEM micrographs of AA2024 showing plate like Al_2CuMg precipitates [95].

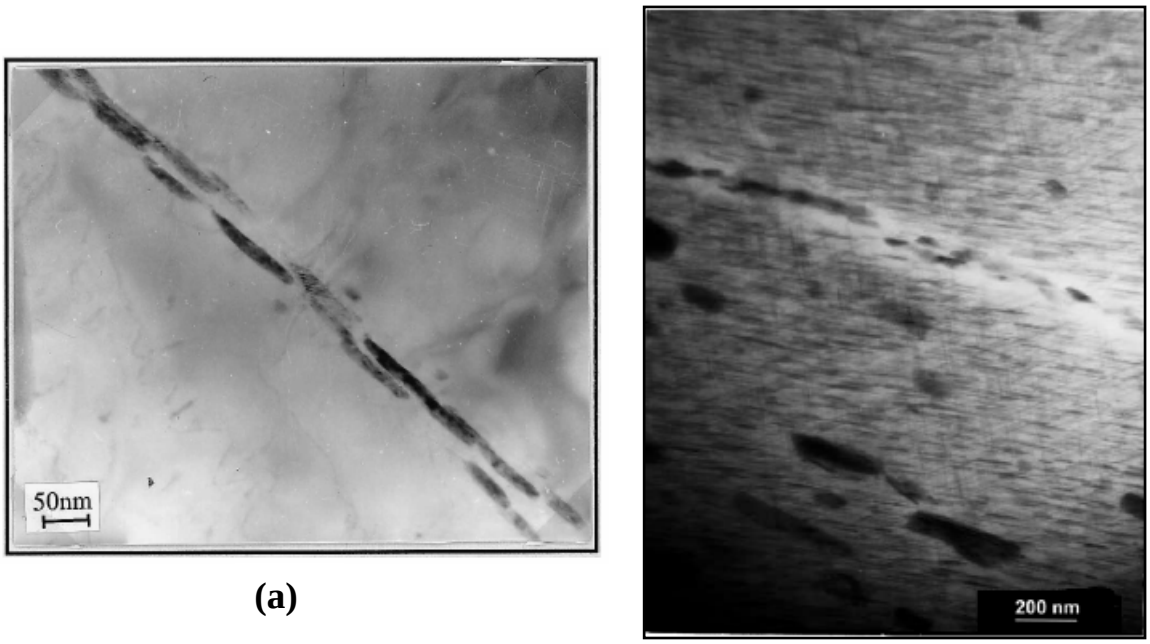

(a) **(b)**

Figure 2.5 TEM micrographs of AA2024 showing (a) Al_2CuMg precipitates in the grain boundary [7], and (b) precipitate free zone around the grain boundary [95].

The effect of aging time and temperature on the hardness of AA2024-T351 is shown in Figure 2.6 [90]. The alloy in the super saturated solid solution condition after quenching has low strength as there are no precipitate particles dispersed in the matrix. Strength of the alloy increases initially during aging as precipitates starts to form. Mechanism behind the increase in the strength involves precipitate-dislocation interaction which is described in Figure 2.1. The rate of increase in hardening with aging time increases with increasing temperature, Figure 2.6. However, peak hardness is found to be lowered with higher aging temperature. With prolong aging, precipitates starts coarsening which results in the drop of the strength of the alloy.

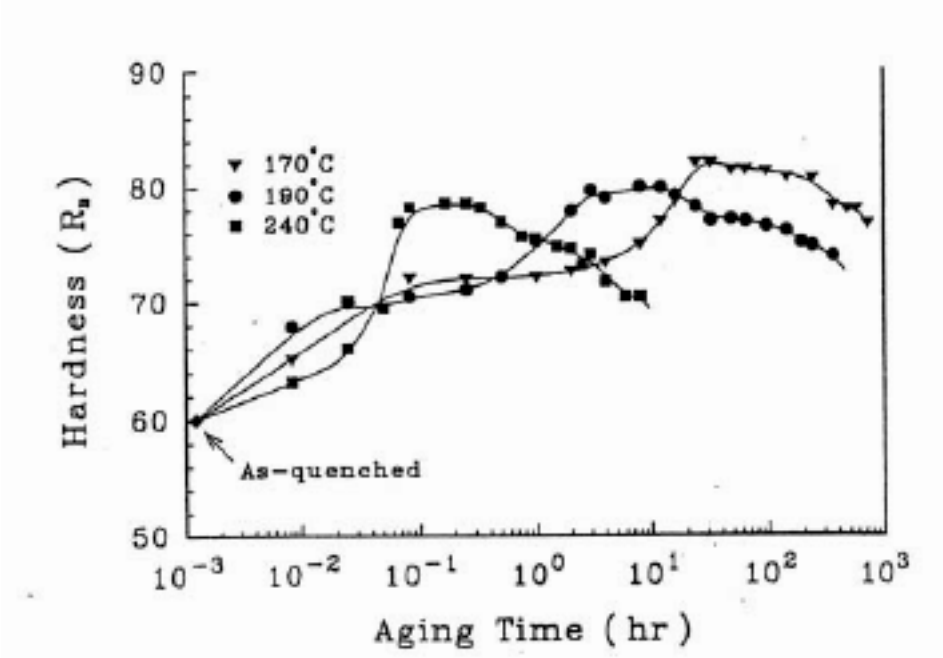

Figure 2.6 Rockwell B hardness a function of aging time at three holding aging temperatures for the stretched (1.5% preaging strain) specimens of AA2024 [90].

2.2 Corrosion of Aluminium and Its Alloys

Aluminium owes its excellent corrosion resistance to the barrier oxide film that is bonded to its surface very strongly. Even if the surface gets damaged, the film can reform very quickly in most environments, **Equation 2.1**:

$$2Al + 3H_2O \rightarrow Al_2O_3 + 6H^+ + 6e^- \qquad \textbf{Equation 2.1}$$

Freshly formed barrier oxide film can be as thin as 1 nm but is highly effective in protecting aluminium from corrosion. The oxide film formed on freshly rolled aluminium exposed to air is very thin and has been measured as 2.5 nm [5] though in most cases it varies between 1 to 5 nm [96, 97]. The inner layer of the oxide film is thinner and more compact than the outer layer which is thicker and more permeable. From the potential-pH diagram (i.e., Pourbaix Diagram) of aluminium in non-complexing aqueous solutions

(Figure 2.7) it can be seen that, the protective film is stable in aqueous solutions of the pH range 4.5-8.5 but dissolves in strong acids or alkalies leading to rapid attack of the aluminium. However, the limits of this range depend on the temperature and on the presence of soluble or insoluble salts that can form various complexes with aluminium [96-102].

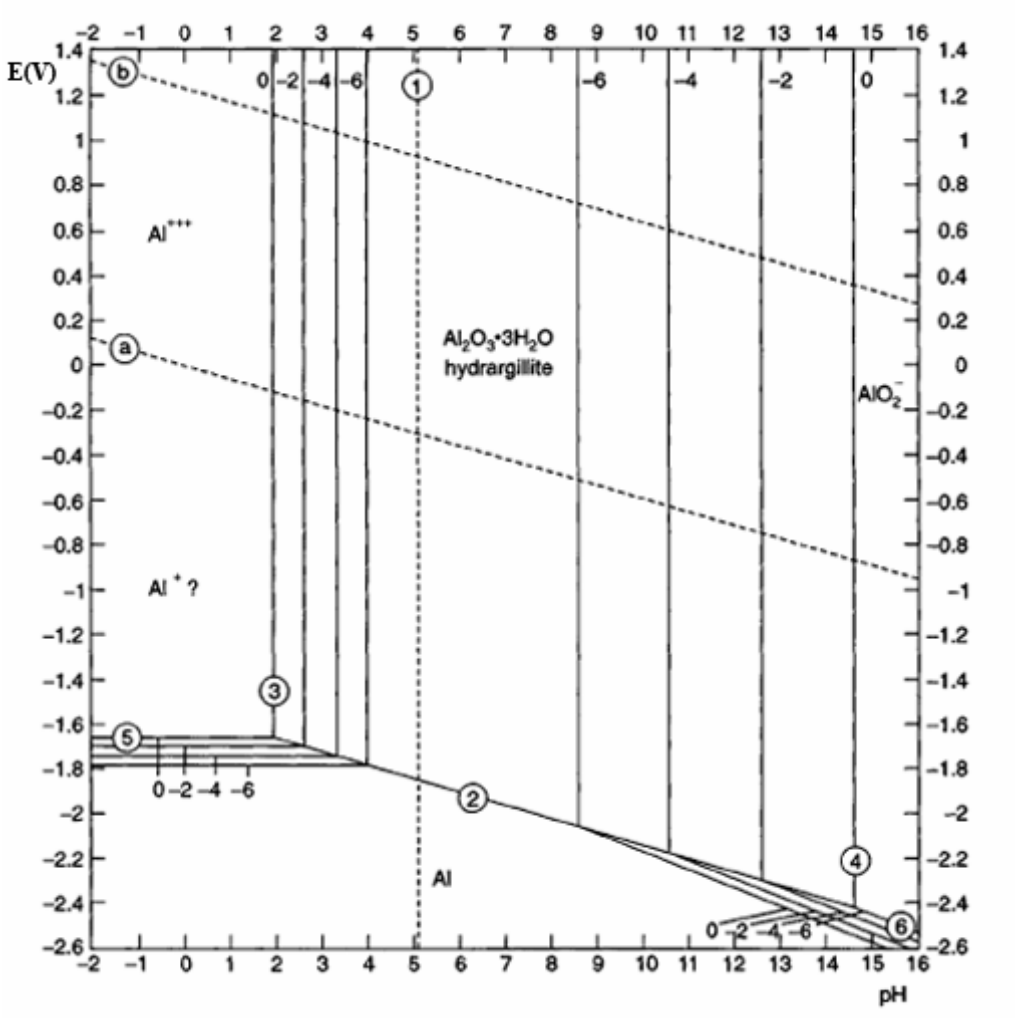

Figure 2.7 Potential-pH equilibrium diagram for the aluminium-water system at 25°C. Dotted line 'a' refers to the reaction $H_2 = 2H^+ + 2e^-$ and line 'b' refers to the reaction $2H_2O = O_2 + 4H^+ + 4e^-$. Water is stable between line 'a' and 'b'. Lines 1-6 represent the relative stability of different phases in aluminium-water system. Details of these reactions involved could be found elsewhere [98].

In acidic solutions, aluminium will dissolve as follows:

$$Al \rightarrow Al^{3+} + 3e^{-}$$ **Equation 2.2**

Whereas, in alkaline environments aluminium will dissolve by forming aluminate ions:

$$Al + 4OH^{-} \rightarrow Al(OH)_4^{-} + 3e^{-}$$ **Equation 2.3**

As stated earlier, the oxide film on aluminium is very soluble in strong alkali and acidic environment [98, 103]. In acidic environment the film dissolves by the following equation (**Equation 2.4**):

$$Al_2O_3 + 6H^{+} \rightarrow 2Al^{3+} + 3H_2O$$ **Equation 2.4**

In the alkaline solutions, the passive film will dissolve through (**Equation 2.5**):

$$Al_2O_3 + 3H_2O + 2OH^{-} \rightarrow 2Al(OH)_4^{-}$$ **Equation 2.5**

The surface oxide film is reported to consist of a composite type of Al_2O_3, $Al(OH)_3$ and AlO(OH), where the respective aluminium cation is bound to oxygen or oxygen containing species in different energies [104]. The structural characteristics of the oxide depend on the material composition, the presence and distribution of micro-defects (vacancies, voids etc.) as well as macro-defects (inclusions, second phase particles its size and shapes), crystal structure and the degree of noncrystalinity of the oxide [105].

2.2.1 Pitting Corrosion

Pitting is the most common form of localized corrosion of passive metals like aluminium and its alloys. Like other localized corrosion processes, pitting is also a multiple step process and generally gets aggravated in the presence of aggressive halide ions such as Cl^- and Br^- [97, 105-120]. Occurrence of pitting corrosion can be exceedingly destructive since pits can cause perforation of components and also can provide sites for cracks initiation.

2.2.1.1 Passive Film and Theories of Pit Initiation

Several fundamental mechanisms associated with different stages of localized corrosion have been extensively studied over the last few decades. During pitting corrosion of passive metals and alloys, local dissolution occurs leading to the formation of cavities within a passivated surface area [106]. The local breakdown of passivity of commercially available engineering materials, such as stainless steel and aluminium, occurs preferentially at sites of local heterogeneities, such as inclusions, second phase precipitates, solute segregated grain boundaries or even dislocations [112, 121]. Normally in aluminium alloys pitting is associated with the intermetallic/constituent particles [8, 47, 122, 123] and will be described in the following sections in detail.

In this current section the available theories for passive film breakdown mechanisms and pit initiation in pure aluminium without the presence of intermetallic particles in the matrix will be discussed. It should be noted that, the nature and type of the passive film associated with the matrix in an aluminium alloys could be similar to the passive film of pure aluminium (though in some cases the behaviour of the oxide film

may be modified by alloying additions [124]). Hence these theories could also be used to explain the interaction of chloride ions with the matrix in aluminium alloys. With the help such available theories, researchers [125] have tried to explain the chloride ion attack on the passive oxide film and resulting breakdown in the places of the intermetallic particles in an aluminium alloy.

Chemical or electrochemical behaviour of these pits largely depend on whether pit initiation is followed either by repassivation (metastable pitting) or stable pit growth [112]. Although pitting corrosion of passive metals and alloys is commonly observed in the presence of chloride or other halides, evidence of pitting corrosion in the absence of halides raises the question whether halides are always an essential requirements for pit initiation at all [110]. Initial studies on localized corrosion focused on treating the breakdown potential as a singular point associated with pit initiation. However, it is now clear that the breakdown potential is associated with pit propagation and stabilization [126, 127]. Recent researches have been focused on the metastable pitting phenomena prior to the stable pitting and it is accepted that metastable pitting plays a crucial role in better understanding the pitting of metals and alloys.

Based on numerous experimental investigations of the pitting process, several theories of pitting corrosion initiation involving the localized loss of the oxide protective properties have been developed in recent years. However in many cases, explanation of the experimental evidences are found to be contradictory to each other and thereby adding more ambiguities over the much debated issue of pit initiation. Some of these initiation theories/models are similar to each other and many are composed of elements taken from different ideas [18].

Different theories[3] for pit initiation can be summarized as follows [112, 114, 121, 128-135]:

Adsorption Theory

Anion Penetration and Migration Theories

Mechno-Chemical Model

Point Defect Model for Pit Initiation

Localized Acidification Theory

Chemical Dissolution Theories

Depassivation-Repassivation Theory

Though it is not easy to classify these theories precisely into a specific group of models, the most commonly used pit initiation theories can be grouped into three main mechanisms: penetration mechanisms, adsorption mechanisms and film breaking mechanisms [112, 120, 136]. It should be noted that, most of the above mentioned theories deal with the breakdown of passive films on pure aluminium or pure metal systems rather than on aluminium alloys or real alloys where pitting is typically associated with the existence of intermetallic particles (or inclusions) as will be described in the following section.

Penetration mechanisms for pit initiation involve the transport of the aggressive anions through the passive film to the metal/oxide interface where aggressive dissolution is promoted. Adsorption theories of initiation were based on the notion of competitive adsorption of chloride ions and oxygen. Pit initiation by film-breaking mechanisms

[3] A detailed overview of these theories is presented in Appendix A.

considers that the thin passive film is in a continual state of breakdown and repair. These mechanisms are schematically represented in Figure 2.8. Mechanical stresses at weak sites or flaws may cause the local breakdown of the passive films, which then rapidly heal in nonaggressive environments [18, 112, 137].

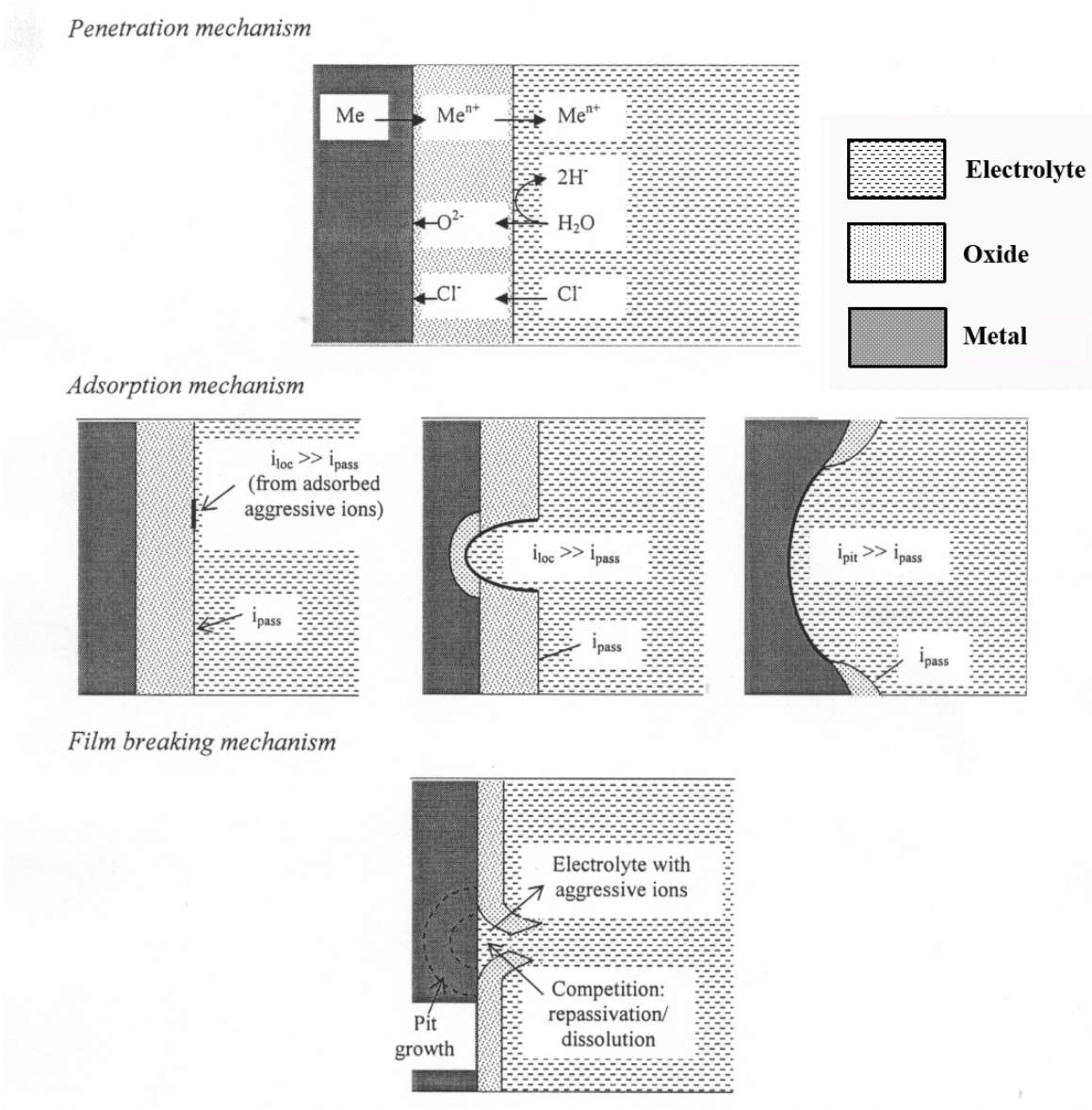

Figure 2.8 Schematic diagrams representing different pit initiation mechanisms [112]. Penetration mechanism involves the transport of the aggressive ions through the passive film, adsorption mechanism deals with the competitive adsorption of chloride ions and oxygen, whereas film breaking mechanism considers continual breakdown and repair of the thin passive film.

It has to be noted that none of these pit initiation theories are totally complete or globally accepted as none of them fully explain all the observed phenomenology of pit initiation such as induction time, transition from metastable to stable pits, potential dependence, randomness of attack etc.

Foley [107, 110, 138, 139] was among the earliest to describe the localized corrosion of aluminium as a sequence of steps - adsorption of the reactive anion on the oxide film, chemical reaction between the adsorbed anion with the oxide film, thinning of the oxide film by dissolution, and direct attack of the exposed metal by the anion. The last step is sometimes called as pit propagation stage.

In a recent review, McCafferty [120] tried to describe the sequence of steps in the pitting corrosion of aluminium slight differently than that discussed by Foley. McCafferty also thoroughly reviewed the experimental evidences as shown by several researchers in support of different individual stages involved in the pitting corrosion of aluminium. Adsorption of Cl^- ions on passive films of aluminium at the open circuit potential as well as at applied anodic potential has been revealed by several analytical techniques such as SIMS [140] , radiotracer technique [118, 141, 142], X-ray absorption spectroscopy [143, 144], Auger spectroscopy and X-ray photoelectron spectroscopy [141-146]. The structure of the oxide film and the role of Cl^- species in pitting corrosion has also been studied extensively [147, 148]. However, the adsorption of the aggressive anions on the metal surface is nonuniform because of the existence of heterogeneity on the surface due to imperfections or flaws in the oxide film which can act as a place for preferential anion adsorption [137, 149].

Chemical reactions between the adsorbed species and the oxide film in the second step have resulted in the formation of intermediate soluble complexes such as $AlCl^{++}$, $AlCl_4^-$, $Al(OH)Cl_2$ and $Al(OH)_2Cl$ [150, 151]. Galvele *et al.* [152] found a logarithmic

dependence of the pitting potential on chloride concentration, **Equation 2.6**, (where E_p is defined as the pitting potential) which was later supported by Stirrup *et al.* [150] and McCafferty [153].

$$E_p = E_p^{\,0} - B.\log[Cl^-] \qquad \textbf{Equation 2.6}$$

The mechanisms behind the thinning of the protective oxide film (described as the third step in pitting corrosion) have been a subject of debate over the years and the exact mechanism by which chloride ions penetrate the oxide film is not well understood. It has been assumed that chloride ions can diffuse through the oxide lattice, and several theories have been put to support this [112, 120, 153-156]. It is also believed that chloride ion penetration can occur by the formation of soluble compounds or transitory species at critical sites [110, 157].

The fourth step in the localized corrosion process is sometimes referred to as pit propagation. Proposed models/mechanisms for pit propagation will be discussed later in detail.

2.2.1.2 Metastable Pitting

Although the distinct definition of the stages of pitting have been a subject of controversy for a long time, it has been more or less agreed that when exposed to chloride environment aluminium alloys exhibit both metastable and stable pitting by undergoing some form of passive film breakdown, metastable pitting and then passivation or finally stable pit growth [112, 158, 159]. Metastable pits are pits that initiate and grow for a

limited period before repassivating. The resulting current transients due to metastable pitting (see Figure 2.9c) differ widely with respect to the peak current height as well as the lifetime. Sizes of the metastable pits are typically in the range of microns to sub microns and the lifetimes are normally in the order of seconds. Metastable pitting can be found much below (i.e., more negative in potential) the pitting potential which is generally associated with the initiation of the stable pit, see Figure 2.9 [134]. It is also reported in recent investigations that the metastable pitting events could possibly be correlated (i.e., one metastable pitting event will enhance the likelihood of subsequent events) [160, 161].

Metastable pitting of stainless steel has been well studied whereas very few studies have been performed on metastable pitting of aluminium and aluminium alloys. Researchers have observed transients in both stainless steels and aluminium alloys, but the origin of those transients, their behaviour as a function of metallurgical and electrochemical variations, the reasons behind the repassivation of the metastable pits, the controlling factor for the metastable pit growth (ohmic controlled vs. mass transfer controlled), and the relation between metastable pitting and stable pit growth has not been fully understood, as yet, and still remains a subject of much debate [158, 162-166].

Recently Pride *et al.* [134, 167] studied the metastable pitting of pure aluminium and Al-4Cu alloy in detail. Critical potentials seems not to be the complete means of describing pitting corrosion of aluminium and its alloys as metastable pitting has been found at potentials much below[4] both pitting and potentiodynamically determined repassivation potential. In case of Al-Cu alloys, metastable pits are believed to initiate due to the galvanic coupling between the intermetallic particles and the grain boundaries.

[4] Here 'below' refers to a potential which is higher than the open circuit potential, but lower than the pitting potential in the anodic domain.

A metastable pit could repassivate and die because of the limited supporting cathodic current or dilution of the concentrated pit environment. However, if, via hydrolysis, the pH within the pit reaches such a lower value that aluminium oxide formation becomes unfavourable, the pit can no longer passivate and become a stable pit [158].

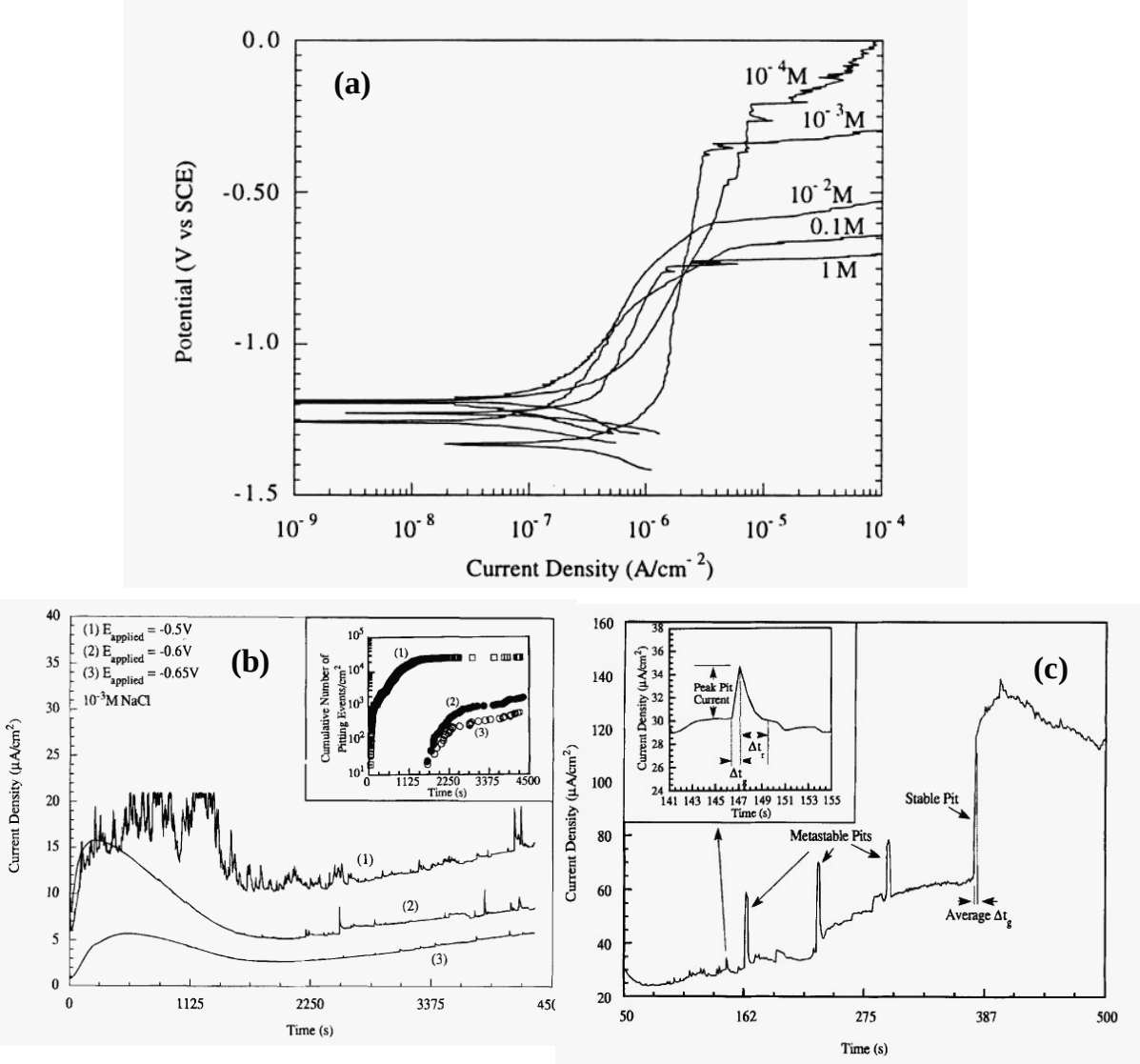

Figure 2.9 Typical potentiodynamic scans and time series of high purity aluminium in deaerated NaCl solutions at different concentrations. (a) anodic Polarization, (b) time series showing effect of potential on anodic current spikes associated with metastable pitting in deaerated 10^{-3} NaCl solution, and (c) time series showing the transition from metastable pitting to the formation of a stable pit in deaerated 10^{-3} NaCl solution at -0.05 V [134].

Galvele and De Micheli [152] found a clear relationship between pitting and intergranular corrosion. It was believed that localized galvanic coupling between the anodic phases (Cu-depleted zone) and cathodic phases (intermetallic particles) leads to the formation of metastable pits and intergranular corrosion. Galvele found that at potentials below the critical pitting potential, the number of metastable activities per unit time increases as the potential increases. Trueman [158] argued that the alloying constituents in aluminium alloy may have an effect upon the type, frequency and location of flaws within the oxide that result in metastable pits, but not on their occurrence. The transition from metastable to stable pitting would be expected to occur in a similar manner to pure aluminium.

Although metastable pitting is not usually considered a real corrosion risk from an engineering point of view, studies of metastable pitting as a precursor to stable pitting may provide valuable insights into fundamental aspects of pitting corrosion [106]. It is well accepted that pit initiation as well as the transformation of metastable into stable pits are key factors in localized corrosion process,

2.2.1.2.1 Transition from Metastable Pit to Stable Pitting

Modelling of corrosion of aluminium alloys has become a subject of great interest to the aircraft manufacturers and maintainers as it potentially offers significant cost savings by more accurate determination of reduced component lifetimes due to corrosion damage. Thus for any kind of pitting corrosion model, the probability of stable pit formation in a particular environment is an important and essential input. One of the critical issues in the metastable pit studies are the transition process of metastable pits to the stable pits and the electrochemical factors that influence this transition. Several

researchers have tried to come up with a relationship that will predict the transition of metastable pit to stable pit based on the pit current and the pit size. Williams *et al.* [126] have established such a criterion of pit stabilization for stainless steel. According to Williams, I_{pit}/r_{pit} must exceed 4×10^{-2} A/cm for stable growth (where I_{pit} is the current within the pit, and r_{pit} is the radius of the pit). Below this value metastable pit are formed. Similarly, Galvele [114] determined that stable pit growth would occur at $x.i \geq 10^{-2}$ A/cm, where x is the pit depth and i is the pit current density. Pride [134] carried out extensive studies on the metastable pitting of pure aluminium and Al-Cu alloys. He established a similar kind of criterion for pit stabilization in aluminium alloys. Pride *et al.* [167] found that the apparent metastable pit current density is ~ 0.1 to 10 A/cm^2 and the apparent metastable pit radius is ~ 0.1 to 6 μm. Metastable pits on pure aluminium increase with an increase of the anodic potential at a constant concentration of chlorides, and with increasing concentration of chloride at a constant potential. It was found that, as the potential is increased, the metastable peak pit currents and apparent pit radii at peak pit current both increase towards $I_{pit}/r_{pit} = 10^{-2}$ A/cm. Instantaneous growth of stable pits maintains I_{pit}/r_{pit} greater than 10^{-2} A/cm throughout, whereas metastable pits never achieve this critical ratio during their growth. Pride [134] also tried to develop a new analytical method called the Statistical Pit parameter (SPP) which is based on the criteria that pit stabilization occurs when $I_{pit}/r_{pit} \geq 10^{-2}$ A/cm.

As an input parameter for the pitting corrosion model and to determine the probability of stable pit formation in a particular environment, the information about the thermodynamics of pitting corrosion as measured by the pitting potential, as well as information about the kinetics of pitting corrosion is needed. In a recent study Trueman [158] claimed that to date no electrochemical methods are available to determine the kinetics of the initiation of corrosion pits on aluminium alloys or other passive metals.

This led to an effort to develop a method of determining the stable pit initiation kinetics (SPIK) on aluminium and its alloys. For determining the probability of the transition from a metastable pit to a stable pit, the statistics of the occurrence of metastable pits of given volume as a function of time was obtained. Trueman argued that the pit stability criteria used by Galvele [114] and Pride [167] (i.e., $x.i \geq 10^{-2}$ A/cm) does not hold in all conditions as these models assume a simplistic cylindrical shape of the pit where only bottom of the cylinder is corroding and took no account of pit caps and their effects on diffusion.

In a heterogeneous alloy like AA2024-T3, the growth of the metastable pits may depend on several factors including the locality of intermetallic cathodic sites and ohmic drops related to those metastable pits. Using statistical analysis to find distribution parameters Trueman [158] showed that it is possible to calculate the largest expected pit and the probability of a metastable pit of a given size forming within a given time period. It is also statistically possible to determine the probability of a metastable pit that will develop into a stable pit. However it has to be taken into account that it is extremely difficult to determine the transition size from metastable to stable pitting as the stable pit continues to grow. Using optical method and potentiostatic current transient techniques Trueman [158] concluded that the metastable pit size to transition into stable pit was 20 μC, equivalent to a 13.7 μm diameter of hemispherical pit. These estimates are similar to those found by Pride *et al.* [167] in aluminium.

2.2.1.3 Pitting Corrosion of Aluminium Alloy 2024

Pure aluminium is too soft for most of the engineering application and hence it is alloyed with metals like copper, or zinc to strengthen it. Copper in solid solution increases

the corrosion resistance of the alloy by decreasing the rate of active dissolution [168]. Unfortunately when intermetallic particles enriched with copper form during solidification or copper rich precipitate form during heat treatment, the areas adjacent to the particles get depleted with copper and thereby the corrosion resistance of those areas decreased. Moreover, pitting corrosion could occur in those copper depleted zones. It is also found that microsegregation of impurities such as Fe could also increase the tendency for pitting at open circuit [168].

Passive films on intermetallic particles are more conductive and thinner than the passive film on the matrix. This makes electron transfer easier through the film on the intermetallic particles and they serve as a place for cathodic reaction [46, 48, 169, 170]. It has to be remembered that corrosion of aluminium alloys is frequently limited by the cathodic reaction which is typically oxygen reduction [97, 171-174], **Equation 2.7**.

$$O_2 + 2H_2O + 4e^- \rightarrow 4OH^- \qquad \textbf{Equation 2.7}$$

On the matrix of commercial alloys, the cathodic reaction is limited by the transport of electrons across the insulating oxide film [105, 172, 175] as shown in Figure 2.10.

Dissolution of aluminium and magnesium from the intermetallic particles will leave behind copper which will then act as an efficient cathode to increasing the local pH as a result of oxygen reduction. This change in local pH will lead to the grooving adjacent to the cathodic intermetallic particles (see Figure 2.10).

Some author [48] argued that these grooves/cavities may switch to an acid-pitting mechanism at later stages. Whereas other researchers refer to the alkaline attack itself as

pitting [11, 170] or tried to describe the grooving phenomena as galvanic corrosion between particle and matrix [9]. These theories will be described in details later in Section 2.2.1.3.1.

Thinning down of the protective oxide film exposes the highly reactive metallic aluminium which ensures rapid attack and pit propagation (see Figure 2.10). The basic difference of the propagation step from the initiation step is that the initiation step involves chemical or physical interaction of the oxide film with the solution environment, whereas the growth of the pit involves the interaction of aluminium metal directly with an environment that is changing as the reaction proceeds.

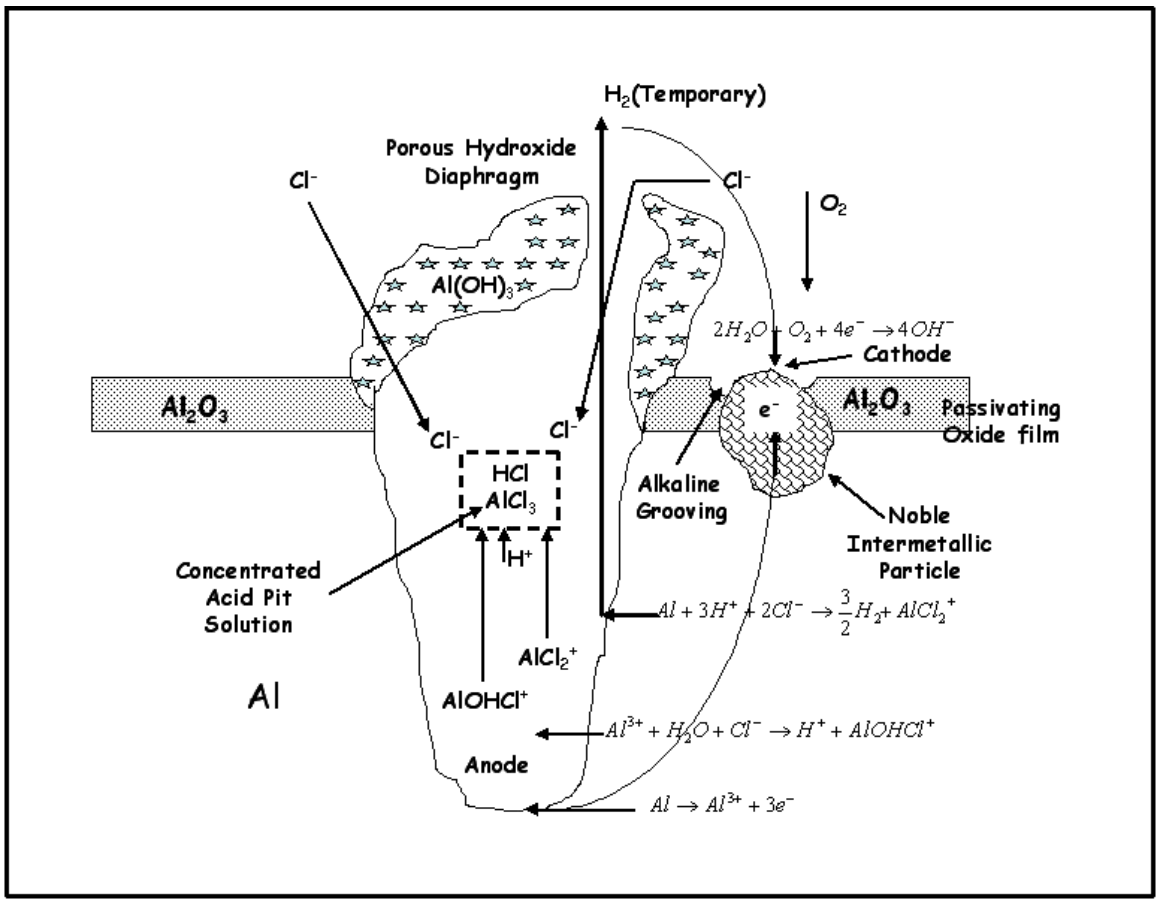

Figure 2.10 Schematic illustration of aluminium alloy corrosion along with the mechanism of pit propagation in chloride solution (adapted from ref. [103, 110]).

Pit growth is a self propagating or autocatalytic process [111, 112, 176-178]. Once the oxide film is sufficiently thin, chloride ions will directly attack the matrix and rapid dissolution of aluminium will occur, **Equation 2.2**. Copious anodic production of positively charged Al^{3+} attracts negative anions (e.g., Cl^-) to the initiation site for maintaining the charge neutrality. Hydrolysis of Al^{3+} by produces local pH reductions at the initiation sites, **Equation 2.8**.

$$Al^{3+} + H_2O + Cl^- \rightarrow H^+ + AlOHCl^+ \qquad \textbf{Equation 2.8}$$

The acid chloride solution further accelerates anodic dissolution, which in turn further concentrates chloride inside the pit. The combination of high chloride content and low pH makes the environment inside the pit very aggressive which will favour continued dissolution over repassivation and the pit will continue to grow. Chloride ions migrate into the pit to form aluminium chloride ($AlCl_3$) which dissolves in the solution. Because of the low pH, the aluminium alloy may also corrode with the evolution of hydrogen, **Equation 2.9**.

$$2Al + 6H^+ \rightarrow 2Al^{3+} + 3H_2 \qquad \textbf{Equation 2.9}$$

However, to stabilize a pit and continue its growth, a pit needs to maintain a very high concentration of cations which largely depends on the balance between the cations produced by the dissolution reaction and migration of cations from the pit (i.e., the production rate of cations must be higher than their escape rate from the pit) [121, 169, 176]. At the same time, the high specific gravity of the corrosion products causes leakage

out of the pit in the direction of gravity, inducing breakdown of passivity wherever the products come into contact with the alloy surface [178]. This accounts for the shape of pits elongated in the direction of gravity, as is often observed in practice. Frankel [112] has argued that under mass transfer limited growth, pits will be hemispherical with polished surfaces. But at lower potentials, in the absence of salt films, pits could be crystallographically etched or irregularly shaped. Cathodic reduction of a dissolved oxidiser such as oxygen consumes the electrons liberated by the anodic pit reaction.

In an aluminium alloy, the galvanic coupling between particles and the matrix could be an important growth contributor [11, 175, 179, 180]. The spacing between the intermetallic particles inducing pitting at the surface and the subsurface particles sometime play crucial role in determining the propagation rate. Pit could initiate and then cease if the spacing is too great [11, 175, 179]. Shallow pits were found to be associated with isolated intermetallic particles, whereas severe pitting was observed to be associated with particle clusters, Figure 2.11 [11, 179].

2.2.1.3.1 Role of Various Intermetallics in Localized Corrosion

As described in Section 2.1.1.1, two predominant categories of constituent intermetallic particles have been distinguished on the surface of aluminium alloy 2024. The first type appeared as round and smooth with size range of 1-5 μm and they are identified as Al_2CuMg (‘S’ phase). In very few cases these ‘S’ phase particles appeared to be as big as 10 μm in diameter. Second type of particle (consists of Al-Cu-Fe-Mn) is in the range of 10 to 30 μm with a rectangular or elongated shape and identified with the composition of $Al_6(CuFeMn)$ or other stoichiometric relationship [commonly referred as ‘Fe-Mn’ particle/Fe-rich intermetallic particle].

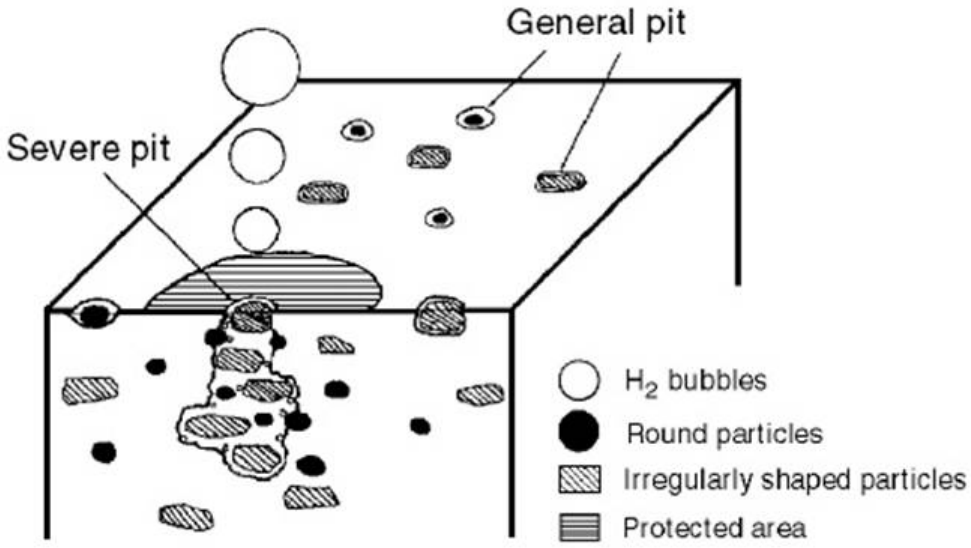

Figure 2.11 Conceptual model for particle induced pitting corrosion [11]. General pitting is observed on the isolated surface particles which are far away from their nearest subsurface particles. Severe pitting develops at subsurface particle cluster.

Normally pitting in aluminium alloys is associated with these intermetallic/constituent particles. However the mechanism of pit initiation is not fully understood in this context. The role of different intermetallic particles on corrosion of aluminium alloys have been investigated by different researchers in the last few decades [8-11, 14, 15, 37, 38, 40, 42, 47, 48, 82, 123, 171, 173, 175, 181-197]. The reactivity of the intermetallic particles as well as the pit morphologies induced by them have been investigated by several techniques such as confocal laser scanning microscopy [37, 38], fluorescence microscopy and near field scanning optical microscopy [174, 195, 196, 198-200], micro-capillary electrochemical cell technique [39-42], scanning electron microscope with EDX [7-9, 11, 19], scanning Kelvin probe force microscopy [43, 44], and AFM [45-48]. Buchheit *et al.* [9] performed detailed analysis to identify the intermetallic particles present in 2024-T3 alloy and kind of roles they play during corrosion. Results indicate that approximately 60% of the particles in the size range greater than 0.5 to 0.7 μm, are Al_2CuMg ('S' phase). This fraction corresponds to 2.7% of

the total surface area. $Al_6(CuFeMn)$ ['Fe-Mn' particles] intermetallic were revealed as the second most frequent type constituting about 12% of all intermetallic particles. It is also believed that an inhomogeneous distribution of Cu in AA2024-T3 associated with intermetallic particles results in galvanic cells that lead to localized attack [9].

The role of intermetallic constituent particles is often described in terms of their galvanic relationships with the surrounding matrix phase, solute-depleted zones, and other intermetallic particles as it is speculated that intermetallic compounds are associated with the formation of a solute depleted zones around them [15, 18, 123]. The corrosion potentials of different intermetallic particles have been measured on simulated, synthesized bulk alloys to have a better understanding of the importance of the intermetallic particles as initiation sites for corrosion [15, 201, 202]. Corrosion potentials of different phases present in Al-Cu-Mg alloy has been compiled by Buchheit [14, 191]. These measurements on bulk intermetallic samples indicate the relative nobility of the two main types of particles in AA2024-T3; Fe-Mn particles should be more noble relative to the Al matrix, whereas 'S' phase particles should be more active [191]. Researchers [203] argued that as all intermetallic particles except 'S' phases are composed of metals nobler than aluminium, they should show cathodic character. The 'S' phase particles not only contain nobler copper, but they also contain active magnesium which might trigger the initial anodic behaviour of the 'S' phase particles. Corrosion potentials of metals, alloys and intermetallic compounds relevant to localized corrosion of Al-Cu-Mg alloys are summarized in Table 2.2. Lower corrosion potential indicates the anodic nature of a material, whereas the cathodic (more noble) nature of a material is characterized by a higher corrosion potential.

2.2.1.3.1.1 The ‘Fe-Mn’ Particles

It is believed that Fe-Mn intermetallic particles act as cathode during the corrosion process [8, 11]. Unlike the ‘S’ phase particles, Fe-Mn particles do not show selective dissolution, though pitting sometime occurs at their periphery [7, 8, 11, 175, 186, 187]. This is in agreement with the literature where it was shown that Fe-Mn particles could have a nobler corrosion potential than the matrix [191, 204]. The cathodic nature of these Fe-Mn particles were indicated by the Cu deposition/replating as observed by Chen *et al.* [8] and later supported by Liao *et al.* [11]. In some cases attack on Fe-Mn particles had been observed due to their heterogeneous nature [43, 44].

Seegmiller *et al.* [187] found that both Cu-rich and Fe-rich intermetallic particles act as cathodes for O_2 reduction with similar efficiency during investigations using a wall-jet flow cell. Results indicate the possibility of inhibiting cathodic corrosion by buffering the solution which in turn prevents the matrix dissolution and consequent activation of the surface. In contrast, Shao *et al.* [12], using microreference electrode technique, concluded that the pitting attack around these Al-Cu-Fe-Mn particles is less severe than around Cu-rich particles and these particles are less effective cathodes.

The effect of bulk solution pH on the intermetallics corrosion and their morphology was studied by Kolics *et al.* [193]. In an acidic solution, Al_6(Cu,Fe,Mn) particles did not show any significant sign of attack or morphological changes. These particles behaved slightly more active in neutral solution and produced some dissolution zone around the particles. When the solution was alkaline, Al_6(Cu,Fe,Mn) particles showed a smooth surface morphology with enrichment of Cu and Mn.

Table 2.2 Corrosion potentials for metals, alloys, and intermetallic compounds relevant to localized corrosion of Al-Cu-Mg alloys.

Material	E_{corr} (V_{SCE})	Environment	Aeration	Reference
Al_2CuMg	-0.88	1 M NaCl (pH 5.6)	N_2 sparged	[14]
Al_2CuMg	-0.91	53g/L NaCl + 3g/L H_2O_2	Open to air	[14, 18, 191]
Al_2CuMg	-0.93	0.5 M NaCl	Open to air	[14]
Al_2CuMg	-0.93	0.5 M NaCl	Air sparged	[14]
Al_2CuMg	-0.93	0.5 M NaCl	N_2 sparged	[14, 18]
Al_2CuMg	-0.850	0.005 M NaCl + 0.1 M Na_2SO_4	Open to air	[37, 204]
Al_2Cu	-0.44	53g/L NaCl + 3g/L H_2O_2	Open to air	[18, 191]
Al_2Cu	-0.59	1 M NaCl	N_2 sparged	[191, 205]
Al_2Cu	-0.70	0.5 M NaCl	Open to air	[18, 191, 206]
Al_2Cu	-0.621	3% NaCl	Not stated	[18, 191]
Al_2Cu	-0.400	0.005 M NaCl + 0.1 M Na_2SO_4	Open to air	[37, 204]
$Al_{20}Cu_2(MnFe)_3$	-0.340	0.005 M NaCl + 0.1 M Na_2SO_4	Open to air	[37, 204]
99.999% Al	-0.84	0.6 M NaCl	Air sparged	[14, 207]
99.999% Al	-1.01	0.6 M NaCl	Ar sparged	[14, 207]
99.998% Al	-1.07	0.005 M NaCl + 0.1 M Na_2SO_4	Open to air	[37, 204]
Mg	-1.64	53g/L NaCl + 3g/L H_2O_2	Open to air	[14]
Cu	+0.20	0.2 M NaCl	Not Stated	[14]
Cu	-0.11	53g/L NaCl + 3g/L H_2O_2	Open to air	[14]
99.999% Cu	-0.100	0.005 M NaCl + 0.1 M Na_2SO_4	Open to air	[37, 204]
Al-4Cu (Solid Solution)	-0.60	53g/L NaCl + 3g/L H_2O_2	Open to air	[14]

Liao *et al.* [179] carried out a galvanic coupling study of model alloys with pure aluminium. Results suggest that pitting corrosion is induced by the galvanic interaction between the particle-matrix couple, with the particles promoting matrix dissolution. It can be concluded from their study that the galvanic coupling is responsible not only for the nucleation but also the growth of pits.

Localized corrosion of aluminium alloys associated with the intermetallic particles was also explained by a cathodic trenching phenomena which was originally introduced by Nisancioglu *et al.* [208]. The oxygen reduction reaction occurs on these particles as they behave cathodically towards the matrix. Moreover, the oxygen reduction reaction on the particles will increase the pH locally, thereby dissolving the matrix adjacent to them as the oxide film is not protective in an environment of high pH (Figure 2.10). These types of trenching formation between the matrix and the intermetallic particle has been extensively discussed in the literature [8, 40, 43, 47, 48, 171, 175, 186, 198, 209].

Figure 2.12 shows examples of trench formation from the morphological studies of the corrosion attack on the intermetallic particles of AA2024-T3 using in situ confocal laser scanning microscopy [38]. Trenching was found in both alkaline and acidic solution. After 18h of exposure, the width and depth of the trench was found to be only approximately 0.5-1 μm and 1.3-2.3 μm, respectively. Although these studies led to the development of a cathodic model, the actual mechanism behind the trench formation remains unclear.

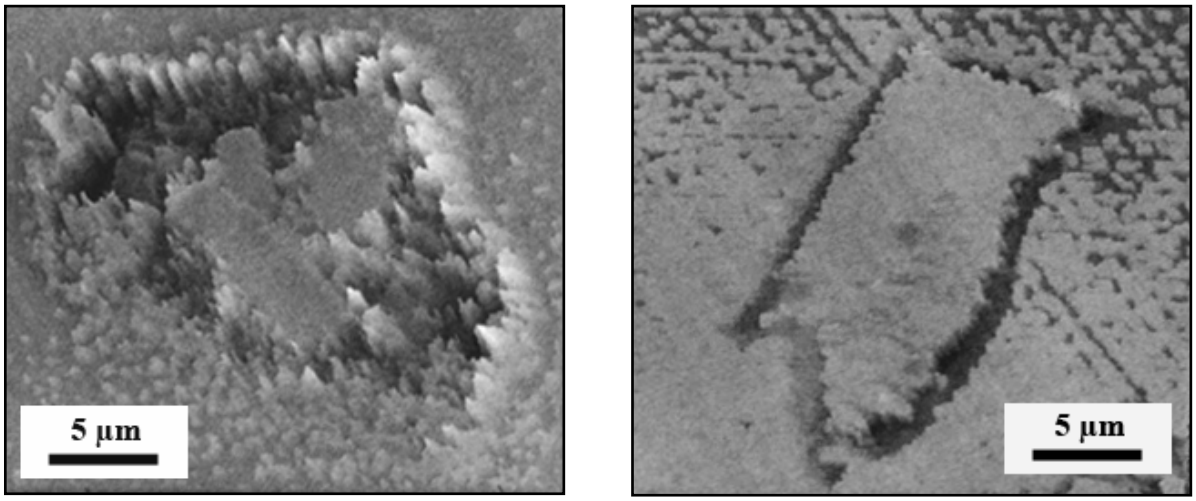

(a) **(b)**

Figure 2.12 Trench formation in (a) alkaline solution, pH 10 after 9h of immersion; (b) acidic solution, pH 3 after 18h of immersion. Electrolyte: 0.1 M Na_2SO4 + 0.005 M Cl^- adjusted to different pH [38].

Rynders *et al.* [47] used in situ atomic force microscopy (AFM) to study the trench formation near the iron rich inclusions in AA6061-T6 immersed in 0.6 M NaCl solution. The shape evolution of the trenches around iron rich intermetallic particles was investigated in both open circuit condition and under cathodic overpotential. Though this study has been done in AA6061 and on Al_3Fe intermetallic particles but the same analogy can be extended to the Fe-Mn particles in AA2024-T3 which are also cathodic in nature. Figure 2.13 presents a series of AFM images of an iron rich intermetallic particle (i.e., Al_3Fe) over a period of 24 hours of exposure in 0.6 M NaCl. Rynders *et al.* [47] observed that initial trenching around the particles could be non uniform and is normally observed in the regions where the ratio of intermetallic particles to host matrix surface area was high. Once the trench was formed around the particle, dissolution of the surrounding matrix was uniform and proceeded radially outward from the inclusion edge. The radial size of the trench was an order of magnitude greater than the trench depth. It was also

found that a trench was formed around the intermetallic particle that grew to form circular attack.

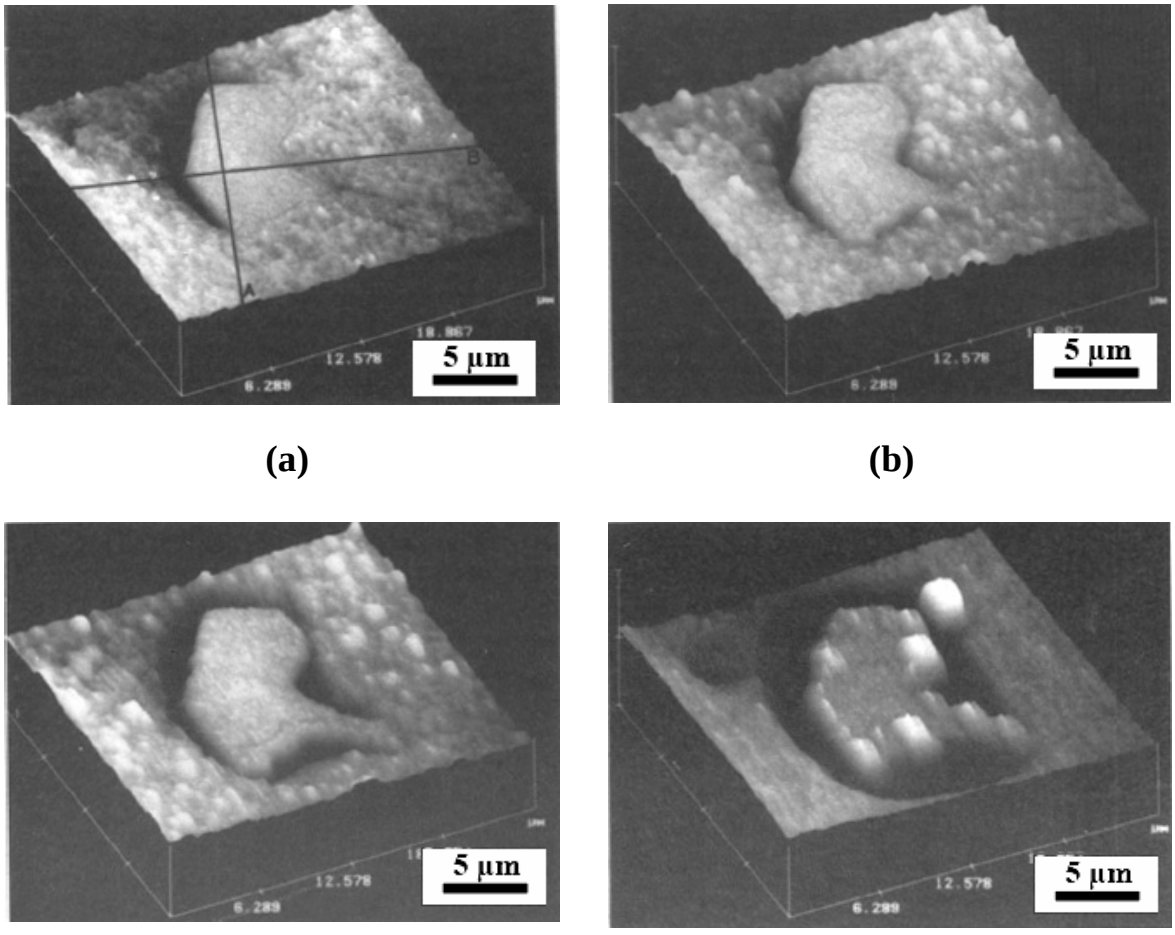

Figure 2.13 AFM images of an iron rich inclusion of AA6061-T6 (a) in air and (b) in situ exposure to 0.6 M NaCl at the open circuit potential for 1 h, (c) 2h, and (d) 24 h [47].

Rynders *et al.* [47] tried to explain the mechanism of shape evolution of the initial non uniform trenches around the particles based on the size and shape of the inclusions, local accumulation of hydroxide, and rate of oxygen transport. For example, in Figure 2.13c, the rate of oxygen transport to the inclusion tip which extends to the bottom right, would be higher than the rate of transport into the two "side pockets" on either side of the inclusion peninsula. As a result generation of hydroxide would be more at the tip than in

the side pockets. However, as the diffusion at the tip is faster, hydroxide accumulation at the tip would be lower than in the side pockets where diffusion is restricted. As a result in those restricted areas, local pH would increase to such a level where the oxide film is no longer stable.

Rynder's group extended their investigations to understand the role of Fe-rich intermetallics in the corrosion process of AA6061 using scanning pH microelectrodes [48]. The evolution of local environment around the intermetallic particles was investigated and presence of an alkaline region was confirmed. From this investigation, it was evident that the local alkalinity around the intermetallics causes breakdown of the passive film around the intermetallics. At the start of exposure, the dissolution process around the intermetallic particles is independent of the size of the particles, but in the later stages, they become very much dependent on the size of the particles. AFM studies of AA6061 immersed in buffered aerated 0.6 M NaCl solution (pH 5.5) did not show any evidence of dissolution of the aluminium alloy matrix around the intermetallic particles. These measurements indicate that Al_3Fe particles in AA6061 serve as local cathodes and a high pH develops around the intermetallic particles and creates cavities in the alloy matrix.

Park *et al.* [48] proposed a model mechanism (for Al_3Fe intermetallic particles in AA6061) to explain how the interactions among a cluster of intermetallic particles supporting cathodic reactions causes a large number of slowly dissolving alkaline cavities to evolve and coalesce into a small number of rapidly dissolving acidic pits (Figure 2.14). As this proposed mechanism involves the increase in local alkalinity in the vicinity of intermetallic particles which are cathodic in nature and to some extent depends on the size and shape of the intermetallic particles, this theory could also potentially be applicable to Fe-Mn phases in AA2024. As discussed earlier, during initial time period following

immersion, the intermetallic particles support the cathodic oxygen reduction reaction which results in an alkaline environment around the particle as shown in Figure 2.14a. An increase in the pH would destabilize the passive film and the aluminium matrix around the particle would dissolve (Figure 2.14b). Due to the fact that size and shape of the intermetallic particles influence the local dissolution, so at some places local dissolution would be faster than at others. This would result in generation of more Al^{3+} than it could be neutralized by OH^- produced on the surface of the intermetallic particle. It is also possible that dissolution of aluminium can occur faster than the precipitation of $Al(OH)_3$ as it is well known that hydrolysis of Al^{3+} to form $Al(OH)_3$ proceed slowly. Under these circumstances the dissolved aluminium ions would generate local acidity in the occluded regions, as indicated in two of the cavities shown in Figure 2.14c. With the increase in the acidity, the rate of local dissolution will increase and to support this increased local dissolution rate, nearby intermetallic particles would start to act as local cathodes and their anodic dissolution would cease. Therefore, after some time, a small number of intermetallic particles would have anodic regions that are dissolving more rapidly and thereby cathodically protecting the rest of the inclusions. Finally anodic regions begin to compete with one other and extend dissolution. This type of extended dissolution caused evolution of shape as shown in Figure 2.14d. It can be seen that two intermetallic particles have become undercut by dissolution and have fallen out. At the centre of Figure 2.14d, it is indicated that detachment of the inclusion did not change the acidic region and dissolution continued further. Such cavities thus take on characteristic features of pitting corrosion.

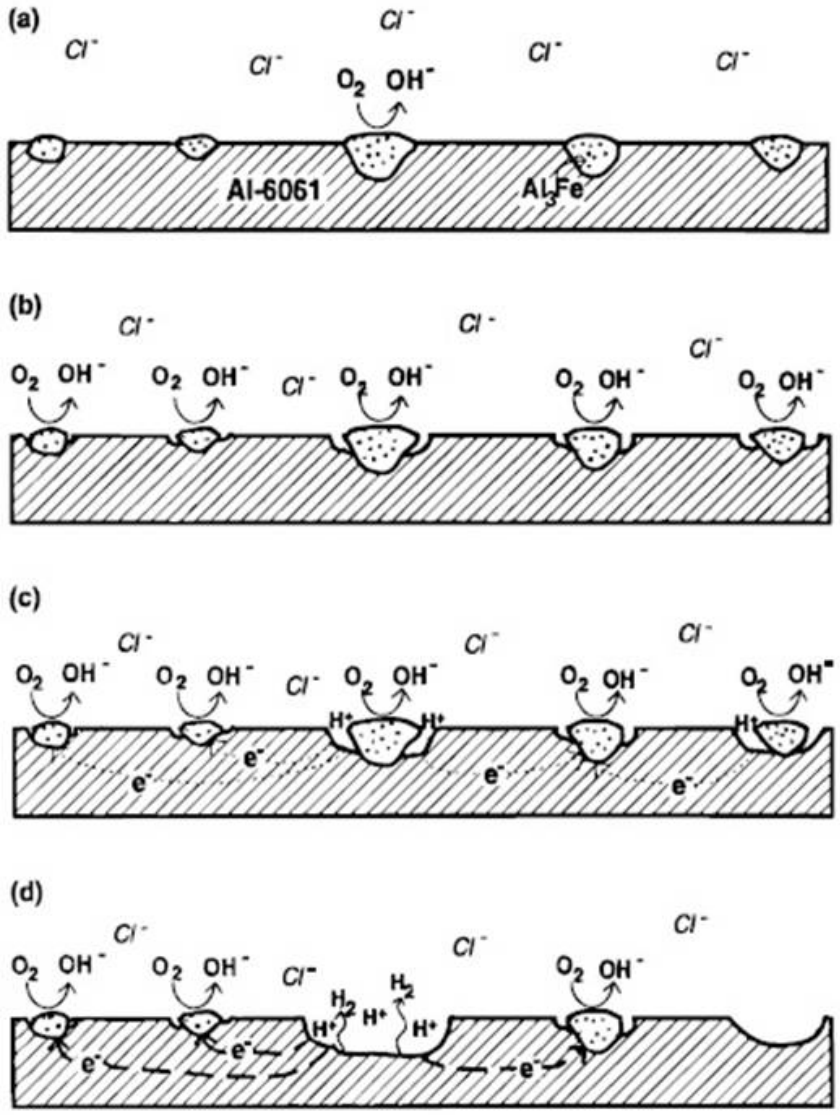

Figure 2.14 (a)-(d) Schematic representation of initial stages of pit initiation around iron rich intermetallics during 2-3 h of immersion into aerated NaCl solution [48].

In the alkaline model (i.e., cathodic trenching phenomena) the main reason for trenching is thought to be the increase in the local pH [208]. But this model is not efficient enough to rationalize trenching at low pH and also it does not properly explain different trenching phenomena associated with different types of particles. In order to resolve the discrepancy, Schneider *et al.* [38] developed an alternative anodic trenching

model based on the assumption that the galvanic coupling between the matrix and the particles cause preferential breakdown or enhanced passive dissolution.

Formation of copper rich intermetallics leads to the depletion of Cu in the adjacent matrix [7, 9, 173, 194]. Guillaumin *et al.* [7] found a 500 nm wide dispersoids-free zone around coarse intermetallic particles in AA2024. Lower local Cu content in the matrix will lower the pitting potential and promote pitting at specific locations [37, 210]. According to the anodic trenching model, Al-Cu-Fe-Mn particles (referred as 'Fe-Mn' particles in this current study) have less copper than the Al-Cu-Mg particles, leading to less depletion of copper in the surrounding matrix of Al-Cu-Fe-Mn particles. Thus Al-Cu-Mg particles should be more susceptible to trenching than Al-Cu-Fe-Mn particles. This assumption was later supported by the studies of Zhu *et al.* [211] where immersion testing was performed on AA2024-T3 in 0.6 M NaCl solution. Illevbare and Scully [204] reported the corrosion potential of Fe-Mn particles to be approximately -0.35 V/SCE in chloride containing solutions which is 0.2 V/SCE positive compared to the AA2024-T3 matrix (i.e., -0.65 V/SCE). Based on this data Zhu [211] assumed that in principle there should be galvanic coupling between the anodic Al matrix/cathodic Fe-Mn particles and that this would induce the dissolution of the surrounding aluminium matrix. However, no significant dissolution of aluminium matrix surrounding the Fe-Mn particles was observed even after 72 hrs of immersion in 0.6 M NaCl solution. This phenomenon was then tried to be explained with the help of cathode to anode area ration during galvanic coupling. Zhu *et al.* [211] argued that, higher the cathode to anode area ratio, higher the magnitude of galvanic corrosion. In the case of Fe-Mn particles, it was shown that the induced galvanic attack spreads over a greater area of anodic aluminium matrix and corrosion activity on the anode is therefore weakened. As a result, severe dissolution of the aluminium matrix is avoided.

Comparing the results and arguments provided by different researchers, it can be summarized that both “alkaline model” and “anodic model” have their own limitations in explaining the presence of trenching around intermetallic particles in aluminium alloys. The alkaline model is not efficient enough to rationalize trenching at low pH and different trenching phenomena associated with different types of particles. On the other hand, the anodic model describes the preferential breakdown phenomena of the surrounding matrix of a particle as a consequence of galvanic coupling between the particle and the copper depleted adjacent matrix. However, the described copper depletion has not always been found around all intermetallic particles. According to both of the models, probability of pit initiation is higher in the adjacent matrix around the Fe-Mn particles (due to passive film dissolution or due to breakdown associated with galvanic coupling), though in some cases attack on Fe-Mn particles had also been observed [43, 44]. Hence, the pit initiation phenomena associated with the Fe-Mn seems to be complex with the possibility of more than one operating mechanism.

2.2.1.3.1.2 The ‘S’ Phase Particles

‘S’ phase intermetallic particles are a key contributor to the poor corrosion resistance of Al-Cu-Mg alloys [12-15]. It should be noted that, the corrosion studies as will be discussed in this section are performed on the ‘S’ phase as an intermetallic particle and not as a precipitate. However, initial behaviour of the ‘S’ phase particles with respect to the matrix was a subject of debate among researchers. ‘S’ phase particles show lower open circuit potential than the open circuit potential (OCP) of 2024-T3 [9, 191] which suggest that that the ‘S’ phase is active. A number of researchers have confirmed the anodic behaviour of ‘S’ phase particles by showing initiation of pits on the particles [8,

12, 37, 43, 46, 174, 185, 198, 203]. Based on these observations it is believed that the dissolution of the 'S' phase particles occurs at the first stage of pitting corrosion [12-15]. On the other hand, the Volta potential measurements clearly show a cathodic character of 'S' phase particles when compared to the alloy matrix [6, 212-214]. In a few cases, pit morphology revealed the presence of pits adjacent to the particles which is also evidence of the particle being cathodic in nature [12]. These contradictory observations raise the question of why predominantly cathodic intermetallics exhibit high anodic dissolution activity.

Buchheit's theory [9, 14, 82, 123, 181, 182] of selective dissolution of Mg and Al from the particles attempts to resolve the conflict. This theory explains that 'S' phase particles initially behaves anodically which results in the dealloying of Mg and Al from the particle. The particle soon become rich in Cu and starts acting as a cathode, as Cu is a better surface supporting for oxygen reduction [173, 175, 186, 187]. In several papers, Buchheit *et al.* [9, 14, 82, 123, 181, 182] described the phenomena of Cu distribution on the surface during the corrosion process. Based on the finding that metallic copper clusters were present in the corrosion product layer, a mechanism was proposed to explain the formation of Cu ions during Al-Cu-Mg corrosion. The overall mechanism is schematically represented in Figure 2.15.

The diagram (Figure 2.15) indicates the dealloying of the Al-Cu-Mg intermetallic particle which is polarized anodically by the surrounding matrix. This dealloying leads to the formation of very fine and porous copper rich particle remnant which will then coarsen to 10 to 100 nm diameter metallic copper clusters to minimize the surface energy. These metallic copper clusters are then detached from the particle remnant, gets captured by the corrosion product and move away by the mechanical action of film growth or solution movement [182].

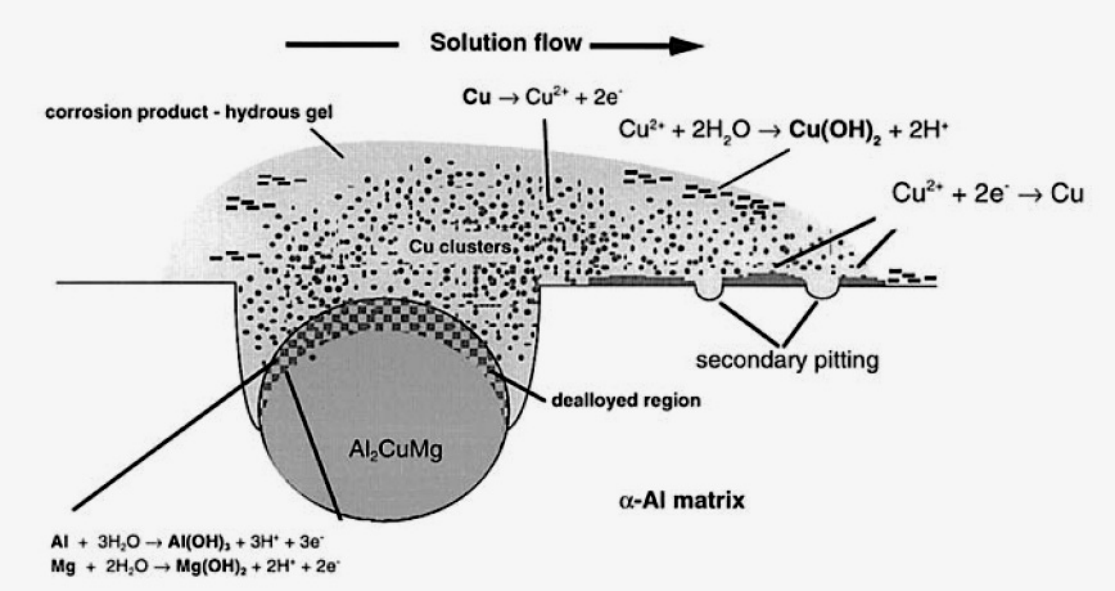

Figure 2.15 Schematic illustration of a mechanism for redistribution of Cu by dissolution of large copper bearing intermetallic particles in Al alloys [182].

Once these copper clusters are isolated their OCP rises from the OCP of the alloy (i.e., -0.550 to -0.700 V_{SCE}) to the OCP of Cu (i.e., -0.050 to 0.0 V_{SCE}) and as the OCP of copper in near neutral chloride containing solution is higher than the reversible potential of copper (E_{Cu}), oxidation of the clusters will generate copper ions. Precipitation or reduction of Cu ions will serve as local cathodic sites that stimulate secondary pitting. It was also concluded that Cu release is more strongly influenced by overall alloy Cu concentration than by volume fraction of Cu-rich intermetallic particles.

Rapid anodic and cathodic reaction kinetics of the 'S' phase contribute to the instability of the compound and subsequent liberation of Cu [14]. This nonfaradaic liberation of Cu clusters from dealloyed Al_2CuMg was supported experimentally by Buchheit *et al.* [14] through electrochemical characterization of bulk synthesized 'S' phases. In this study Buchheit proved that the 'S' phase is most active, Cu depleted zones (e.g. pure Al) are intermediate, and the α-Al matrix phase (i.e., Al-Cu solid solution) is

the most noble. Galvanic relationship between the matrix and particle is thought to change depending on the localized phenomena. Dealloying of ‘S’ phase particles could lead to the enrichment of Cu on their surface and thereby changes the galvanic relationship with the surrounding microstructure [7, 9, 15, 179]. Cu rich remnants on ‘S’ phase particles moves its potential to more positive direction and caused the anodic dissolution of the alloy base at its adjacent periphery [9]. It is speculated that the formation of these copper rich phases would lead into the depletion of copper at the adjacent matrix [7, 173, 194]. Local galvanic coupling between the depleted zone/alloy matrix and depleted zone/S-phase is also thought to influence the local dissolution phenomena. However, there are some ambiguities about the presence of Cu depleted zones around the particles. Buchheit [9] could not identify the presence of the depleted zone and gave an explanation that as these particles are more or less stable, they may not consume solute from the surrounding matrix. In the case where depleted zones have been observed, ‘S’ phase intermetallic particles may nucleate and grow during cooling after solution treatment and thereby creating solute depleted zone at the adjacent area.

Guillaumin *et al.* [7] found a copper depleted dispersoids free zone around the ‘S’ phase particles. While performing potentiodynamic scans in 1 M NaCl, two different breakdown potentials of AA2024-T3 were found by Guillaumin *et al.* [7]. It was concluded that the first breakdown potential was indicative of the dissolution potential of ‘S’ phase particles whereas the second breakdown potential corresponded to the matrix breakdown potential. ‘S’ phase particle contains more copper than the Fe-Mn and hence it was thought that the depletion of copper around the ‘S’ phase particles would be more than that of the matrix around the Fe-Mn particles. This hypothesis seems was proposed to explain the faster dissolution kinetics of the matrix surrounding the Al_2CuMg than that of matrix adjacent to the Al-Cu-Fe-Mn containing particles [7, 12].

In a recent study Zhu *et al.* [211] suggested that pitting initiates around the 'S' phase particles as exhibited by the dealloying of Mg and Al from the particle and the severe dissolution of the surrounding aluminium matrix. Using SEM/EDX analysis after the exposure of AA2024-T3 in neutral 0.6M NaCl as a function of time, observations of the dealloying of Al and Mg with the dealloying of Mg being severe was confirmed. Although this work agreed that corrosion of AA2024-T3 starts from the dealloying of 'S' phase particles as a result of galvanic corrosion driven by the galvanic coupling of the anodic 'S' phase with the cathodic Al matrix, it does not agree with the copper redistribution mechanism and the change in the galvanic coupling mechanism between the particles and the matrix as the cause of surrounding aluminium matrix corrosion as proposed by Buchheit *et al.* [9] and other researchers [7]. According to Zhu the aluminium dissolution in the vicinity of 'S' phase remnants is likely to be caused by local alkalization from cathodic reactions (i.e., as a result of oxygen reduction local pH increases to such a value where the passive film is not stable). Zhu did not find any significant increase in the extent of attack around the 'S' phase particles between 3.5 hrs and 72 hrs of immersion. It was argued that if the attack happens due to the local change in the galvanic relationship (i.e., Cu enriched particle become the cathode and matrix acts as an anode), severe attack would be expected after long exposure as the particle become more enriched in copper and hence more cathodic. To resolve this issue an attempt was made to explain the corrosion behaviour of dealloyed 'S' phase remnants with the help of cathode to anode area ratio during galvanic coupling. Zhu argued that the higher the cathode to anode area ratio, the higher the magnitude of galvanic corrosion. The extensive dealloying of 'S' phase particles during the first few hours of immersion occurs as the 'S' phase particles have small area compared to the large surrounding cathodic aluminium matrix. In later stage 'S' phase remnants become cathodic because of copper enrichment,

but the anodic aluminium matrix surrounding them will still be higher in area. Therefore these small cathodes will not be able to induce severe dissolution of the anodic aluminium matrix at the peripheries due to the effect of small cathode to anode area ratio.

Irrespective of the initial behaviour of 'S' phase particles, most researchers agreed that after an extended exposure to an aqueous solution 'S' phase particles act as net cathode because of the copper enrichment and redistribution. A Ce decoration technique was used by Kolics *et al.* [215] and Aldykewicz *et al.* [216] to detect cathodically active sites, where the higher the Ce deposition, higher the cathodic reactivity. Kolics *et al.* [215] found the highest Ce deposition on the 'S' phase particles followed by Fe-containing particle and the alloy matrix, whereas Aldykewicz *et al.* [216] found Ce deposition only on 'S' phase particles.

Vukmirovic *et al.* [175], Chen *et al.* [8] and Dimitrov *et al.* [173] have agreed with the dealloying mechanism of 'S' phase particles proposed by Buchheit and identified the copper redistribution to be an important aspect in the localized corrosion event. It should be noted that, intermetallic particles serve as the primary sites for oxygen reduction regardless of the operative copper distribution mechanism. It was observed that 'S' phase particles are responsible for corrosion by dissolution and the extent of attack is a function of pH of the solution. It was also suggested that the main corrosion damage by particle-nucleated pitting results from the pit coalescence process rather than single pit growth. Dimitrov *et al.* [173] performed experiments to elucidate the effect of convection on the Cu redistribution process. It was confirmed that convention enhances the copper redistribution process and thereby supports Buchheit's assumption.

Similar types of experiments were performed by Seegmiller *et al.* [187] investigating the cathodic activity of Cu-rich intermetallic particles using a wall-jet flow cell. The primary aim was to discern when and to what extent the Fe-rich and Cu-rich

intermetallic particles act as sites for oxygen reduction. The cathodic corrosion that occurs due to the oxygen reduction on the intermetallic particles (and could occur in the absence of chlorides) could be an influential factor for determining the corrosion performance of the alloy. It was also observed that the protective oxide layer around the intermetallic particles is reactive to the OH^-. This helps in forming trenching and cavities around the particles. Both Cu-rich and Fe-rich intermetallic particles are found as cathodes for O_2 reduction with similar efficiency. In another paper Dimitrov *et al.* [186] investigated the dealloying process of bulk synthesized 'S' phase (Al_2CuMg) in alkaline (0.1 M NaOH) media. The development of a porous structure with 2 nm average ligament size was observed during the initial stages of the dealloying process.

Kendig *et al.* [188] demonstrated the development of dealloyed Cu-rich phase of nanometre scale particulates. They found that the enrichment of the surface with Cu and Mg by cathodic corrosion (i.e., corrosion induced by the increase in local alkalinity as a result of oxygen reduction reaction) of the Al component of the phase. The Cu-rich layer inhibited dissolution of the underlying material though it was itself catalytic for reduction reactions. Reference was also made to the presence of a 'pseudo-passive' layer which results in the dissolution rate higher than common passivity.

Kolics *et al.* [193] studied the effect of bulk solution pH on the intermetallics corrosion and their morphology. Two kinds of corrosion products around the intermetallics were observed. Corrosion product enriched with aluminium oxide was found around both Al_6(Cu,Fe,Mn) and 'S' phase intermetallic particles in slightly acidic condition. Deposits rich in copper were only found around the 'S' phase particles. Kolics summarized the behaviour of 'S' phase particles as a function of pH, namely acidic, neutral and alkaline condition in 0.1 M NaCl. At lower pH, most of the 'S' phase particles showed porous grain structure and selective dissolution of Mg and Al at the particles

periphery, while no evidence of redeposited Cu around the intermetallics was observed. Slight increase in pH (from pH 3 to 4) resulted in an extensive deposition of aluminium oxide corrosion product around 'S' phase particles. In neutral solution a strong dissolution of the matrix adjacent to the particles was observed which developed a porous structure. As demonstrated by Buchheit *et al.* [9], copper deposits were also found in this study as a result of selective dissolution of Mg and Al. In higher pH (~ 13), S-phase particles are reported to have undergone copper enrichment and aluminium dealloying. As the Cu enrichment in the bulk matrix lowered the potential difference between 'S' phase particles and the matrix, galvanic action was not as severe as it was in the lower pH environment. However, Kolics *et al.* [193] concluded that the Cu content in the bulk matrix played an important role by contributing to the significant amount of surface Cu in acidic and alkaline media. Bulk pH also played crucial role to the extent of S-phase dealloying and the resulted Cu redeposition.

There have been arguments between different researchers about the source of Cu that enriches the area around the Cu-rich intermetallic during the corrosion process. Two possible explanations have been proposed about the source of Cu. It could either come from the intermetallic particles [182] or from matrix phase dealloying [171, 173, 186]. Some researchers explained the presence of Cu-enriched layer around the intermetallic particles by the dissolution of the surrounding matrix [171, 173, 186]. According to this theory, the enriched copper does not come from the intermetallics, but comes from the surrounding matrix. According to this theory the 'S' phase particles dealloy very quickly leaving behind Cu-rich remnants. This Cu supports the cathodic reactions at much faster rate. The cathodic reaction will increase the local pH promoting dissolution of adjacent aluminium matrix.

Boger *et al.* [194] performed rotating ring electrode to discern the amount of Cu-release from both intermetallics and Al-Cu alloys. Attempts were made to find and compare the amount of Cu released by both mechanisms. The intermetallic Cu-release was divided by the total Cu-release by both mechanisms and found that the precipitate released Cu only account for about 15% of the total Cu release. As this percentage is larger than the volume fraction of precipitate in the microstructure, Boger concluded that the Cu-release from the precipitates is high, relative to the matrix. However, it was observed that Cu-release from the matrix phase occurred and could result in Cu-release in real alloys. The work proved that copper redistribution is not simply a function of matrix phase dealloying or intermetallic dealloying, but both mechanisms have an influence on the corrosion behaviour.

As discussed earlier, the dealloying mechanism leads to the formation of porous Cu remnant which then acts as an efficient cathode. It has been predicted that oxygen reduction will change the local alkalinity and drive preferential dissolution of aluminium from the alloy matrix [171, 173, 186]. Missert *et al.* [185] attempted to capture this localized change in pH during in-situ scanning confocal microscopy with addition of fluorescein indicator. It was observed that particle dealloying shows transient acidity, but although localized corrosion occurred at the majority of the 'S' phase particles, surprisingly only a minority of sites showed transient acidity. This could be due to the fact that only sites with high reaction rates contribute to pH changes and that in the majority of the sites pH alteration does not occur due to locally balanced production of H^+ and OH^-. Missert concluded that localized pH changes occur as a result of accelerated attack at a minority of sites and pH change does not necessarily drive localized corrosion of the alloy. Local pH gradient is influenced by the spacing between the cathodic particles. Anodic dissolution of aluminium was observed beneath the noble particles.

Highly alkaline region created by the cathodic reaction on the individual particles are reported to overlap when the particle spacing is less than 50 μm.

In a similar study to Chen *et al.* [8], Liao *et al.* [11] investigated the importance of intermetallic particle-matrix galvanic couple in promoting localized pitting corrosion. In agreement with earlier work it was observed that most of the intermetallic particles eventually behaved cathodically, irrespective of their original anodic or cathodic character relative to the matrix and promoted matrix dissolution. Based on this study, a conceptual model of pitting was proposed which identified intermetallic particles to be responsible for growth and location of severe pits (Figure 2.11). The proposed model categorized two different types of particle induced pitting corrosion. General pitting was observed on isolated surface particles which are far away from their nearest subsurface particles, while severe pitting develops at subsurface particle cluster.

Anodic dissolution of the constituent particles and the extension of that dissolution into the surrounding matrix was investigated by Ilevbare *et al.* [37] using in situ confocal laser scanning microscopy in very low chloride solution of varying pH. OCP and polarization data indicated that at all pH levels, Al-Cu-Mg particles predominantly behave as an anode, while Al-Cu-Fe-Mn particles behaved as cathodes. Metastable pitting activity in the alloy at open circuit was also observed and attributed to the low pitting potential of Al-Cu-Mg particles. Pride's [167] pit stability criteria was used and localized pit growth was found in the Al-Cu-Mg (S-phase) particles. If the local cathodic reactions are high enough to support the pit growth, pits from intermetallic particles are predicted to propagate into the matrix. The bigger the intermetallic particle clusters, the greater the chance of Cu replating which could support cathodic reactions and thereby help in the formation of stable pits.

Alodan *et al.* [174, 198] used confocal laser scanning microscopy (CLSM) to detect the localized corrosion in 2024 in chloride solution by adding fluorescence dye which helped to identify any change in local pH around different intermetallic particles. Strong fluorescence signal from Cu rich intermetallics were observed after immersion which indicated changes in pH around those particles. The pH gradient around the particle was dependent on the bulk pH. At a bulk solution of pH 4, the gradient was sharp and reached the bulk value within a distance of 0.5 μm from the surface of the particle. Elemental analysis after the aqueous exposure revealed a compositional change in the Mg rich Al_2CuMg (i.e., 'S' phase particles) which showed signs of Mg dealloying. Particles containing Mg present a more negative OCP than the matrix and act as anodes. As a result, in the initial stage Mg dissolves to leave corrosion products on the surface. Corrosion products entrap fluorescein and confine the fluorescein signal to the surface only.

Like other researchers, Shao *et al.* [12] also identified the Al_2CuMg intermetallics to be mainly responsible for corrosion using a microreference electrode technique. An attempt was made to capture the events associated with each particle during immersion in chloride containing solution. Different behaviours of 'S' phase particles have been reported in this study. In a few cases 'S' phase particles dissolved very quickly while in other cases dealloying of Mg from 'S' phase particles was observed. The dealloying resulted in attack in the periphery of the particles (Figure 2.16a). Significant amount of dealloying was observed when EDX analysis of the same particle before and after exposure was performed. This selective dissolution of Mg resulted in Cu-rich remnant which acts as a cathode to facilitate the localized corrosion for AA2024. Some 'S' phase particles were found to be non-reacting with no attack around the periphery (Figure 2.16b). It was assumed that these particles must have been protected by some form of

film that dissolves very slowly in NaCl solution [43]. After the removal of the film the 'S' phase was found to be dissolved very quickly.

(a) **(b)**

Figure 2.16 SEM image of (a) Al_2CuMg (i.e., 'S' phase) particle showing attack in the periphery (b) Intact Al_2CuMg particle; after 2h of immersion in 0.01M NaCl [12].

Schmutz *et al.* [43, 44] also reported the presence of a surface film on 'S' phase particles when ex situ AFM topographic and Volta potential mapping (Kelvin Probe Technique) experiments were used to examine the corrosion that occurred at different intermetallics particles in AA2024-T3 during immersion in NaCl solution. Due to the presence of surface film, Al-Cu-Mg particles showed noble Volta potentials in air, which was in contrast to the active potential reported for intermetallic particles in solution. This noble potential decreased with time and as soon as the particles become active relative to the matrix, it rapidly dissolved.

Findings of different researchers as discussed above seem to strongly indicate that the 'S' phase intermetallic particles not only function either as a cathode or as an anode during the corrosion processes but also play a complex role combining cathodic and anodic activity together in the same particle.

Complexity of the processes associated with ‘S’ phase particle corrosion is concisely summarized in a recent study by Yasakau *et al.* [203]. Figure 2.17 shows the schematic representation of the mechanisms involved in ‘S’ phase particle corrosion in chloride solution. Yasakau *et al.* [203] described the possibility of chemical dealloying of ‘S’ phase particles along with electrochemical dissolution at different stages of the corrosion process. Due to the presence of a thinner and more defective oxide film [12] on the ‘S’ phase intermetallic particles compared to that of the alloy matrix, the chloride ions interact with the native oxide film of AA2024 (Figure 2.17a) leading to its breakdown at the weak places originated from the ‘S’ phase particles [125]. Fast chemical dealloying of active Al and Mg from the ‘S’ phase particles (Figure 2.17b) starts immediately after solution comes in contact with the surface of the intermetallics [14, 173, 186, 210, 213] leaving copper rich remnants behind. Local increases in pH around the ‘S’ phase particles in combination with enrichment of their surfaces by copper then shift the dissolution processes from chemical to electrochemical.

During the electrochemical dissolution, the intermetallic ‘S’ phase particles play the role of both active anode and cathode at the same time and cause further localized dealloying. The aluminium and magnesium cations can react with hydroxyl ions (generated from the oxygen reduction reaction at the copper enriched cathodic areas) and form various insoluble hydroxide sediments or soluble hydroxyl complexes (Figure 2.17d) depending on the pH values. It is hypothesized that the $Al(OH)_4^-$ complex can diffuse to the bulk solution. After reaching the zones of the solution with lower pH (approximately 8), the complex anions can be transformed into thermodynamically stable, insoluble $Al(OH)_3$ and form an insoluble deposit at a certain distance from the active intermetallic (Figure 2.17d).

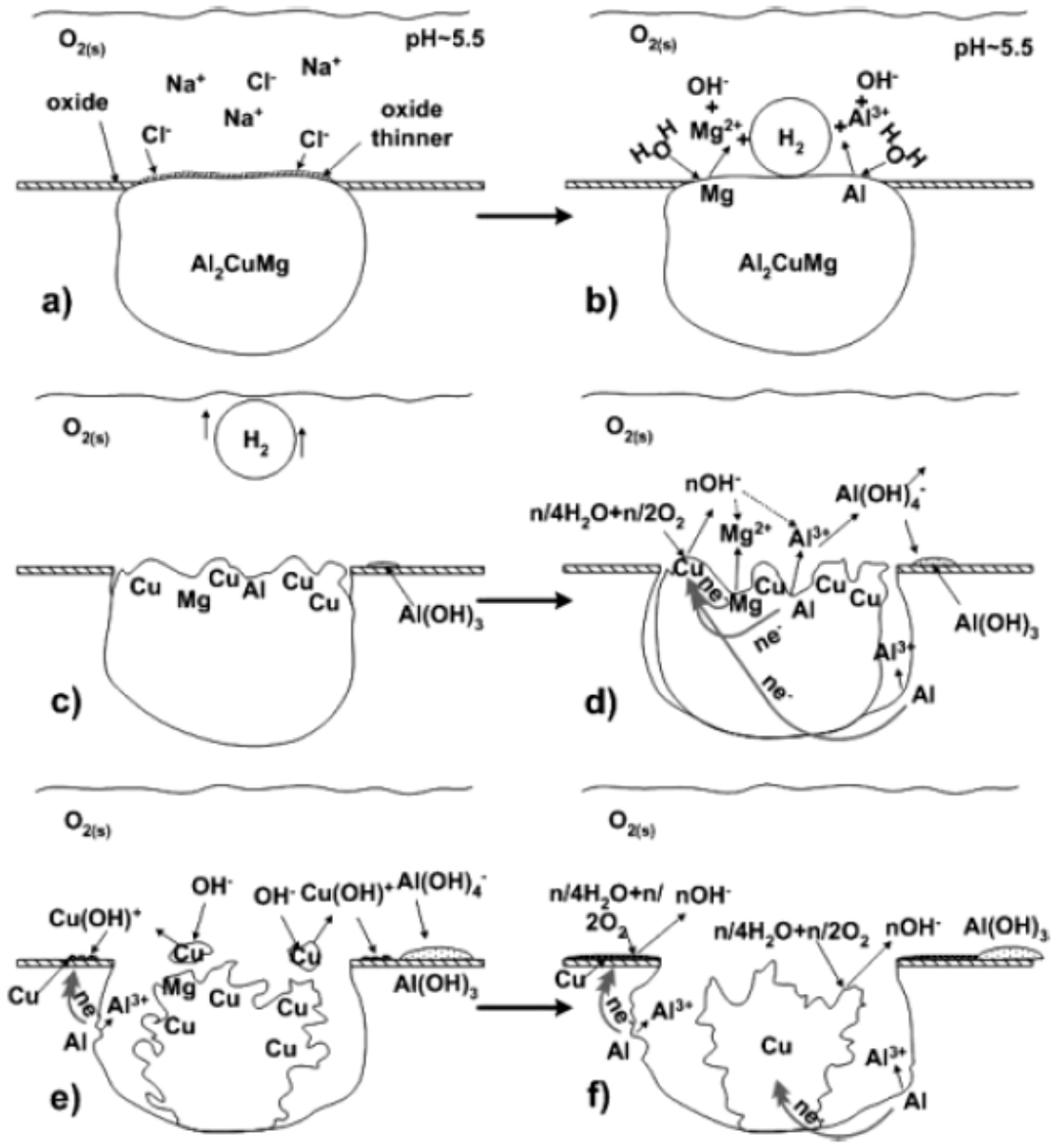

Figure 2.17 Schematic representation of 'S' phase corrosion mechanism during the immersion of AA2024 in chloride solution [203].

Thus, with longer exposure time, an active pit can be covered with a hydroxide dome. Redistribution and redeposition of nano sized copper particles have been extensively discussed in the literature and reemphasized in Figure 2.17e. The redeposited

copper increases the effective surface area for the cathodic reaction and thereby plays an important role in further development of the localized corrosion

2.2.1.3.1.3 Microelectrochemical Characterization of Intermetallic Particles in AA2024

Suter and Alkire [40] used a micro-capillary electrochemical cell to study the mechanism of localized corrosion during the initiation processes at single intermetallic particles. The unique aspect of this work is the use of very small exposed area which reduces the noise and thereby increases the sensitivity of the tests. It was observed that a decrease in the exposed area increases the pitting potential which in general is fixed by the most active intermetallic particle. Therefore, the larger the area, the higher the chance of having active intermetallic particles exposed to the solution resulting in a low pitting potential. Interestingly reduction in the number of active intermetallic particles not only increases the pitting potential, but also leads to higher corrosion potentials and higher cathodic current as well. As the potentiostat measures the net current, cathodic currents are lower in large scale experiments because of their anodic nucleation current.

Suter and Alkire [40] chose three different areas (capillary diameter of 20, 50, and 100 μm) containing only Al-Cu-Mg, only Al-Cu-Fe-Mn and a mixture of both kind of particles to study the electrochemical behaviour of the different intermetallic particles. The pitting potential of the areas containing Al-Cu-Mg or a mixture of both kinds of particles was always observed to be 200-300 mV less than the area containing only Al-Cu-Fe-Mn particles. It was seen that pitting starts in the adjacent matrix before the Al-Cu-Mg particles completely dissolved. Further studies on the single intermetallic particle were performed using a smaller capillary size (20 μm diameter). Both types of particles

showed a range of pitting potential, but, on average, Al-Cu-Fe-Mn particles were more corrosion resistant than the Al-Cu-Mg particles. EDX analysis at the edge of the Al-Cu-Mg particles after the microelectrochemical tests indicated a preferential dissolution of Mg. In comparison, Fe and Mn dissolution was observed at the edge of Al-Cu-Fe-Mn particles. Pit initiation at lower potential resulted pitting at the adjacent matrix of the 'S' phase particles. On contrary, initiation of the pits at high potential leads to the faster dissolution of intermetallic particles and pitting underneath the dealloyed Cu-rich remnant. No adsorbed copper around the intermetallic particles was observed when the experiments were stopped during pit initiation (I_{max} : 10 nA), while adsorbed copper was found when the experiments were stopped during pit propagation (I_{max} : 1 μm).

Figure 2.18 shows the summary of the pitting potentials of different inclusions and areas without inclusions. All the experiments were performed after the initial cathodic potentiostatic hold at -1000 mV_{SCE} for 1 min and then potentiodynamically scanned at 1 mV/s. This initial cathodic hold might have an effect on the results as large scatter is evident in the pitting potential data.

As discussed earlier, the predominant cathodic reaction for aluminium corrosion is oxygen reduction which produces local alkalinity. Increase in the local alkalinity will dissolve the passive film and complete removal of the passive film will expose pure aluminium during the experiment. Similar phenomena could happen during a longer period of cathodic hold. Surface film on top of the matrix or particles is modified and could result into scatter of the breakdown potential data.

It is also interesting to note that Suter's [40] potentiodynamic scans in the areas without any intermetallic particle showed higher cathodic reactivity compared to the scans in the areas with intermetallic particles. It would be expected that the intermetallic

particles have higher cathodic reactivity than the pure matrix as particles serve as a better places for cathodic reaction (i.e., oxygen reduction).

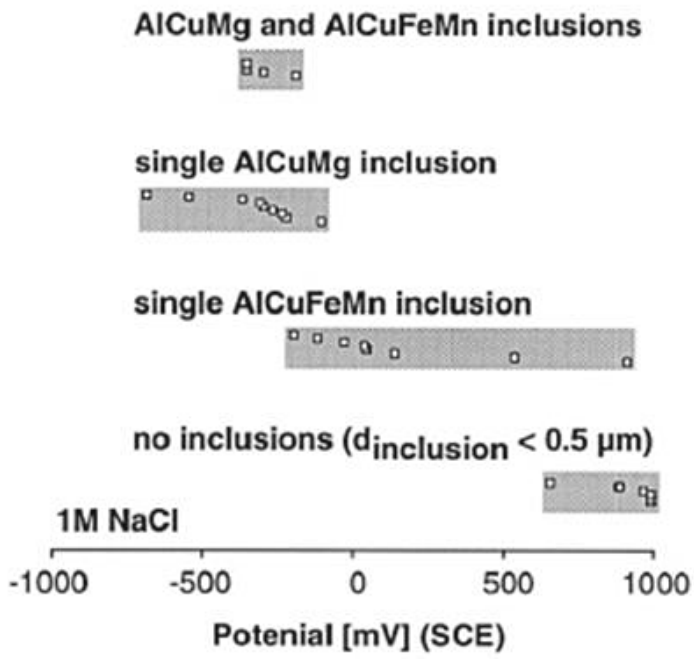

Figure 2.18 Pitting potentials of areas with AlCuMg and AlCuFeMn inclusions when scanned from -1000 mV_{SCE} at 1mv/s after initial potentiostatic holding for 1 min at -1000 mV_{SCE}. Capillary of 20 µm diameter was used for single inclusion and without inclusion tests whereas 50 µm diameter was used for areas with both types of inclusions [40].

In a recent study Birbilis *et al.* [42] used micro-capillary electrochemical cell to characterize the electrochemical behaviour of bulk synthesized 'S' phase (Al_2CuMg). Earlier studies on bulk synthesized 'S' phase [14] with a large exposed area did not reveal any passive region in the anodic portion of the potentiodynamic scans. In this study Birbilis *et al.* [42] used capillary sizes of 20-50 µm diameter and reported pitting potential of 'S' phase particles between 80 mV_{SCE} to 135 mV_{SCE} depending on the chloride concentration. It was observed that the corrosion potential of 'S' phase particles was less noble than that of the matrix while the breakdown potential of 'S' phase particles showed

a higher value than the matrix. These results would lead to the belief that ‘S’ phase is cathodic to the matrix. This misleading behaviour of ‘S’ phase particle could be explained by taking into consideration that the dissolution characteristics of the ‘S’ phase are complex and have been shown to incorporate a dealloying mechanism, leading to Cu enrichment [14]. Therefore, the large current densities observed prior to the final breakdown and the breakdown potential itself could actually be due to the presence of redistributed pure copper [14, 182]. It may be assumed that the ‘S’ phase particle does not dissolve as a unique entity, but may undergo a dealloying process leading to selective dissolution of the Mg and Al components of the intermetallic.

Therefore, from the above discussion it could be summarized that ‘S’ phase particles have poor corrosion resistance properties compared to the matrix or the Fe-Mn particles. It has been agreed that initially ‘S’ phase particles behave anodically resulting into dealloying of Mg and Al from the particle and enriching the surface by Cu. However, reason for the dissolution of the surrounding aluminium matrix along the ‘S’ phase particles still remain a subject of debate. Both ‘alkaline corrosion’ and ‘galvanic coupling’ mechanisms have been proposed to explain presence of grooving in the adjacent matrix. According to the findings of several researchers, pit initiation sites in 2024-T3 could include the Al-Cu-Mg particles, the periphery of Cu enriched Al-Cu-Mg particles that have been dealloyed of Al and Mg and the matrix adjacent to Al-Cu-Mn-Fe particles (though in some cases attack on Fe-Mn particles had also been observed).

2.2.2 Intergranular Corrosion

Intergranular corrosion (IGC) is a type of localized attack at and adjacent to the grain boundaries as a result of an enhanced thermodynamic and/or kinetic tendency for corrosion relative to the grain matrix. [111, 217]. IGC is operated by pre-existing active dissolution paths based on compositional/structural heterogeneity. The most prevalent and technologically significant forms of IGC occur when either a segregant is enriched at the grain boundary (GB), an actively corroding precipitate phase forms at the boundary or a beneficial element normally in the solid solution is depleted from the boundary region [217].

High strength age-hardening Al-Cu alloy like AA2024 derive most of their strength from the precipitation of copper enriched phase (e.g., Al_2Cu, Al_2CuMg) in the grain matrix. IGC susceptibility in Al-Cu and Al-Cu-Mg alloys is strongly dependent on the quench rate over the temperature range from 400 to 315˚C and on subsequent natural aging. Alloys such as AA2024-T3 require quench rates faster than 500˚C/s to avoid IGC [217]. This requirement is associated with Cu-depletion mechanism that minimizes grain boundary precipitations and formation of Cu-depleted profiles. Copper remains in solid solution when it is quenched fast enough from homogenizing temperature of about 480˚C and improves the corrosion resistance of the alloy. Precipitation takes place slowly at room temperature with progressive strengthening of the alloy. However, if the alloy is quenched slowly or after quenching if it is artificially aged above 120˚C, copper enriched precipitates form preferentially along the grain boundaries [178]. This result in a copper depleted zone adjacent to grain boundary precipitates and rapid anodic attack in this copper depleted zone make the alloy susceptible to intergranular corrosion. It is rationalized that in Al-Cu and Al-Cu-Mg alloys IGC dependency is related to the Cu

depletion at grain boundaries [97, 152, 168, 205, 207, 217-221]. IGC in aluminium alloys may also result from the segregation of a corrosion stimulating element or by the formation of harmful anodic precipitate [7, 217, 222-225].

Sinyavskii *et al.* [226] found two types of IGC in aluminium alloys. In low alloy or pure aluminium crystallographic IGC is caused by the formation of corrosion active areas at high-angle boundaries of recrystallized grains at certain stage of recrystallization. This is thought to be possible due to the local accumulation and coalescence of vacancies. The second form (i.e., structure-decomposition IGC) occurred in high or medium alloyed Al, and is associated with the formation of active corrosion areas in close proximity to incoherent or partly coherent phase particles located at GB. Susceptibility to structure-decomposition IGC can be reduced by controlling the heat treatment conditions to achieve uniform precipitation throughout the matrix.

Zhang and Frankel [95] emphasized on the fact that though the solute depleted zones (SDZ) near the grain boundary (GB) are considered to be the site for local attack, but Cu-rich ‘S’ phase particles at the grain boundary could also play an important role in corrosion initiation. These particles have been shown to release Cu. Deposition of Cu on the grain faces linking the GB crevice would protect those faces from attack. Those also provide a cathodic site that would consume current generated by IGC at the attack front. Since most of the current would not escape from the GB crevice, the dissolution rate of the front would not be strongly dependent on the external applied potential [227]. However, arguments presented by Zhang seems differ with the findings of Muller and Galvele [168] who found that in an Al-3.5Cu binary alloy intergranular corrosion rates are potential dependent, the lower the potential the lower the corrosion rate. Muller also reported a range of potentials below which no intergranular corrosion could be found.

The electrochemical framework mechanism of intergranular corrosion of Al-Cu alloys as proposed by Galvele and De Micheli [152] is schematically represented in Figure 2.19. Cu depleted grain boundary zone exhibits more negative (i.e., lower) critical pitting potential compared to matrix. Al- 4%Cu alloy is proposed as a system with three distinct microstructural features/regions which can act as anodic or cathodic zones. The copper depleted zone along the grain boundaries is the anode, whilst the grain matrix and the intermetallic Al_2Cu act as cathodes. IGC of Al-Cu is described as a process in which a very small anode is in contact with a large cathode. It was also argued that intergranular attack is not due to a difference in corrosion potentials between grain boundaries and grain matrix, but to a difference in the breakdown potentials of these phases. The difference in potentials between the grain boundaries and the grain matrix is on the order of 100 mV.

Galvele and De Micheli [152] summarized the requirements for IGC in a Al-Cu alloy as, (a) the alloy must have a solute depleted zone along the GB, (b) the corrosive medium should contain anions capable of breaking down the passivity of the Al, (c) the breakdown potential of the depleted zone must be lower than that of the grain matrix, (d) the corrosion potential of the alloy must be over the breakdown potentials of the depleted zone, and under the breakdown potential of the grain matrix.

Though Galvele [152] and others [168, 205, 228, 229] argued that IGC in Al-Cu alloy occurs due to the difference in the pitting potential between the copper depleted zone adjacent to the grain boundary and the copper enriched matrix, but it is also believed that the difference in electrochemical potentials (which is approximately 120 mV) between those areas form a strong galvanic cell which could be responsible for intergranular corrosion of Al-Cu alloys [97, 221]. Furthermore, the anodic copper-

depleted zone is small in area compared with the area of the cathodic grain matrix, resulting in a high driving force for rapid intergranular corrosion.

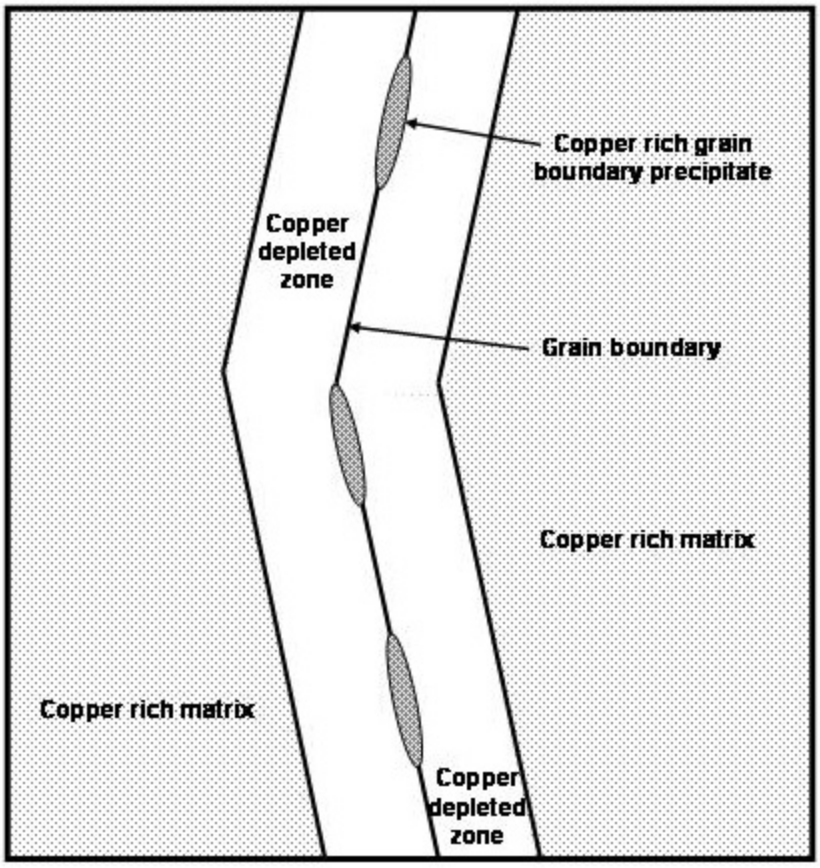

Figure 2.19 Schematic of grain boundary region in an Al-Cu alloy (adapted from [221]). Copper depleted zone is more susceptible to corrosion (with lower breakdown potential) as compared to copper rich matrix. Copper rich anodic precipitates (e.g. Al_2CuMg in case of AA2024) in the grain boundaries also contribute to the intergranular corrosion.

However, the mechanism of potential differences between cathodic and anodic phases does not explain why the presence of halide ions (chloride ions, in particular) is necessary for intergranular corrosion, since galvanic corrosion should occur in any electrolyte of comparable ionic conductivity. Therefore, an alternative mechanism based on the development of a preferential anodic path along grain boundaries resulting from localized active phase precipitation is proposed [222, 230, 231]. However, it should be

noted that due to the complexity of the combination/interaction of microstructural features and electrochemical conditions for producing IGC, the exact contribution from each of the proposed mechanisms is not fully understood. It is quite possible that all the proposed mechanisms have their contribution on the intergranular corrosion of aluminium alloys.

As mentioned earlier, a prominent factor in the IGC susceptibility in Al-Cu-Mg alloy is grain boundary Cu depletion as a result of heterogeneous nucleation of Cu-containing grain boundary phases. Precipitate phases at the GB can be cathodic or anodic in nature [217]. Precipitates such as Al_2Cu which are cathodic in nature can not account for an anodic electrochemical path that enables IGC in Al-Cu alloys. However anodic precipitate like Al_2CuMg can actively dissolve and therefore could account for IGC.

IGC which is produced by intermetallic particles are not altered by the thermal treatment or artificial aging. Sometimes pitting induces IGC [217]. Galvanic corrosion can take the form of cathodic trenching due to enhanced cathodic reactivity or halide induced acid pitting adjacent to the Cu-rich constituent particles. The primary role of initial pitting or cathodic trenching in the context of IGC is to produce the local environment necessary to develop differences in the corrosion behaviour of grain interiors compared to the GB region.

So, it is clear from the above discussion that if IGC occurs due to the formation of copper depleted zone adjacent to the grain boundaries, its extent will depend on the cooling rate and subsequent aging heat treatment given on that particular alloy. It should be remembered that aging heat treatment is almost compulsory for the high strength Al-Cu alloys as they get their strength from the precipitation of second phase particles in the matrix. Normally aluminium alloys are given solutionizing heat treatment to dissolve the alloying elements and then cooled rapidly to keep them in the solid solution. As described

earlier, the cooling rate following the solution heat treatment are found to affect the susceptibility to intergranular corrosion [45, 63, 97, 178, 207, 217, 221].

The effect of temperature and time on the corrosion behaviour of AA2024 is illustrated by the time-temperature-corrosion diagram in Figure 2.20. It can be clearly seen from Figure 2.20 that the intergranular corrosion susceptibility increases as the quenching rate decreases. As discussed earlier, susceptibility to structure-decomposition IGC can also be reduced by controlling the heat treatment conditions to achieve uniform precipitation throughout in the grain matrix. Generally fast growing precipitates in the grain boundary leads to the formation of copper depleted zone adjacent to the grain boundaries. Solute atoms from the grain matrix will diffuse to the grain boundary and then they will diffuse along the grain boundary to contribute to the growth of grain boundary precipitates by a “collector-plate” mechanism [217].

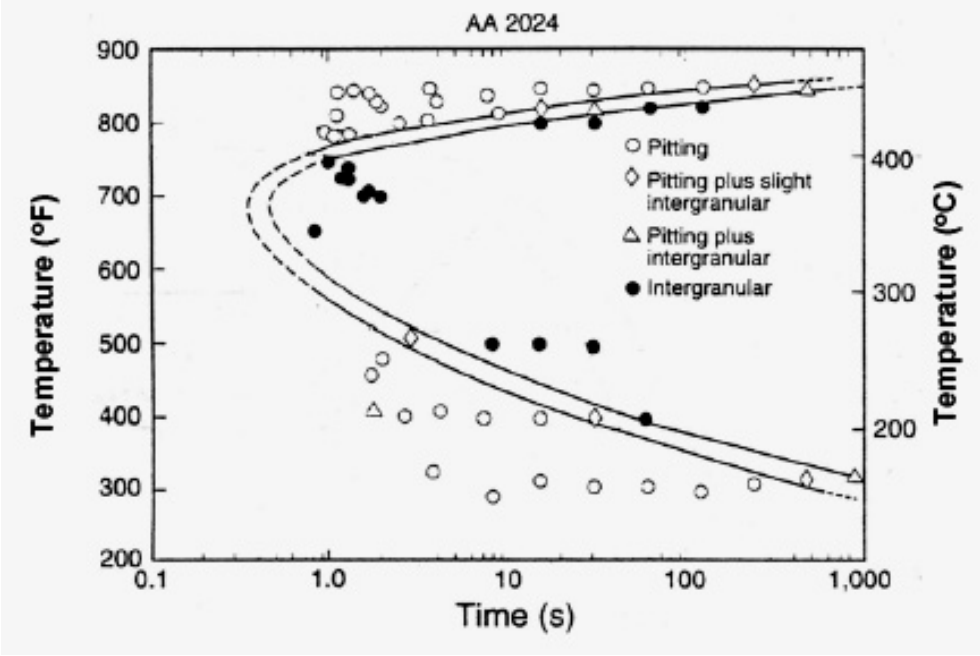

Figure 2.20 Effect of temperature and time in interrupted quenching experiments following solution heat treatment on type of attack developed in AA2024-T4 sheet by an accelerated corrosion test [62].

Figure 2.21 shows the region for intergranular corrosion susceptibility in AA2024 as a function of aging time at 170˚C [205, 217, 228]. Copper remaining in the solid solution increase the pitting potential and corrosion resistance of the alloy. Figure 2.21 emphasizes the fact that, intergranular corrosion occurs only in a specific range of potential: $E_{pit(GB)} < E_{IGC} < E_{pit(matrix)}$, where $E_{pit(GB)}$ is the pitting potential for the copper depleted zone associated with the grain boundary, E_{IGC} is the potential for intergranular corrosion and $E_{pit(matrix)}$ is the pitting potential form the grain matrix.

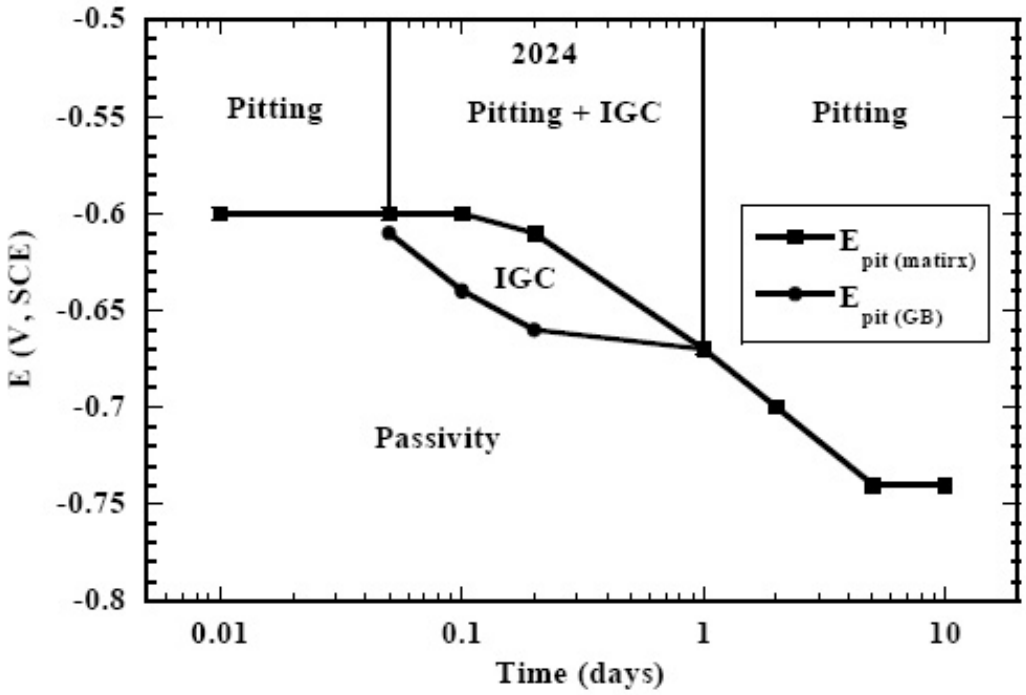

Figure 2.21 The change in pitting potentials for the grain matrix, $E_{pit(matrix)}$ and Cu-depleted zones associated with grain boundary, $E_{pit(GB)}$ in AA2024 with aging time at 170˚C [217, 228]. IGC is found to occur in a specific range of potential: $E_{pit(GB)}<E_{IGC}<E_{pit(matrix)}$, where E_{IGC} is the potential for intergranular corrosion.

It can be seen from Figure 2.21 that severely over aged alloy 2024 shows tendency for pitting rather than intergranular attack. This could be explained from the fact that, prolong over-aging leads to significant precipitation and solute depletion in the grain

interiors as well as at the grain boundaries. Depletion of copper from the matrix brings the pitting potential down and as a result pitting is more probable than the intergranular attack. The maximum susceptibility to intergranular corrosion is obtained when the difference between the pitting potential of the matrix and the copper depleted zone reaches the maximum as it was argued by Galvele and De Micheli [152].

Figure 2.22 represents the schematics of solute depletion along the grain boundaries and in the matrix of a Al-Cu alloy as a function of aging time [232]. Figure 2.22a shows the under-aged condition where the boundary has the heaviest concentration difference in solute between Cu-depleted zones and the supersaturated matrix. In peak-aged condition (Figure 2.22b) the Cu-depleted zones around the Cu-containing precipitates begin to overlap at the boundaries as well as in the matrix. This leads to an overall lowering of the global copper content in solid solution in the matrix. A continuous path of solute depleted zone which could promote intergranular attack at the grain boundaries can be found in this condition. Figure 2.22c shows the schematic of the copper depleted matrix that would be associated with an extremely over aged condition. With the long aging times more nanoscale precipitates will form. As the preferential copper depleted path along grain boundaries is eliminated and the matrix is also depleted with copper, pitting corrosion is more likely to occur in this condition rather than intergranular attack (which is also emphasized in Figure 2.21).

It is interesting to note that the Al_2CuMg phase increases in size and density upon over-aging but maintains the same composition. Thus the presence of Al_2CuMg on grain boundaries could not readily explain the decrease in IGC susceptibility of the alloy upon over-aging [232].

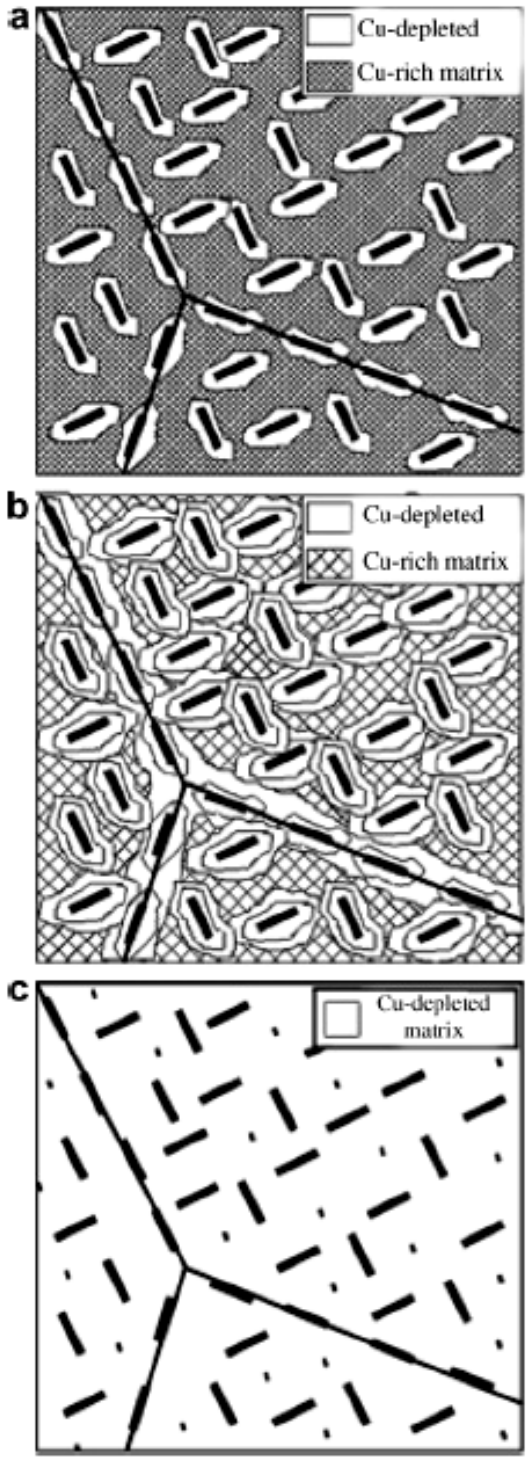

Figure 2.22 Schematic of solute depletion around plate-shaped Cu-bearing precipitates along grain boundaries and in the matrix. (a) Shows an under-aged condition (highest Cu in the matrix. (b) Represents a peak-aged or over-aged condition (lower Cu in matrix). (c) Represents an extremely over-aged condition (lowest Cu in matrix) [232].

2.2.2.1 Growth Kinetics of IGC in Aluminium Alloys

Growth kinetics of localized corrosion (pitting and intergranular) in aluminium alloys have been studied predominantly using two techniques:

1) Foil penetration technique [29, 49-52]
2) X-ray radiography [53-55]

Foil penetration is one of the most simple, and direct methods of measuring localized corrosion growth rate in materials and was first developed by Hunkeler and Bohni [49, 50]. In this technique, the growth kinetics is measured by the time required to penetrate a thin foil. Different test parameters such as sample thickness, sample orientation, test environment, and applied potential could be varied to determine the kinetics of the fastest growing localized corrosion growth regardless of the corrosion growth path [51]. Thus, using foils of different thicknesses penetration depth as a function of time can be measured. The growth rate of localized corrosion exhibits a strong anisotropy in AA2024 plate and sheet owing to the different grain structure in each direction due to the rolling process [52, 233]. The three different directions with respect to the grain structure of AA2024-T3 are illustrated in Figure 2.23.

Growth in the longitudinal (L) and long transverse (LT) directions is much faster than it is in the short transverse (ST) direction. The grains get elongated in the rolling direction during rolling. As a result, it is easier for the intergranular corrosion to follow this path rather than along the more tortuous grain boundary route observed in the through-thickness (short transverse, ST) or the transverse (T) direction. Grains in a ST direction are more rounded than other two directions, so IGC through this direction would have to follow a longer path.

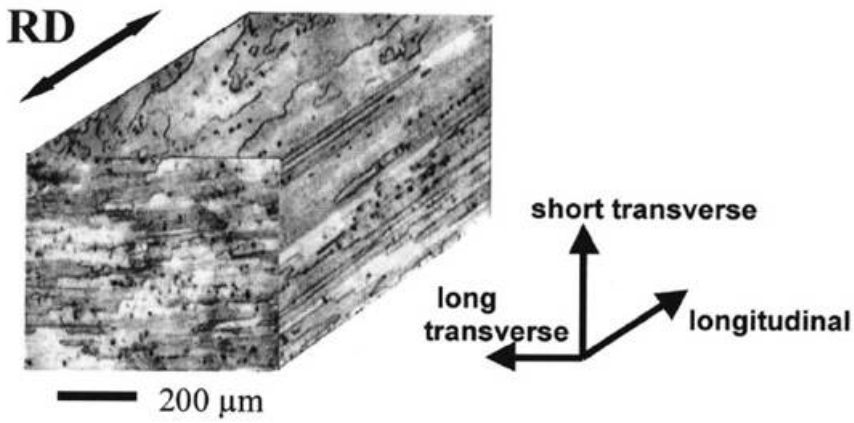

Figure 2.23 Metallographic sections of AA2024-T3 showing grain structure in each direction along with the terminology used for different sections. RD is rolling direction [233].

Results gained from statistical models based on this hypothesis seem to be in agreement with foil penetration data [234]. It was also found that the penetration rate of corrosion attack depends on the applied potential and stress state with samples showing higher penetration rate when subjected to a remotely applied load. Effect of stress on the localized corrosion growth kinetics will be discussed later in detail. The foil penetration technique has some distinct advantage over the serial exposure and metallographic sectioning technique. It has been shown that the kinetics determined from the longest site in each metallographic section are slower than those determined by the foil penetration technique [55]. This emphasizes the fact that the fastest growing sites are often missed by metallographic sectioning.

However the main disadvantage with the foil penetration technique is that it determines the growth kinetics of the fastest growing localized corrosion sites. It is also possible that the exposed sample contains many slow growing localized corrosion sites or there could even be some sites that initiate much later than the fastest growing corrosion site. Though the presence of these corrosion sites will affect the structural integrity of the material but they will remain unidentified by the foil penetration technique. To overcome

these problems imposed by the conventional foil penetration technique, Zhao *et al.* [55] studied the intergranular corrosion of aluminium alloys using an X-Ray radiographic technique. It was found that the growth kinetics determined from radiographs of the samples were slower than growth kinetics determined by the foil penetration technique. However, the resolution of these X-ray radiographic studies was quite low. As a result, though these studies gave an idea about the IGC growth in two dimensions, it was difficult to quantify the evolution of IGC morphology within the microstructure. Localized corrosion growth normally follows a t^n penetration relationship which is represented as [29, 49, 50, 52, 55, 217, 219]:

$$d = Kt^n \qquad \textbf{Equation 2.10}$$

Where d is the depth of penetration, K is a constant, t is time and n is a fraction between 0 and 1.

The two most predominant forms of localized corrosion, pitting [49-51] and intergranular corrosion [29, 52, 55] are reported to follow the above relationship. Zhang and Frankel [52] found the localized corrosion growth to follow a $d = Kt^{0.5}$ parabolic relationship for AA2024-T3 in all three direction. Values of K are 0.271, 0.209 and 0.123 in L, LT and ST sections respectively. In stressed conditions, the penetration depth of IGC in the L-T and T-L orientations were reported to vary approximately with $t^{0.5}$ similar to what has been observed for pitting corrosion and IGC in unstressed samples [29]. The X-ray radiographic study of IGC growth kinetics of aluminium alloys showed similar relationship to those reported via the foil penetration technique [55]. Growth in the T direction was found to follow the general law $d = Kt^n$, where n was ~ 0.33 and K was 0.23 to 0.34 for values in hours and d in mm.

Rota and Boehni [218, 219] found that IGC penetration behaviour depends on the sheet thickness under investigation. Due to the transition in attack morphology with increasing sheet thickness and the formation of a fine-meshed localized corrosion attack network resulting in macroscopic grain dissolution at the specimen surface after long exposure, it was impossible to formulate an integral attack growth kinetics valid for the entire range of attack depths. So, to correlate the current time records with the attack morphologies, the intergranular corrosion growth kinetics was divided in three distinct stages with decreasing penetration velocity: 1) activation/initiation – represented by linear increase of total current I with time, 2) transition stage – where corresponding total current I shows a flat maximum, and 3) stable macroscopic grain dissolution – characterized by constant total current I. Based on the experimental findings it was concluded that the growth kinetics of intergranular corrosion are related to the number of active attack sites per unit volume. This specific number of actively growing attack sites depends on the grain size and on the electrochemical conditions and, for given parameters, on the exposure time and therefore on the sheet thickness. Figure 2.24 shows the schematic diagram summarising the critical findings from Rota's research [219].

Rapid growth of IGC to a certain depth and its subsequent cease could be explained by the self-limiting effect of localized corrosion as discussed by Lifka [221]. IGC initiate and grow rapidly to a limiting depth at which mass transport no longer provides sufficient oxygen and corroding species down the narrow corrosion path. Branching of IGC networks make it extremely difficult for oxygen to diffuse down to the active tip to provide necessary cathodic support for continuing anodic dissolution.

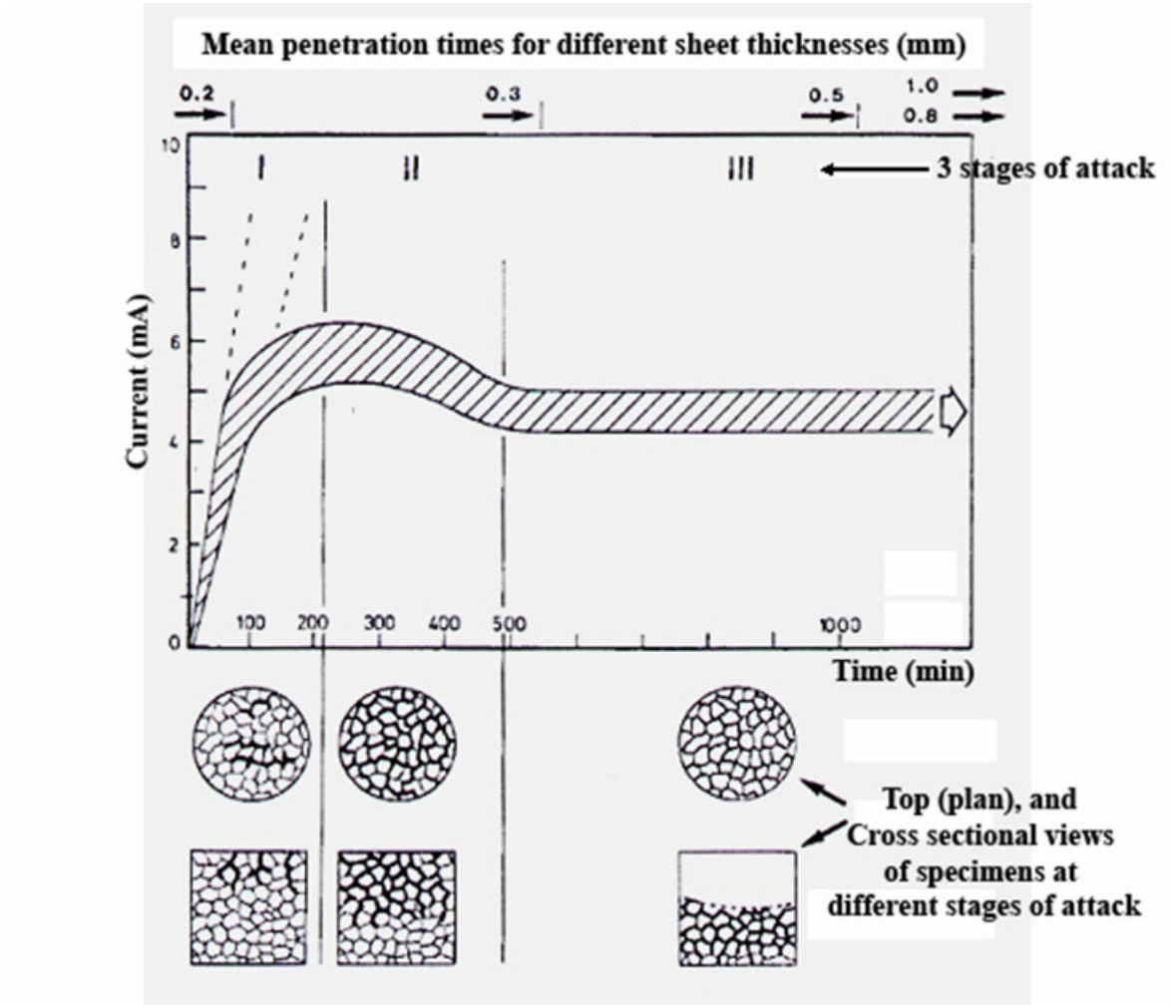

Figure 2.24 A schematic representation of the current time curves for perforation time measurement in sheets of a fine grained commercial AA2024 alloy, showing the three stages of IGC growth. The mean perforation times for different sheet thicknesses in 0.1M NaCl, pH 7, at a measuring potential of -500mV are indicated by the arrows at the top of the graph and are related to the time scale at the bottom. Top and cross sectional views of the attack morphologies corresponding to the three subsequent stages of intergranular corrosion are shown in the lower part of the figure [219].

When penetration of IGC in a certain direction ceases, it begins to spread laterally through the material in other directions [221]. This theory has been experimentally supported by the three dimensional visualization of IGC by Fox [235], who found that IGC sites rapidly penetrate a susceptible alloy until a limiting depth at which point the

electrochemical driving force for corrosion would start favouring the grain interiors rather than the grain boundaries. At this point widening of IGC will occur as found by other researchers [52]. The dissolution of the interior grains could also result due to the possible change in chemistry inside a dissolving boundary. Kotsikos [236] *et al.* suggested that aggressive ion accumulation inside an active tip of an IGC can occur within a few hours. This increase in aggressiveness could play an important role in spreading the dissolution from the boundaries to the grain interiors.

Intergranular corrosion of aluminium alloys could also be associated with an induction period prior to the initiation as indicated by several researchers [70, 95]. The reason behind this is not fully understood as yet, but it could well be correlated with the time to passive film breakdown and with the time to accumulate the necessary aggressive environment required for the initiation of intergranular corrosion.

2.2.3 Stress Assisted Localized Corrosion

Application of stress can change the local microstructural features and electrochemical activity for localized corrosion site initiation. Previous investigators have shown that applied stress affects the localized corrosion behaviour of structural metal by influencing dissolution rate [20-22], passivity [23-25], and localized corrosion initiation and propagation [26-34].

Gutman and his co-workers [21, 237, 238] tried to explain the change in the corrosion behaviour of materials under the application of stress using ‘mechanochemistry’ or ‘mechanochemical’ models. These models are focused towards the deformation induced microstructural changes and their subsequent interaction with the

corroding media rather than passive film oriented theories of local breakdown in stressing condition. Applied tensile stresses below the yield strength does not rupture the electrochemical continuity of oxide film on aluminium as was unambiguously shown by impedance measurement [237]. Therefore it was concluded that, deformation acceleration of anodic dissolution manifests itself only in the sections that are subjected to dissolution before applying stress and corrosion rates before and after deformation refer to the same surface. According to Gutman's theory, stress induced microstructural changes such as, slip band formation, and dislocation pile up play a crucial role in determining the corrosion of that particular material. Various features of anodic electrochemical behaviour of materials are due to the different values of chemical potential of the metal sample at different stages [21]. Mechanochemical behaviour of the metal can be correlated with the known change of dislocation substructure during plastic deformation. When stainless steel is plastically deformed, the active area of metal dissolution could be limited by the regions of maximum deformation induced activation of the metal.

Gutman *et al.* [21] also argued that the mechanochemical behaviour of the metal are equivalent in both passive and transpassive state and independent of the surface oxide film. Local potential measurements on the slip planes showed more negative (i.e., more anodic) potential than the potential of the rest of metal the surface [237]. The potential difference grows with the increasing predeformation of the specimen. A potential change of ~ -100 mV was observed in local regions adjacent to slip planes for 18-8 stainless steel. The active dissolution occurs in local areas of slip plane exit, while the remaining surface of a metal is passivated. In most cases, applied stress to the yield stress of the material or even beyond will cause a change in the chemical potential of about ~ 20-30 mV maximum. Also, the local potential difference between the slip planes and the rest of the metal surface normally varies between 5-20 mV [237]. So, ambiguity still remains

with this theory of 'mechanochemical activation of solid' on whether this theory is strong enough to explain some of the dramatic changes in the localized corrosion behaviour of materials under the application of stress.

Bombara *et al.* [25] investigated the possible role of oxide films under straining conditions in initiating localized corrosion which can potentially act as precursor sites for stress corrosion cracking at later stages. It was assumed that the primary effect of stress is to produce fresh metal areas disbanded from the overlaying passive coverage. These freshly exposed areas without passive films may show high dissolution rate as well as becoming active crevices at any film rupture by the sequence schematically represented in Figure 2.25. The micro-crevice at the base of the slip step will be deeper and more critical for the more ductile oxide layer. Effect of stress on the pitting susceptibility is also described by the influence of stress on the mechanical integrity of the protective oxide film [34, 239]. Structural and compositional variations within the oxide film are thought to provide weak points for mechanical fracture and subsequent anodic activity may lead to the formation of pits.

Vignal *et al.* [30] reported that the presence of microcracks near inclusions from an applied load could be the possible controlling factor in localized corrosion initiation in steel. Detailed study using the micro-capillary electrochemical cell showed the influence of plastic deformation on the electrochemical behaviour of inclusions in stainless steel on a microscopic scale. It is known that the inclusions at the surface of stainless steels are good precursor sites for the nucleation of cracks during fatigue loading. Detailed SEM observations by Vignal *et al.* [240] revealed the presence of two types of microcracks at the MnS inclusion of steel. In the first case numerous microcracks were observed both in the inclusion and at the inclusion/matrix interface. In the other case microcracks were only observed at the inclusion/matrix interface. Based on their findings they concluded

that these microcracks play a crucial role in the localized corrosion initiation and certain morphology of microcracks is necessary to obtain stable pitting.

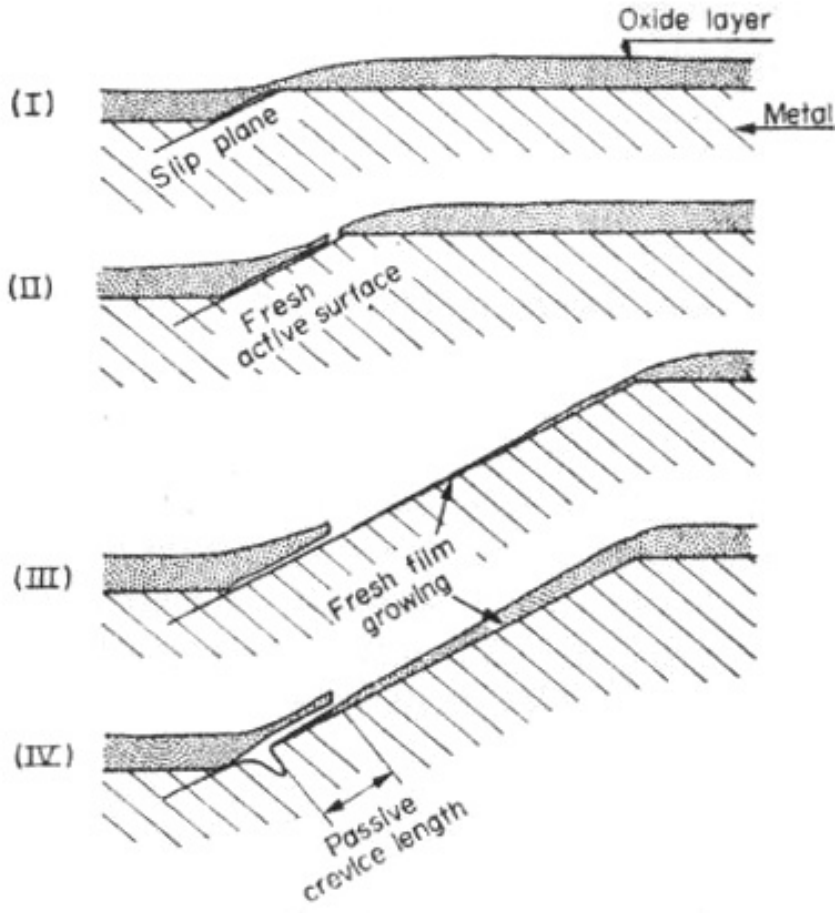

Figure 2.25 Schematic representation of the sequential steps of passive film rupture by application of stress and thereby creating potential sites of initiating crevice attack [25]. (I) Emergence of slip step with a necking effect on the oxide film. (II) Rupture of the oxide film at the leading edge and crevice activation. (III) Partial passivation of the crevice area and notching attack at the active foot of the slip step.

Vignal *et al.* [30] developed a method to calculate the stress field around the inclusion and it can be used with certain limitations for predicting where microcracks can initiate. Electrochemical characterization was then performed via the micro-capillary

electrochemical cell at the microcracks near the inclusions for better understanding of pit initiation.

Suter *et al.* [28] investigated the influence of applied stress on the pitting behaviour of stainless steel. Most of the inclusions were deformed by the rolling process and depending on their orientation, different corrosion behaviours were observed. Cracks were found to form within the MnS inclusions by applied stress and subsequently formed a preferable geometry to accumulate high concentrations of aggressive species causing stable pitting. Using microcapillaries of 100 μm diameter, it was found that applied stress shifted the MnS dissolution potentials more negative (i.e., lower) and increased the dissolution rate.

Whereas the effect of stress on the localized corrosion of stainless steel has been explored during last few years, limited research has been performed with aluminium alloys. Connolly [36] studied the effect of stress on the particle behaviour and its effect on localized corrosion in aluminium alloy 2024. Application of tensile stress above the yield stress was found to increase the electrochemical reactivity for the localized corrosion site initiation (Figure 2.26). It can be seen from the figure that application of plastic stress decreased both open circuit potential and breakdown potential of AA2024 when tested in 0.1 M NaCl. If a current density of 10^{-5} A/cm^2 is chosen as an appropriate metric to measure representative breakdown potential (E_b), stressed sample shows almost 100 mV lower (i.e., more negative) E_b than the unstressed sample. SEM analysis in conjunction with in situ stressing revealed that delamination occurs at constituent particle/matrix interfaces when the 2024-T351 samples are subjected to load greater than 90% of YS (Figure 2.27). These delaminated areas could form micro/nano crevices which can accumulate aggressive ions and thereby acting as potential sites for corrosion initiation.

A significant portion of the stress assisted localized corrosion work in aluminium alloys investigated the effect of stress on intergranular corrosion. Contribution from the stress component in the intergranular corrosion process of high strength aluminium alloys has remained unclear.

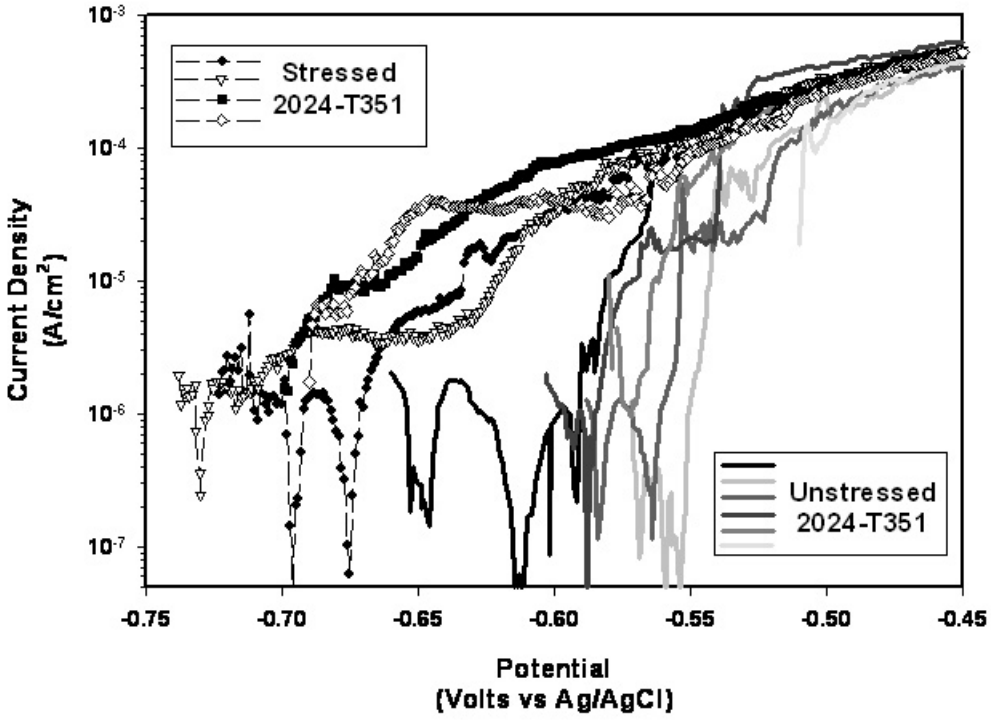

Figure 2.26 Anodic potentiodynamic scans in 0.1 M NaCl characterizing the effect of applied stress on the pitting potentials of AA2024-T351. The applied stress was oriented parallel to the rolling direction [36]. Current density of 10^{-5} A/cm^2 is taken as a representative current associated with breakdown event. Application of stress brings down both open circuit potential and breakdown potential of the alloy. Average breakdown potential of stressed sample (~ -675 mV vs. Ag/AgCl) is about 100 mV lower than unstressed sample (~ -575 mV vs. Ag/AgCl).

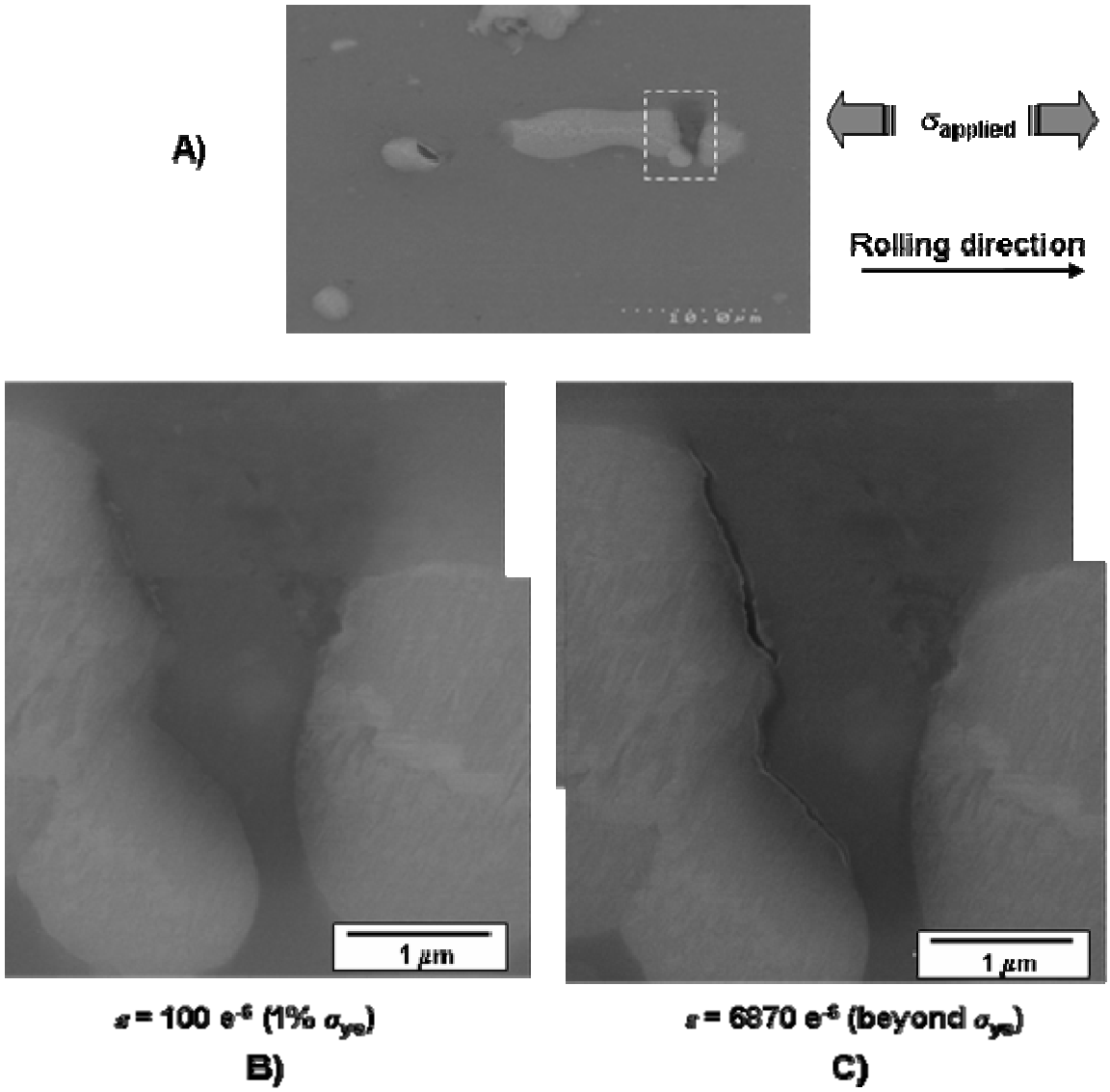

Figure 2.27 In situ FEG-SEM documentation of a constituent particle/matrix interface upon application of plastic strain. A distinct delamination occurs along the interface perpendicular to the applied stress. The load in this case was applied parallel to the rolling direction of the 2024-T351 [36]. Delamination between the particle and matrix can act as potential microcrevices for aggressive ion accumulation.

However, few questions are still to be answered as the reported experimental results are sometime contradictory while explaining the role of stress in intergranular corrosion [218]. Debate still continues among the researchers on whether stress assisted intergranular corrosion can simply be termed as intergranular stress corrosion cracking;

or, if actually stress play an influential role in aggravating the intergranular corrosion growth rate itself rather than turning the intergranular corrosion into crack.

It has often been seen that, the role of intergranular corrosion of an unstressed material has not been considered in the SCC investigations. Based on the available data in the open literature Rota and Boehni [218] divided the effect of stress on the intergranular corrosion into four groups:

(i) Stress induced intergranular corrosion: Mechanically stressed specimens show intergranular attacks in less aggressive electrochemical environment as compared to the unstressed condition.

(ii) Stress assisted intergranular corrosion: Under identical electrochemical conditions, the growth rate of intergranular attacks is higher in mechanically stressed specimens.

(iii) No detectable influence of mechanical stress on the growth kinetics of intergranular attacks.

(iv) In some special cases, tensile stresses are found to reduce the intergranular crack growth rate.

Liu *et al.* [29] tried to find a correlation between intergranular corrosion (IGC) and intergranular stress corrosion cracking (IGSCC). Intergranular corrosion (IGC) is one of the main forms of localized corrosion in high strength aluminium alloys, and IGC can transition into IGSCC under a tensile stress [29, 241, 242]. It has also been reported that tensile stresses increases the penetration rate of IGC and the extent of it depends on the orientation of stress relative to the wrought microstructure [29, 242]. Liu described IGSCC as an enhanced IGC phenomenon due to the presence of applied stress. The

primary mechanism of crack growth for 2xxx series (Al-Cu-Mg) alloys is considered to be anodic dissolution of the grain boundary precipitates [53]. As discussed in the earlier sections, galvanic interaction between the particles and the local surrounding matrix can lead to preferential dissolution of anodic particles or dissolution of the adjacent matrix surrounding noble particles [170, 182, 227]. According to the anodic dissolution mechanism, the function of applied tensile stresses is limited to opening cracks [242]. This theory treats the mechanism of SCC similar to that of IGC, but it does not give any insight why some alloys are susceptible to SCC and not susceptible to IGC (Al-Zn-Mg alloys) or, conversely, susceptible to IGC and unsusceptible to SCC (Al-Mg-Si alloys) [242]. However, the theory of opening of cracks/localized corrosion sites under the application of tensile stresses and thereby increasing the corrosion growth rate could be supported by the findings of Liu *et al.* [241]. It was found in their study of AA2024-T3 that the application of compressive stress at a level halfway to yield significantly reduced the growth kinetics of IGC in the perpendicular direction.

Liu *et al.* [29] studied the effect of tensile stress on the corrosion of 2024-T3 using the foil penetration technique. As discussed earlier, the growth rate of localized corrosion exhibits a strong anisotropy in AA2024 plate and sheet owing to the different grain structure in each direction [52, 233]. It was also found that the penetration rate of corrosion attack depends on the applied potential and stress state with samples showing higher penetration rate when subjected to an applied load. However the main disadvantage with the foil penetration technique is that it determines the growth kinetics of the fastest growing localized corrosion sites. Increase in the IGC rates in the presence of a tensile stress at the surface of the material was also reported by Rota *et al.* [218]. Zhao *et al.* [55] studied the intergranular corrosion of aluminium alloys using X-Ray radiograph and found that growth kinetics determined from radiographs of the samples

were slower than growth kinetics determined by foil penetration technique. In a separate study Zhao and Frankel [35] investigated the effect of prior deformation on localized corrosion of aluminium alloys. AA2024-T3 showed increased corrosion rate after pre-stressing, but little change in breakdown potentials. It is speculated that the increase in the current density with increase in pre-strain is due to the deformation induced defects.

Liu *et al.* [29] agreed with Zhang and Frankel [52] that in AA2024-T3 showing two breakdown potentials during polarization scan; the first breakdown is triggered by the transient 'S' phase attack whereas IGC is responsible for second breakdown. In the stressed samples, IGSCC was more prominent above second breakdown whereas pitting was predominant between two breakdown potential. It has been found that the penetration rate of corrosion attack depends on the applied potential and stressed sample showed higher penetration rate. With the application of stress a smooth transition from IGC to IGSCC has been observed which indicate that both these phenomenon could be operated through same mechanisms [29].

Zhang and Frankel [52] found that under stressing condition for AA2024-T3, penetration depth of IGC in L-T and T-L orientations vary approximately with $t^{0.5}$ similar to what has been observed for pitting corrosion and IGC in unstressed samples [29]. The effect of stress on growth kinetics depended on the sample orientation and n was found to vary from 0.15 to 0.46 when curves were best fitted. Applied stress had a tendency to increase the value of K and slightly decrease n.

Rota and Boehni [218, 219] carried out experiments to find out the effect of stress on the intergranular corrosion growth rate of aluminium alloys using the foil penetration technique. Different stages of IGC growth according to Rota's study were summarized in the earlier section. Effect of stress was found to be only in the first stage where a small number of parallel cracks/localized attacks were active. In the second stage those

localized attacks starts to form a branched network thereby making effect of stress less predominant. In the third stage, grain dissolution starts and growth kinetics become independent of applied stress. It was tried to explain the effect of stress based on stress induced widening of the localized attacks which not only reduces the integral ohmic resistance of the system but also improves the mass transport conditions between the localized corrosion path and the bulk electrolyte. Rota argued that the widening of localized attack depends on the stress distribution in the whole specimen rather than on the stress intensity at the tip of the localized corrosion path. With the generation of large number of parallel cracks/localized attacks and network formation, chances of stress induced widening of IGC attacks diminished. This phenomena result into the disappearance of stress effect in the presence of large number of parallel IGC attacks. However it must be noted that Rota's model of stress induced IGC growth kinetics is based on the results obtained from a modified foil penetration test which measures the fastest growing localized attack in two dimensions.

2.3 Surface Treatment

Surface treatment of AA 2024 is almost always necessary prior to any kind of engineering applications. Pretreatment of the aluminium alloy substrate is essential in order to obtain a strong and stable bond between the alloy substrate and the relevant protective coating (or bonding) [243, 244]. In order to achieve this, the naturally formed surface oxide on aluminium alloy has to be removed and replaced with a new, continuous, solid, and corrosion resistant oxide layer [243]. The most successful and widely used treatments in the aerospace industry involves formation of chromate conversion coating

(CCC) on the top of the substrate as these coatings are generally considered to give the best improvement in the corrosion behaviour of the aluminium alloys along with good paint adhesion [245]. However, the production, storage and application of chromate solutions cause large environmental and health related problems as they contain hexavalent chromium compounds that have several toxic effects (i.e., carcinogenic in nature). This fact has driven research toward more environment friendly pretreatment methods for aluminium alloy.

It has been reported that on aluminium alloys, the cathodic nature of the intermetallic particles promote filiform corrosion which occurs by the microgalvanic coupling between the aluminium matrix and electrochemically nobler second-phase particles [246-248]. Chromate conversion coating is widely used as a pretreatment technique because of its ability of inhibiting the cathodic oxygen reduction reaction on the intermetallic particles [74, 249, 250]. Although the general trend of the present age is to move away from the CCC technique, researchers have tried to maintain the advantages offered by those coatings especially in terms of its effectiveness in inhibiting the cathodic reaction and thereby minimising corrosion.

Therefore, alternative pretreatment methods have been developed to etch/remove the cathodic particles from the surface [251]. It has also been shown that effective removal of such intermetallic particles by controlled etching can significantly improve the corrosion resistance of bare aluminium alloy [249, 251, 252]. For example, Lunder *et al.* [249] studied the effect of α-Al(Fe,Mn)Si particles removal from the surface of AA6060 using different treatment methods. It was found that removal of the intermetallic particles by immersion in HNO_3-HF or by potentiostatic etching in chloride solution and HNO_3 respectively, reduce the cathodic reactivity of the alloy.

A typical surface treatment mainly consists of three steps; cleaning, coating and finally painting [19]. However, this present review will be concentrated only on the first step. A typical cleaning process includes degreasing, etching in alkaline solution and then desmutting and/or oxide removal. Normally cleaning also helps to improve the adhesion of subsequent treatments. In the degreasing step, organic solvents such as methyl-ethyl-ketone are normally used to remove any contamination from the surface [76].

The effect of chemical etching on aluminium substrates was studied by Moffitt *et al.* [253]. Many commercial alloys, frequently containing relatively high levels of iron, resulting in the presence of second phase material are subjected to alkaline etching to remove millscale, residual oil and subsurface defect [254]. The behaviour of aluminium alloys during alkaline etching and the resultant surface morphology have been examined previously [255]. It was found that both alkaline and acid cleanings modify the aluminium oxide structure above complex alloys and at times copper surface enrichments were detected. Alkaline etching helps to remove thin cold-work layers. It also removes some oxide left on the alloy surface after processing and etch the aluminium matrix [256]. In case of 2024, alkaline etching leaves a black smut on the surface which is enriched with copper [257, 258]. The dissolution of the alloy and surface enrichment could be represented by the following equation, [76] :

$$2Al + 6H_2O + 2OH^- \rightarrow 2Al(OH)_4^- + 3H_2$$ **Equation 2.11**

Nitric acid desmutting is a practical way to remove the smut enriched with copper compounds. It has been observed that the nitric acid is most effective within the first 30s of immersion and sometimes attack the intermetallic particle [76, 258]. The desmutting

procedure removes the residual copper left on the surface after etching and any insoluble oxides formed during the alkaline etch. It appears, however, that nitric acid desmutting does not remove thin enrichments beneath an established oxide [253]. Lunder *et al.* [243] used alkaline etching of AA6060 in hot NaOH followed by desmutting in nitric acid and found improvements in the corrosion and mechanical properties compared to surfaces only degreased with acetone.

Complete removal of enriched copper on the surface is not always possible even after the nitric acid desmutting. The copper enrichment on the surface is thought to be due either to the replating of dissolved copper or undissolved solid solution copper left during the dissolution of the aluminium matrix [259]. The etching process does not remove the intermetallic particle because in the alkaline environment Mg is stable and protects the 'S' phase. It has been reported in the literature [19, 260] that the addition of rare earth chloride in the nitric acid bath has a beneficial effect in removing the intermetallic particles and therefore decreasing the surface reactivity. Addition of cerium chloride in the nitric acid bath helps in removing the 'S' phases which act as cathodic sites during corrosion [258]. The disappearance of cathodic sites helps in improving the corrosion properties of the alloy.

2.4 X-Ray Microtomography

X-ray tomography is a relatively new non-destructive technique which has been used recently in many areas of materials science and engineering for obtaining 3D information of the interior of materials with a spatial resolution on the micron scale [261-267]. High resolution X-ray computed tomography with spatial resolution of at least 50-

100 μm is termed as X-ray microtomography [267]. Normally most of material characterizations are performed in conventional two dimensional (2D) techniques using light or electron microscope. Though 2D techniques are used to obtain three-dimensional (3D) information because of their stereological relations [268], there are several limitations in 2D technique that can not be overcome. The true size distribution and connectivity of phases with complex shapes can not be obtained from a 2D section and strong differences can be observed between 2D and 3D measurements [268]. X-ray microtomography can overcome these limitations and gives information about what happens within the bulk material. Reconstruction of the 3D volumetric data from this technique allows us to analyze the microstructure, defects, phase distribution or damage in the bulk material along with the ability to view two dimensional cross sections at any particular plane or orientation.

Though the mathematical principle of X-Ray tomography was developed in the second decade of the twentieth century, the electronic, instrumental, and computer hardware limitation delayed the physical construction of computed tomography device until the early seventies [269]. The initial use of the computed tomography was limited in the medical field due to rather low spatial resolution in the range of 300-1000 μm. The requirement of high spatial resolution for the use of tomography in the materials science field constrained its use until very recent times. New generation synchrotron sources combined with new detectors have now made it possible to obtain 3D reconstructed image with spatial resolution close to micron to submicron level and thereby encouraging the researchers to explore the possibility of making microtomography an useful materials characterization technique [261, 262, 266, 267].

2.4.1 The Principles of X-Ray Tomography

The basis of X-ray tomography is similar to the X-ray radiography. The underlying mechanism for X-ray tomography explores the fundamental interaction of photon with the material as described by Beer-Lambert law (**Equation 2.12-Equation 2.13**) [261, 266, 267, 270],

$$I = I_0 \exp[-\int \mu(s)ds] \quad \textbf{Equation 2.12}$$

$$\int \mu(s)ds = \ln\left(I_0 / I\right) \quad \textbf{Equation 2.13}$$

where, I_0 is the intensity of the unattenuated X-ray beam, I is the beam's intensity after it transverse a material thickness of s, and μ(s) is the linear absorption coefficient at position s along beam path (s).

The intensity of the transmitted beam depends on the density (ρ), atomic number (Z) and the energy of the incident beam (E). For a monochromatic X-ray beam of constant energy E, the relation between the attenuation of the beam by the object with the atomic number and the density is given by the **Equation 2.14**, [261, 270],

$$\mu = K\rho\left[\frac{Z^4}{E^3}\right] \quad \textbf{Equation 2.14}$$

where K is a constant.

Figure 2.28 shows the schematic of the way the integral of the attenuation coefficient (μ) is calculated using **Equation 2.13**, and thereby representing the total attenuation of the beam by the object along the considered path [270]. The term μ (x, y) represents the value of the linear attenuation coefficient at the point (x, y). Repeating such measurement along a sufficient number of straight lines within the same slice enables the reconstruction of the μ (x, y) of the slice and record it on a CCD based X-ray detector [270].

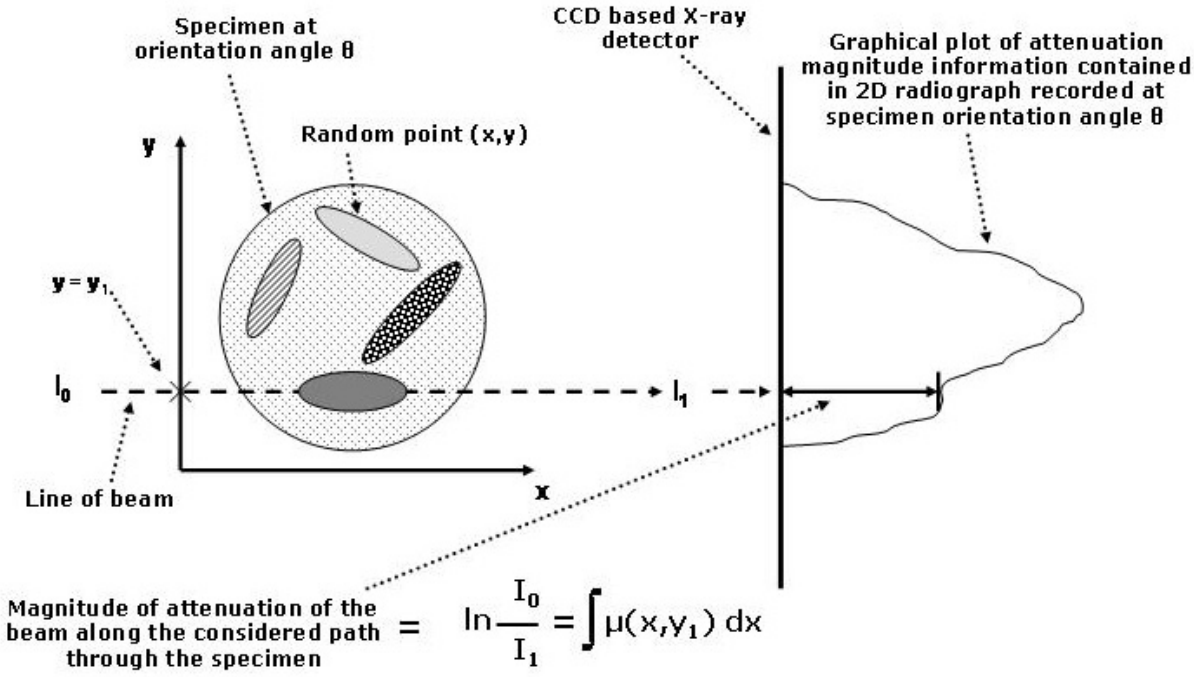

Figure 2.28 Schematic of the physical basis of transmission tomography inside a slice and the resulting beam attenuation [235, 270].

As the X-ray beam is sent through the sample and the transmitted beam is recorded on a CCD detector while the sample is being rotated from 0° to 180° in small

incremental steps. The recorded two dimensional (2D) radiographic projections of the samples are then used to reconstruct a three dimensional (3D) map of the X-ray attenuation coefficient of the material using an appropriate algorithm based on the filtered back-projection [261, 267, 271]. Most of the studies in X-ray tomography have been carried out using the conventional absorption mode though there are three different modes available to perform tomography [266]:

1. *The Absorption mode*: In this mode the contrast is generated due to the difference between the linear attenuation coefficients of two different materials. Attenuation coefficients depend on the atomic number of the elements and the density. As a result, the larger the difference in the density the better the contrast.

2. *The Phase Contrast mode*: The contrast is due to interference after propagation between parts of wave at either side of an interface that have suffered different phase retardation. This is observed when the beam is partially coherent and when the distance between the sample and the detector is increased in comparison to the absorption mode.

3. *The Holotomography mode*: In this mode, images are taken at several samples to detector distances and then using a specific algorithm the quantitative distribution of the optical phase can be retrieved. Using this mode, quantitative analysis of the density in the material in 3D can be done.

Different set up can be used to perform X-ray tomography. They all comprise an X-ray source, a rotation stage on which the object is fixed, and an X-ray detector. The set up can be either medium resolution microtomography or high resolution tomography.

2.4.1.1.1 X-Ray Tube Tomography

Medium resolution microtomography can be done by using a classical microfocus X-ray tube as a source [261]. In this case X-rays are emitted from a metallic target and a polychromatic divergent beam is generated from it. The sample is placed in between the source and the detector and can be moved in order to adjust the magnification and the subsequent resolution which generally lies between 10 and 500 µm [272]. To fit the sample in the field view of the detector, a compromise must be found between the maximum sample size and the spatial resolution. This set up is mainly used in absorption mode since the incoherence of the beam limits the use of phase contrast mode.

2.4.1.1.2 Synchrotron Radiation Tomography

Best quality images with very high spatial resolution allowing high resolution microtomography are obtained by the use of synchrotron radiation. Synchrotron radiation is produced by ultra-relativistic electrons is a storage ring when they are accelerated by a magnetic field [261]. Synchrotron sources deliver a very high flux at very small size of the incident beam (at least 1000 times larger than X-ray tubes for third generation synchrotrons) [267, 273]. As the source and the tomography set up is very large, the X-ray beam becomes practically parallel and coherent in nature which helps the beam to be used in phase contrast or holotomography mode [266]. In some experimental set up a

monochromator is placed between the source and the sample in order to obtain a monochromatic beam. Normally CCD based detectors are used to capture the non magnified image of the sample as shown in Figure 2.29. Most of the time the resolution of X-ray synchrotron tomography is limited by the detector system in use [273]. Currently the optimum resolution is in the range of 0.3 – 0.7 μm [262, 274].

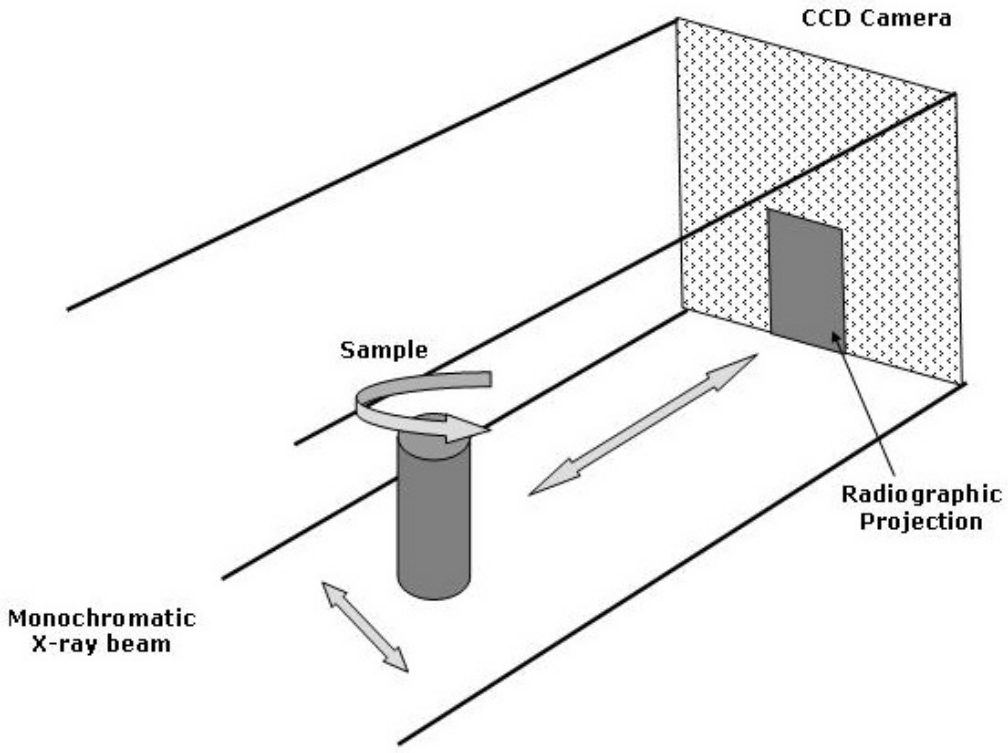

Figure 2.29 A schematic of the X-ray synchrotron tomographic technique using high flux, monochromatic and parallel beam geometry. The sample is not magnified in on the detector [266].

2.4.2 The Application of X-Ray Tomography in Materials Science

The application of X-ray microtomography in the field of material science can be classified into several broad areas: inorganic and metal matrix composites [275-277], foams [268, 278, 279], transport in porous media [267, 280], fatigue crack nucleation [281, 282] and closure [283-286], localized corrosion and stress corrosion cracking [287-290]. The main advantage of X-ray microtomography is that it can reconstruct sample interiors with the spatial and contrast resolution high enough to solve many interesting problems non-destructively.

X-ray microtomography has been used to study the damage accumulation and fracture of both ceramics and metal matrix composites [277, 291-293]. Distribution of the continuous and discontinuous second phases and thermo mechanical fatigue of ceramic as well as metal matrix composites has also been studied. Microtomography was also been successfully used in the electronic industry for non-destructively quantifying the spatial distribution of corrosion products within printed wiring boards [294, 295].

Salvo *et al.* [266] reviewed the use of X-ray microtomography for investigating problems in metallic materials such as superplastic deformation [296], materials in semi solid state and metallic foams [266, 297]. Researchers at the European Synchrotron Facility (ESRF) in France have successfully used high resolution microtomography for showing the evolution of damage during in situ tensile tests [275] and to characterize industrial materials processed by a semi-solid forming technique at a resolution of 2 μm [298, 299]. High resolution microtomography allowed quantification of total liquid volume fraction, the volume distribution, the morphology of the entrapped liquid and its 3D location. The grain boundary wetting phenomena of polycrystalline aluminium in

contact with liquid gallium has also been studied using synchrotron microtomography [300].

Furthermore, synchrotron microtomography is comprehensively used in the field of materials science to study the fatigue crack nucleation and crack closure phenomena [281, 283, 284, 286, 301]. In situ studies helped to understand at what stress intensities and how the crack faces come into contact or separate during a fatigue cycle. Three dimensional observations and modelling of intergranular stress corrosion cracking using synchrotron microtomography in austenitic stainless steel have been reported [287, 290]. In these studies interaction between the stress corrosion crack and the microstructure of stainless steel have been discussed in details. 3D rendering of the material or crack using microtomography proved to be a useful tool to study the history of damage propagation where crack bridging ligaments were observed to develop and fail during crack propagation. In most of the cases these experiments are performed ex-situ and then investigated under X-ray tomography for their microstructural features, phase morphology and connectivity, damage or defect accumulation.

As described earlier, the X-ray tomographic technique shows the difference of what can be derived from the surface observation (conventional 2D technique) and what actually happens within the bulk materials. These features of tomography made it a very attractive tool for in-situ investigations where the imaging is actually done during the experiment itself. Various materials have been studied with different combinations of elevated temperature using furnace, loading stage and in corrosive environments [261, 266, 267, 288].

Use of X-ray microtomography has not been explored in great details to study corrosion problems associated with structural materials like high strength aluminium alloys. Marrow *et al.* [287] were the first to perform in situ experiments in the

synchrotron beam line in a corrosive aqueous environment. Connolly *et al.* [288] and Davenport *et al.* [289] performed in situ experiments for aluminium and magnesium alloy, respectively, to explore this field further.

2.5 Summary

This literature review discusses the various issues related to localized corrosion of aluminium-copper alloys and summarizes the efforts over the past few decades that have been made for better understanding of this phenomenon specifically associated with aluminium alloy 2024. It is generally agreed that intermetallic particles contribute to the poor corrosion resistance of aluminium alloys [8-11, 14, 15, 37, 38, 40, 42, 47, 48, 82, 123, 173, 175, 182-185, 187-189, 191, 193, 194]. Two different types of intermetallic particles have been identified in AA2024, the first category of the intermetallic particles are cathodic in nature (e.g., Fe-Mn particle) [8, 11] while the second type is anodic (e.g., 'S' phase particles) [12-15] with respect to the matrix of AA2024. Discussion on the cathodic model for localized corrosion initiation focuses on the increase in local alkalinity around the intermetallic particle as a result of the oxygen reduction on the particles [208]. Alkaline grooving has been observed around the intermetallic particles and it is believed that these cathodic trenches contribute in the pitting process at later stages by undercutting the particle [48]. However, few researchers refer to the alkaline attack itself as pitting [11, 170]. Other researchers proposed an anodic trenching model based on the galvanic relationships between the particles and the matrix [38]. Anodic phases dissolve via this mechanism and may form a site for accumulating aggressive ions. Pitting attack may initiate and propagate from these preferential sites.

Though the deleterious effects of the intermetallic particles on the corrosion properties of the aluminium alloys have been unambiguously established through the investigations of several researchers in last the few decades, it should be noted that, none of the above mentioned proposed theories are good enough to explain all the corrosion phenomena associated with intermetallic particles independently. It is generally accepted that the inherent variability (e.g., heterogeneity in the composition, difference in morphology etc.) associated with the intermetallic particles provides further challenges to the researchers in establishing any particular corrosion mechanism. However, irrespective of the operative corrosion mechanisms, deleterious effects of the intermetallic particles have further been established when selective removal of these intermetallic particles using different surface treatment techniques is found to improve the corrosion resistance of the alloy [19].

It is essential to investigate the corrosion performance of any alloy subjected to applied loads as stress is an integral part of any structural design/application. It is found that the penetration rate of corrosion attack depends on stress state with samples showing higher penetration rate when subjected to an applied load. However, ambiguities still remain among the researchers about the reasons behind the change in the corrosion properties under stressing condition. Application of stress is thought to produce surface defects such as slip lines, microcracks, decohesion between phases as well as making the surface rougher [35]. It is hypothesized that all of these surface defects could serve as potential sites for pit initiation by making the passive film less stable. It was assumed that the primary effect of stress is to produce fresh metal areas isolated from the overlaying passive coverage and thereby increasing the local dissolution rate [25]. Conversely, proposed ‘mechanochemistry’ or ‘mechanochemical’ models are focused toward the deformation induced microstructural changes and their subsequent interaction with the

corroding media rather than passive film oriented theories of local breakdown under stressing conditions [21, 237, 238]. However, ambiguities still remain with this theory of "mechanochemical activation of solid" on whether this theory has the ability to predict some of the dramatic changes in the localized corrosion behaviour of materials under the application of stress.

However, none of the above mentioned theories under stressing conditions consider the possible role of intermetallic particles in determining the corrosion behaviour of the aluminium alloys. Limited research has been performed on this aspect and it is reported that apart from the stress state, presence of intermetallic particles can also play a crucial role in determining the corrosion property of the alloy under stress. Application of stress creates delamination between the particle-matrix interface which may act as micro/nano crevices and potential site for corrosion initiation [36].

In addition to the significant work that has been performed to understand the corrosion initiation process, significant efforts have been devoted to investigate the localized corrosion growth kinetics in aluminium alloys. In most of the cases the growth rates have been calculated using conventional 2D techniques, mainly using the foil penetration technique [29, 49-52]. Owing to the anisotropic nature of the grains in different directions, corrosion growth is also found to be anisotropic process [52, 233]. Attack penetrates faster in the direction where the grains and grain boundaries are elongated. Localized corrosion growth normally is found to follow a t^n penetration relationship which is represented as $d = Kt^n$ [29, 49, 50, 52, 55, 217, 219]. These 2D techniques have their own limitations as most determine the rate of only the fastest growing corrosion sites. These techniques also do not provide an idea about the distribution of corrosion attack in three dimensions which is very important for life prediction modelling in real engineering situations. In situ X-ray synchrotron

microtomography is reported to be able to overcome the limitations of 2D technique and give real 3D information [266, 267].

Thus the literature review section summarizes the importance of intermetallic particles for corrosion initiation, surface treatment technique for selective removal of harmful phases and thereby improving the corrosion properties, and effect of stress on initiation and propagation of localized corrosion. It is quite clear from the above discussion that limited research has been performed on the effect of stress on the localized corrosion of aluminium alloys. In the unstressed condition, initiation of corrosion has shown to be associated with the presence of intermetallic particles in the aluminium alloy. However, the role of these intermetallic particles in corrosion initiation under stressing condition has not been well investigated. Hence, this work will mainly be focused on the effect of stress on the initiation and propagation of localized corrosion in the aluminium alloys with a special emphasize on the role of intermetallic particles under both unstressed and stressed conditions. It is also evident that better understanding of the propagation rate of localized corrosion in high strength aluminium alloys is essential to develop any effective life prediction modelling tools for components. Hence, this study will also focus on the IGC growth rate measurements in three dimensions using X-ray synchrotron microtomography that can overcome the limitations of the conventional 2D techniques used by most of the previous researchers.